Nanostructured oxygen reduction catalyst designs to reduce the platinum dependency of polymer electrolyte fuel cells

by

Drew Christopher Higgins

A thesis

presented to the University of Waterloo

in fulfilment of the

thesis requirement for the degree of

Doctor of Philosophy

in

Chemical Engineering

Waterloo, Ontario, Canada, 2015

Author's Declaration

This thesis consists of material all of which I authored or co-authored: see Statement of Contributions included in the thesis. This is a true copy of the thesis, including any required final revisions, as accepted by my examiners.

I understand that my thesis may be made electronically available to the public.

Statement of Contributions

This thesis is based upon a combination of published work. Various chapters are adapted from the following list of published work, with specific reference to the published work provided within the chapter.

D. Higgins, F. Hassan, M. Seo, J. Choi, A. Hoque, D. Lee, Z. Chen, "Shape-controlled octahedral cobalt disulfide nanoparticles supported on nitrogen and sulfur-doped graphene/carbon nanotube composites for oxygen reduction in acidic electrolyte", *Journal of Materials Chemistry A*, 3 (2015) 6340-6350.

D. Higgins, R. Wang, A. Hoque, P. Zamani, S. Abureden, Z. Chen, "Morphology and composition controlled platinum-cobalt alloy nanowires prepared by electrospinning as oxygen reduction catalyst", *Nano Energy*, 10 (2014) 135-143.

D. Higgins, Z. Chen, "Recent progress in non-precious metal catalysts for PEM fuel cell applications", *Canadian Journal of Chemical Engineering*, 91 (2013) 1881-1895.

D. Higgins, J. Choi, J. Wu, A. Lopez, Z. Chen, "Titanium nitride carbon nanotube core-shell composites as effective electrocatalyst supports for low temperature fuel cells", *Journal of Materials Chemistry*, 22 (2012) 3727-3732.

D. Higgins, Z. Chen, S. Ye, S. Knights, "Highly Durable Platinum-Cobalt Nanowires by Microwave Irradiation as Oxygen Reduction Catalyst for PEM Fuel Cell", *Electrochemical and Solid-State Letters,* 6 (2012) B83-B85.

Z. Chen, D. Higgins, A. Yu, L. Zhang, J. Zhang, "A Review on Non-precious Metal Electrocatalysts for PEM Fuel Cells", *Energy & Environmental Science*, 4 (2011) 3167-3192.

Abstract

Polymer electrolyte fuel cells (PEFCs) are electrochemical devices that efficiently convert hydrogen and oxygen into electricity and water. Their clean point of operation emissions and fast refueling times have resulted in PEFCs being highly touted as integral components of sustainable energy infrastructures, most notably in the transportation sector. The issues associated with hydrogen production and distribution aside, the commercial viability of PEFCs is still hindered by the high cost and inadequate long term operational stability. A main contributor towards both of these issues is the platinum-based electrocatalysts used at the cathode to facilitate the inherently sluggish oxygen reduction reaction (ORR). These expensive precious metal catalysts comprise almost half of the overall PEFC stack cost, and undergo degradation under the cathode environment that is very corrosive due to the acidic and potentiodynamic conditions. There is therefore ample room for cost reduction if reduced platinum ORR catalysts can be developed with sufficient activity and durability to meet the technical targets set for the use of PEFCs in automobiles.

In this work, two classes of nanostructured catalysts are investigated. The first is high activity platinum or platinum alloy materials with the objective of surpassing the activity of conventional catalysts on a precious metal basis to achieve cost reductions. The second is non-platinum group metal (non-PGM) catalysts, that while intrinsically less active than platinum, can still provide high power output at moderate operating voltages, such as those encountered during automobile operation. These two catalyst technologies are developed and delivered with the ultimate objective of integrating them together into

platinum/non-PGM hybrid electrodes to provide excellent PEFC performance with a reduced platinum dependency.

In Chapter 4, titanium nitride – carbon nanotube (TiN-CNT) core-shell nanocomposites developed by a simplistic two step fabrication procedure are reported. These materials are physicochemically characterized by a variety of microscopy and spectroscopy techniques and used as platinum nanoparticle elelectrocatalyst supports (Pt/TiN-CNT) for the ORR. Through half-cell electrochemical testing in acidic electrolyte, improved ORR activity was demonstrated for Pt/TiN-CNTs compared with state of the art commercial Pt/C. The one-dimensional morphology of the TiN-CNT supports is also conducive for integration into highly porous electrode structures with excellent interconnectivity to ensure reactant access and electronic conductivity throughout the catalyst layer, respectively. The long term stability of this catalyst however remains questionable, likely due to oxidation of the titanium nitride surface that results in a thin passivating layer.

It is becoming increasingly evident that corrosion of platinum nanoparticle supports is inevitable during fuel cell operation. To overcome this, a focus was then placed on the development of supportless nanostructured platinum catalyst designs. Platinum cobalt nanowires (Pt-Co-NWs) were prepared by simplistic, template free microwave-irradiation process as discussed in Chapter 5. Using cobalt as an alloying element was undertaken owing to the documented ability of this transition metal to modulate the adsorptive properties of platinum and induce increased ORR activity. The one-dimensional anisotropic nanostructure can also provide increased platinum stability owing to the reduced surface

energies in comparison to zero dimensional nanoparticles. The Pt-Co-NWs displayed promising ORR activity a through half-cell testing in 0.1 M HClO$_4$. Most notably, using harsh accelerated durability testing (ADT) that consisted of 1,000 electrochemical potential cycles from 0 to 1.5 V vs. RHE at 50 °C, the Pt-Co-NWs maintained the majority of their ORR activity, highlighting exemplary stability. While simple, the drawback of this synthesis approach is that it did not allow for nanowire diameters that were below 40 nm. This resulted in inaccessible platinum atoms within the nanowire cores, highlighting the fact that further improved ORR activity on a platinum mass basis could be achieved with reduced diameters.

To accomplish this, the electrospinning approach was used to prepare PtCoNWs (please note the nomenclature distinction). Through investigations in which synthesis parameters were systematically investigated, electrospinning was found to provide a versatile platform for the synthesis of nanowires with tunable diameters and atomic compositions. PtCoNWs with a near unity stoichiometric ratio, excellent atomic distribution and an average diameter of 28 nm were evaluated for ORR activity. Over a four-fold enhancement in Pt mass-based activity at an electrode potential of 0.9 V vs RHE is obtained in comparison to pure platinum nanowires, highlighting the beneficial impact of the alloying structure. A near 7-fold specific activity increase is also observed in comparison to commercial Pt/C catalyst, along with improved electrochemically active surface area retention through repetitive (1,000) potential cycles. Electrospinning is thereby an attractive approach to prepare morphology and composition controlled PtCoNWs that could potentially one day replace conventional nanoparticle catalysts.

With the development of PtCoNWs established, developing non-PGM catalysts that can be hybridized with the high activity platinum-based catalysts was required. In Chapter 7, single crystal cobalt disulfide (CoS_2) octahedral nanoparticles supported on graphene/carbon nanotube composites were prepared as ORR catalysts. During the simplistic, one-pot solvothermal synthesis, the nanostructured carbon supports were also simultaneously doped with nitrogen and sulfur. Time dependent studies elucidated the growth process of the {111} facet encased octahedra that could only be prepared when carbon support materials were incorporated into the reaction mixture. The impact of carbon support on ORR activity was clear, with the graphene/carbon nanotube composite supported CoS_2 octahedra (CoS_2-CG) outperforming CoS_2 supported on just graphene or carbon nanotubes. Additionally, CoS_2-CG provided an on-set potential (0.78 V vs. RHE) and half-wave potential (0.66 V vs. RHE) that was 60 mV and 150 mV higher than the CoS_2 particle agglomerates formed when no carbon support was included during catalyst preparation. By combining the synergistic properties of the graphene/carbon nanotube composite and unique shape controlled single crystal CoS_2 nanoparticles, CoS_2-CG comprises the highest activity non-precious metal transition metal chalcogenide reported to date, and is presented as an emerging catalyst for the ORR in fuel cells.

Chapter 8 provides a summary of the conclusions of this body of work, along with strategies that can be employed to capitalize on the scientific advancements made through this thesis. The delivery of PtCoNWs and CoS_2-CG that can be reliably prepared by simple techniques provides the crucial first step towards the development of platinum/non-PGM hybrid electrodes. Future projects should focus on the integration of these two catalysts into

new electrode arrangements in an attempt to exploit their individual properties. Through this approach, it is hypothesized that synergistic coupling of these two catalysts can lead to PEFC systems with reduced activation losses from the PtCoNWs, along with CoS_2-CG providing increased maximum power densities at lower cell voltages, all at reduced platinum contents in comparison to state of the art PEFC cathodes.

Acknowledgements

First and foremost I would like to thank my supervisor, Professor Zhongwei Chen, and all of the outstanding colleagues I have had at the University of Waterloo. The support, discussions and sharing of ideas has been crucial to research progress throughout the last several years. I have learned a lot from all of you and am very appreciative to have made some great friends during this time.

I would also like to thank my Ph.D. examining committee, including Professor Michael Pope, Professor Michael Fowler, Professor Bo Cui and Professor Plamen Atanassov (from the University of New Mexico) for their contributions through this important process. In addition I would like to thank Professor Yuning Li for his participation on my comprehensive proposal examining committee.

I also had the valuable opportunity to spend almost one year at the Los Alamos National Laboratory, working with the outstanding fuel cell team that they have there. Special thanks go out to all members of this team that I had the pleasure of working with closely. Of particular note is my mentor, Dr. Piotr Zelenay, and two staff scientists who are truly masters at the art of catalyst synthesis and characterization. Dr. Gang Wu (now at the University at Buffalo, SUNY) and Dr. Hoon Chung, thank you for providing the opportunity to work so closely with you throughout this time, and for all the knowledge you were more than willing to share with me.

Importantly, I would like to most gratefully acknowledge my friends and family. You all provide a constant (and important!) reminder that life is not all about scientific research, and I thank you for all the support, fun and smiles that you provide every day.

Table of Contents

List of Figures

List of Tables

List of Abbreviations

ADT – Accelerated durability testing

CNT – Carbon nanotube

CV – Cyclic voltammetry

DDI – Distilled de-ionized water

ECSA – Electrochemically active surface area

EDX – Energy dispersive x-ray

EG – Ethylene glycol

ESR - Electron-spin resonance

GO – Graphene oxide

HOR – Hydrogen oxidation reaction

ICP – Inductively coupled plasma

MEA – Membrane electrode assembly

MOR – Methanol oxidation reaction

ORR – Oxygen reduction reaction

PEFC – Polymer electrolyte fuel cell

Pt-B – Platinum black catalyst

Pt/C – Carbon support platinum catalyst

Pt-Co-NW – Platinum cobalt nanowires prepared solvothermally (Chapter 5)

PtCoNW – Platinum cobalt nanowires prepared by electrospinning (Chapter 6)

RDE – Rotating disc electrode

RHE – Reversible or reference hydrogen electrode

SAED – Select area electron diffraction

SEM – Scanning electron microscopy

STEM – Scanning transmission electron microscopy

TEM - Transmission electron microscopy

TGA – Thermogravimetric analysis

TOF – Turnover frequency

XANES – X-ray absorption near edge structure

XPS – X-ray photoelectron spectroscopy

XRD – X-ray diffraction

1. Introduction

1.1 The energy challenge

Clean energy initiatives are an increasingly important area for technological innovation owing to rapidly increasing global populations and energy demands. As a society, we continue to have an almost exclusive reliance on fossil fuel reserves to meet these demands. Development of clean energy production, storage and conversion technologies is urgently needed to achieve sustainability of the energy sector, and to proactively deal with climate change and environmental issues before they become detrimental to quality of life.

Polymer electrolyte fuel cells (PEFCs) are highly efficient electrochemical devices that convert the chemical energy of hydrogen and oxygen into electricity and water. Their clean point of operation emissions, fast refueling times and excellent energy density render them promising for a variety of applications, the most notable of which is in the transportation sector. Hydrogen fueled PEFC vehicles would allow us to significantly cut back on the over five billion tonnes of greenhouse gas emissions (CO_2) produced by automobiles each year;[1] however their commercial attractiveness on a device level is still limited by two primary factors: high cost and insufficient durability. The main contributor to PEFC system cost is the high content of platinum required in the electrodes to facilitate the pertinent electrochemical reactions, namely the hydrogen oxidation reaction (HOR) at the anode, and the oxygen reduction reaction (ORR) at the cathode. The monopolized global distribution and limited natural reserves of this precious metal[2] leads to

a very volatile price structure.[3] Furthermore, as it is a natural resource, it is not privy to the economy of scale benefits that can be realized for other manufactured component materials, such as electrolyte membranes and bipolar plates. To this end, under projected conditions of mass PEFC production (500,000 units per year), the platinum-based electrocatalysts are estimated to contribute just short of 50% of the overall PEFC stack cost.[4] Both the anode and cathode rely on expensive platinum-based catalysts, although the majority of platinum content is used at the cathode as the rates of ORR are inherently six orders of magnitude slower than the HOR.[5] Furthermore, the cathode catalysts are exposed to high, transient potentials, which are very corrosive under the humidified, acidic and high temperature environment of the PEFC.[6] This leads to material stability issues, and current catalyst technologies cannot retain adequate activity to meet the 5,000 hours of operation requirement if PEFCs are ever to compete with internal combustion engines. It is therefore extremely desirable to develop new ORR catalyst technologies that can reduce the platinum content of state of the art cathodes, while providing long term stability under the harsh operative conditions.

1.2 Polymer electrolyte fuel cell fundamentals

PEFCs are electrochemical energy devices that directly convert the chemical energy stored in hydrogen and oxygen, into electricity. Initially developed back in the 1960s, PEFCs are attractive for a variety of different purposes due to their efficiency, relatively low operating temperatures, environmentally benign emissions and silent operation. PEFC stacks consist of several cells connected in series in order to achieve useful voltage levels and practical power output. Each individual cell is comprised of three components: (i) the

anode, where the HOR occurs; (ii) the electrolyte membrane, which conducts protons from the anode to the cathode while being impermeable to electron flow; and (iii) the cathode, where the ORR occurs. **Figure 1-1** provides a simple schematic of a single cell, which is commonly referred to as a membrane electrode assembly (MEA).
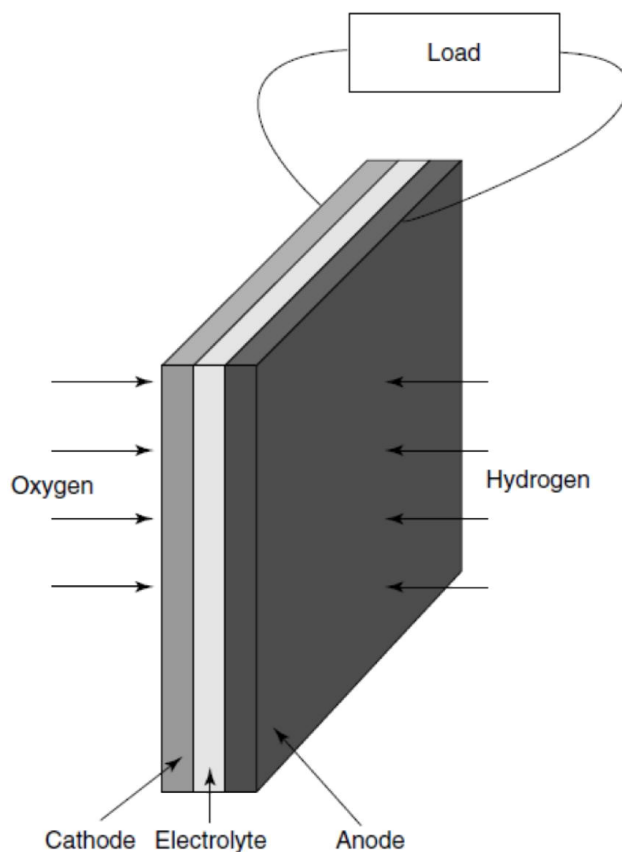
Figure 1-1: Single membrane electrode assembly consisting of an anode, polymer electrolyte and cathode. With permission from [7], copyright John Wiley and Sons, 2003.

Hydrogen is steadily fed as a fuel to the anode, where it will undergo the HOR (Equation 1-1):

$$H_2 \rightarrow 2H^+ + 2e^- \qquad\qquad E^o = 0 \text{ V vs RHE} \qquad\qquad (1\text{-}1)$$

Following this reaction, the generated protons will diffuse across the electrolyte membrane towards the cathode. In PEFC systems, the electrolyte membrane is Nafion, a perfluorinated sulfonic acid membrane. The negatively charged SO_3^- groups have strong interactions with the positively charged protons generated by the HOR. When the membrane is hydrated during PEFC operation, the attraction between the protons and the SO_3^- groups weaken and provide the protons with mobility, upon which they diffuse through the membrane towards the region of lower concentration. It is a stringent requirement that the electrolyte membrane be resistant to electron flow, causing the electrons to flow through the external circuit powering the attached load. After reaching the cathode, the electrons combine with the diffused protons from the HOR, along with oxygen molecules being continuously fed to the cathode where the ORR occurs according to Equation 1-2:

$$O_2 + 4H^+ + 4e^- \rightarrow 2H_2O \qquad E^o = 1.229 \text{ V vs RHE} \qquad (1\text{-}2)$$
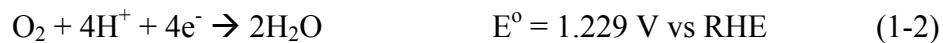
With the HOR and ORR occurring simultaneously during PEFC operation, the theoretical open circuit voltage is given as 1.229 V and the overall full cell reaction can be summarized according to Equation 1-3:

$$H_2 + \tfrac{1}{2}O_2 \rightarrow H_2O \qquad (1\text{-}3)$$
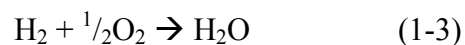
Despite boasting a theoretical open circuit voltage of 1.229, during actual use, observed voltages are always significantly lower than this value and decreasingly so at higher drawn currents. This is due to a phenomenon referred to as overpotential, or irreversible voltage losses than can be attributed to a variety of different factors. **Figure 1-2**

provides an example of a typical PEFC polarization curve. The first thing that can be noticed from this figure is that the open circuit voltage (no current being drawn) is significantly lower than the theoretical 'No loss' voltage marked by the dashed line. This can be attributed to fuel crossover across the membrane,[7] and to some extent, platinum catalyst oxidation.
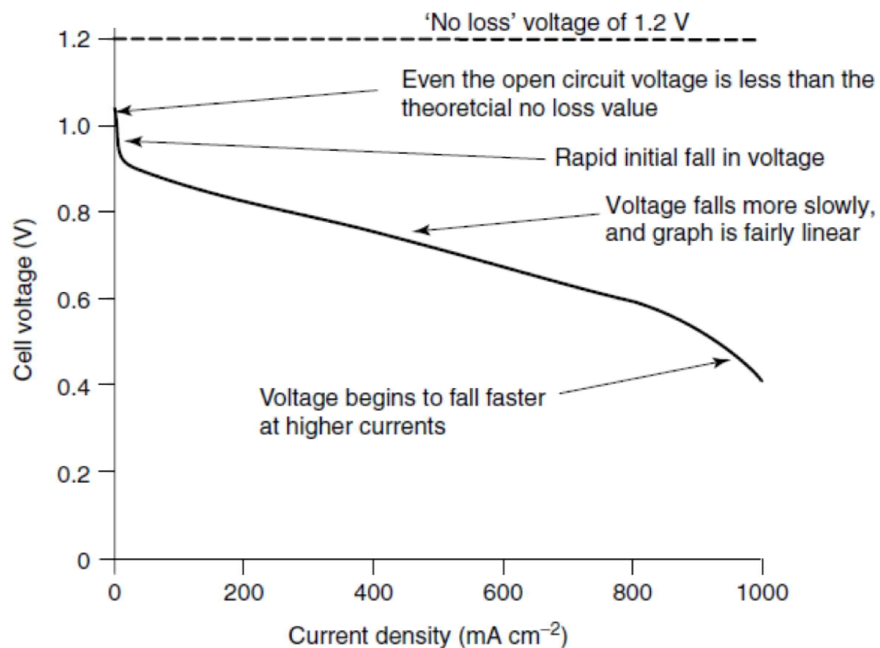
Figure 1-2: Typical PEFC polarization curve showing the various regions of overpotential, or irreversible voltage losses. With permission from [7], copyright John Wiley and Sons, 2003.

Moving to the region where current begins to be drawn from the PEFC, a sharp drop in cell voltage with increasing currents is observed. This region is due to activation overpotential, and is directly related to the slow kinetics of the necessary electrode reactions. This is the most detrimental and important cause of voltage drop in PEFCs, contributed primarily by the cathode due to the very sluggish ORR kinetics in comparison

to the HOR which contributes negligible losses. Using more effective catalysts with deliberately designed nanostructures can serve to overcome these irreversible voltage losses and is a primary research objective of scientists and engineers.

The region displaying a linear loss of cell voltage with increasing currents in the polarization curve provided in **Figure 1-2** is due to ohmic losses. The sources of resistance in PEFCs can arise from the polymer electrolyte, the cell connections or the bipolar plates. These issues can be mitigated by appropriate selection of materials, including electrode structures with high conductivity.

Finally, at excessive current densities, the voltage of the PEFC will drop off dramatically as observed in **Figure 1-2**. This is due to the fact that the necessary electrode reactions are proceeding at a rate faster than the reactants can be delivered to the catalyst surface. Using pure reactant feeds, or increased gas pressures can help to mitigate this occurrence, but also using well designed catalyst layer architectures conducive to good reactant flow and accessibility will increase the current densities attainable in a PEFC system.

1.3 Fuel cell challenges and technical targets

While PEFCs have found marginal commercial success in niche markets such as backup power (*i.e.*, telecommunications) and materials handling fleets (*i.e.*, forklifts),[8] the ultimate target is at scale deployment in the transportation sector. Issues with the storage, handling and distribution of hydrogen aside, there are two device level limitations that currently limit the attractiveness of fuel cells in the automotive market: cost and durability.

To help propel PEFCs to the point that they can one day be integrated into efficient and clean driving light-duty vehicles, technical targets and goals have been established by the U.S. Driving Research and Innovation for Vehicle efficiency and Energy sustainability (DRIVE) Fuel Cell Technical Team (FCTT). The FCTT is a conglomerate organization consisting of members of the U.S. Department of Energy, several of the major automotive manufacturers and various energy companies.

Outlined in the "Fuel Cell Technical Team Roadmap"[9] are technical targets relating to PEFC systems, stacks, MEAs and the various components integral to their performance. Among the various components, the electrocatalysts required at each electrode to facilitate the pertinent electrochemical reactions are the biggest contributors to PEFC cost and durability issues.[10] As electrocatalyst development is the subject of this thesis, all subsequent discussions focus on this important area of research. The FCTT defined technical targets for electrocatalysts are summarized in **Figure 1-3**. The reader is referred elsewhere for in depth information regarding material and design challenges relating to other PEFC components including electrolyte membranes,[11, 12] bipolar plates[13] and overall system designs.[6, 14]

Characteristic	Units	Status	2020 Target
Platinum group metal (PGM) total content[a]	g/kW rated	0.14[b]	0.125
PGM total loading[a]	mg PGM/cm^2 electrode area	0.15[b]	0.125
Loss in catalytic (mass) activity[c]	%	37[d]	40% loss of initial
Loss in high current density performance	mV	10[d]	30 at 0.8 A/cm^2 (Table A-1)
Loss in high current density performance	mV	10[e]	30 at 1.5 A/cm^2 (Table A-2)
Mass activity[f]	A/mg$_{PGM}$ @ 900 mV$_{iR\text{-free}}$	0.47-0.67[b]	0.44
Non-PGM catalyst activity per volume of supported catalyst[f,g]	A/cm^3 @ 800 mV$_{iR\text{-free}}$	60[h]	300

[a] PGM (Pt, Ir, Os, Ru, Rh, and Pd) content and loading targets may have to be lower to achieve system cost targets. The cost impact of the use of other precious metals, e.g., Au and Re, also needs to be considered.
[b] 50 cm^2 with Pt$_3$Ni$_7$, M. Debe, 3M, "Advanced Cathode Catalysts and Supports from PEM Fuel Cells," DOE Hydrogen and Fuel Cells Program 2012 Annual Progress Report, http://www.hydrogen.energy.gov/pdfs/progress12/v_d_1_debe_2012.pdf.
[c] See Table A-1 of Appendix A.
[d] M. Debe, 3M, "Advanced Cathode Catalysts and Supports from PEM Fuel Cells," DOE Hydrogen and Fuel Cells Program 2012 Annual Progress Report, http://www.hydrogen.energy.gov/pdfs/progress12/v_d_1_debe_2012.pdf. 30,000 cycles 0.6-1.0V, 50mV/sec, 80/80/80°C, 100 kPa (abs), H$_2$/N$_2$.
[e] M. Debe, 3M, "Advanced Cathode Catalysts and Supports from PEM Fuel Cells," DOE Hydrogen and Fuel Cells Program 2012 Annual Progress Report, http://www.hydrogen.energy.gov/pdfs/progress12/v_d_1_debe_2012.pdf. 1.2 V for 400 hrs at 80°C, H$_2$/N$_2$, 150 kPa (abs), 100% relative humidity.
[f] Test at 80°C H$_2$/O$_2$ in MEA; fully humidified with total outlet pressure of 150 kPa (abs); anode stoichiometry 2; cathode stoichiometry 9.5 (Gasteiger et al., *Applied Catalysis B: Environmental*, 56 (2005) 9-35.
[g] Volume = active area multiplied by catalyst layer thickness.
[h] P. Zelenay, H. Chung, C. Johnston, N. Mack, M. Nelson, P. Turner, and G. Wu, FY 2011 Progress Report for the DOE Hydrogen Program, p. 816, U.S. Department of Energy, Feb. 2011, DOE/GO-102011-3178.

Figure 1-3: FCTT defined electrocatalyst targets for PEFCs for transportation applications. Reproduced from [9].

Under projected conditions of mass production (500,000 units per year), the cost of the electrocatalyst is estimated to be almost half of the entire PEFC stack cost.[4] This is because platinum is a precious metal with highly monopolized global distribution, and is therefore not privy to the economy of scale benefits that other component materials can benefit from. To lower the cost of PEFC systems, the amount of platinum required must therefore be reduced. Concerted efforts have mainly focused on ORR catalyst development at the cathode. This is because the cathodic ORR is inherently several orders of magnitude slower than the anodic HOR and requires significantly higher platinum contents to achieve

adequate reaction rates. To reduce the platinum requirement at the cathode without a sacrifice in PEFC power output or efficiency, new catalysts must be developed with improved activity on a *platinum mass* basis. This must also be achieved with a simultaneous increase in catalyst stability during long term PEFC operation, and during periods of fuel cell start-up/shutdown.

PEFC electrodes consist of a catalyst coated gas diffusion layer (**Figure 1.4a**). The gas diffusion layer is a carbon paper or carbon cloth that serves as the backing for the electrode structure, and also delivers and diffuses the reactant gas over the entirety of the electrode surface. The current state of electrocatalyst technology consists of uniform sized platinum nanoparticles well dispersed on a high surface area carbon support, commonly abbreviated as Pt/C and illustrated in **Figure 1.4b**. When integrating catalysts into electrode structures, it is important that one maximizes the formation of what is referred to as the *three phase boundary* (**Figure 1.4c**). This three phase boundary is essential, because it brings together all of the necessary ORR reactant species to the catalyst surface (i.e., platinum). This includes: (i) oxygen species that are transported through pores in the catalyst layer; (ii) electrons that are transported through the conductive carbon support particles; and (iii) protons that are transported through the electrolyte and ionomer species present in the catalyst layer.
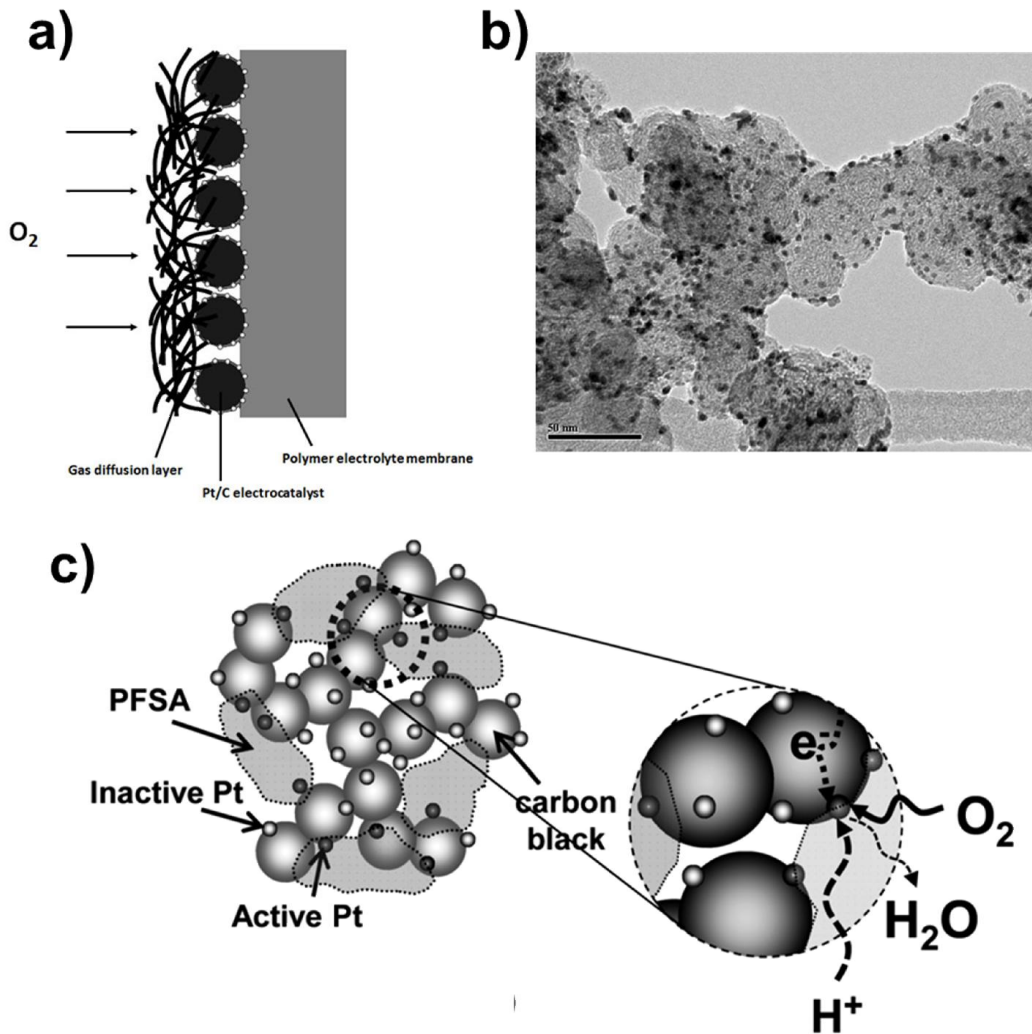
Figure 1-4: (a) Schematic illustration of the cathode portion of a MEA for a PEFC. With permission from [7], copyright John Wiley and Sons, 2003. (b) Typical image of commercial Pt/C showing platinum nanoparticles (dark spheres) dispersed on a high surface area carbon support. (c) Schematic depiction of the three-phase boundary where electrolyte (PFSA) for H^+ transport, pores for O_2 transport and catalyst particles for electron transport all intersect, reproduced from [15], with permission of RSC publishing.

The specific type of catalyst utilized and electrode design will have a direct impact on the activation voltage losses and oxygen mass transport, respectively, which have a

subsequent impact on the power performance of the devices. Increasing the activity of the electrocatalyst materials towards the ORR will have a marked impact on the overall performance output, effectively reducing the overall platinum requirement, system cost and performance. Several strategies to accomplish this involve development of unique catalyst supports,[16-19] alloying with non-precious base metals[20-24] and deliberate nanostructure control.[25-27] These are the approaches that undertaken in the current project.

During fuel cell operation, the cathode will be exposed to potentiodynamic conditions encountered during drive cycles, through start up and shut down procedures or during periods of fuel starvation.[28] Combined with the acidic nature of the polymeric membrane, humidified conditions and elevated temperature, all of these factors culminate in an environment that is very harsh and electrode materials are very prone to degradation and performance loss over time. The specific mechanistic pathways of Pt/C electrocatalyst degradation have been elucidated[6, 29] and can be broken down into three contributions as depicted in **Figure 1-5**, including: (i) corrosion of the carbon support, (ii) platinum nanoparticle dissolution and/or agglomeration, and (iii) catalyst detachment. Contamination or poisoning by species such as CO, CO_2, NO_x and SO_x can also cause performance loss.[30, 31]
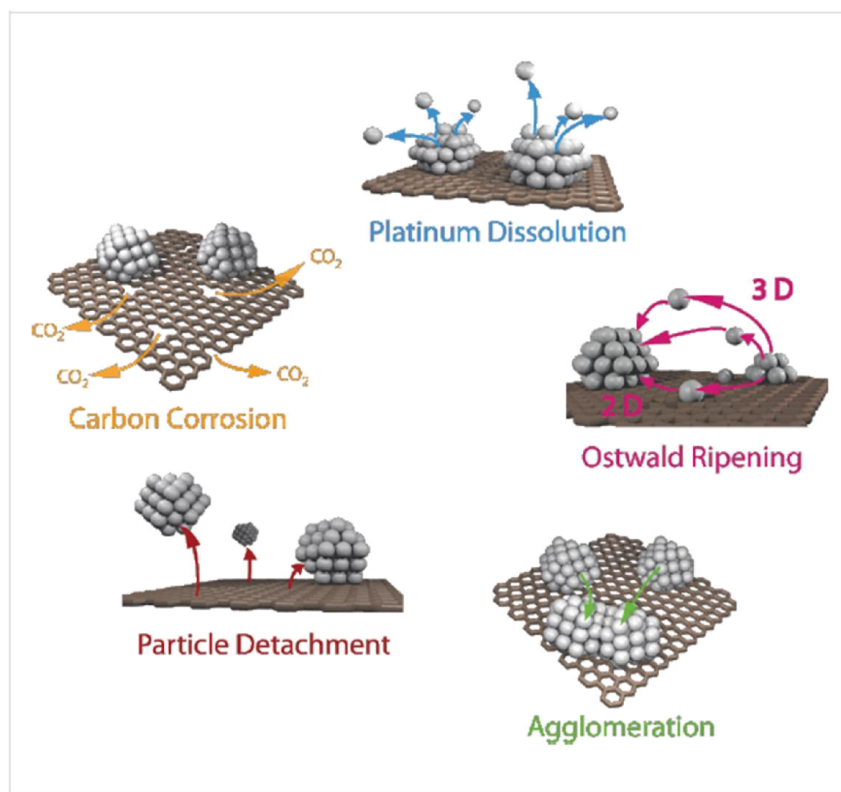
Figure 1-5: Schematic depiction of the primary degradation pathways of conventional Pt/C catalyst. Reproduced from [29] (open access article).

Corrosion (or oxidation) of the carbon support has a relatively low reversible equilibrium potential of 0.207 V *vs.* RHE under standard conditions, and is thus thermodynamically favourable at the conditions encountered as the cathode of PEFCs during operation.[32] It is known to occur according to Equation 1-4:

$$C + 2H_2O \rightarrow CO_2 + 4H^+ + 4e^-$$ (1-4)
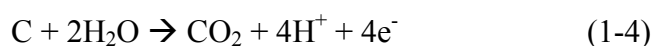
Factors including the presence of platinum, humidity, temperature and the amount of carbon exposure will all play an influential role in carbon corrosion,[6, 32] however potential is the primary governing factor. Carbon corrosion is very detrimental to long term fuel cell

durability and can be mitigated a variety of different ways. One technique is to reduce the amount of platinum utilized as it is known that platinum catalyses the carbon corrosion reaction. Another technique is to use highly graphitized carbon supports, as gaphitic carbon is less prone to corrosion than disordered or amorphous carbon species.[33] Replacing, or compositing carbon materials with materials that are less prone to corrosion is also an effective strategy and can include titanium oxides and nitrides[16, 34, 35] as investigated in the present project.

Platinum nanoparticle dissolution and/or agglomeration will also occur during long periods of PEFC operation. Nanosized platinum particles have very high surface energies that promote their migration and agglomeration into larger particles in order to reduce the surface energy of these materials.[36, 37] This phenomenon is commonly referred to as Ostwald ripening and generally occurs by two different mechanisms. The first is by platinum ion migration through the ionomer layer in the catalyst, and the second is by platinum dissolution and subsequent deposition on neighbouring particles. Particle agglomeration or loss through dissolution lowers the electrocatalyst surface area available to facilitate the ORR, thus resulting in an overall loss of PEFC performance. There are several techniques to overcome this detrimental phenomenon. One of these techniques involves the development of unique catalyst support materials that form stronger bonds with platinum nanoparticles, thereby mitigating the occurrence of dissolution and agglomeration.[38-40] Another technique is by developing platinum or platinum alloy electrocatalysts with controlled nanostructures. Using anisotropic platinum based materials such as nanowires or nanotubes, increased stability is commonly observed[26, 38, 41-44] due to

13

the reduced surface energy of platinum in this morphology in comparison to nanoparticle form.

1.4 Nanostructured catalyst approaches

The aforementioned challenges with ORR electrocatalysts highlight the need to develop innovative material solutions. Three common approaches are taken through various research and development activities to simultaneously reduce platinum contents and increase stability (**Figure 1-6**). These include the development of: (i) unique platinum nanoparticle supports, (ii) extended surface platinum alloy nanostructures, and (iii) non-platinum group metal (non-PGM) catalysts. This section will provide background information and a survey of currently available literature on each of these subjects. It is quite possible that advanced electrocatalyst solutions will comprise a combination of two or more of these approaches. Therefore intensive research efforts, such as those reported within this thesis, are highly warranted both independently and in tandem with each other.
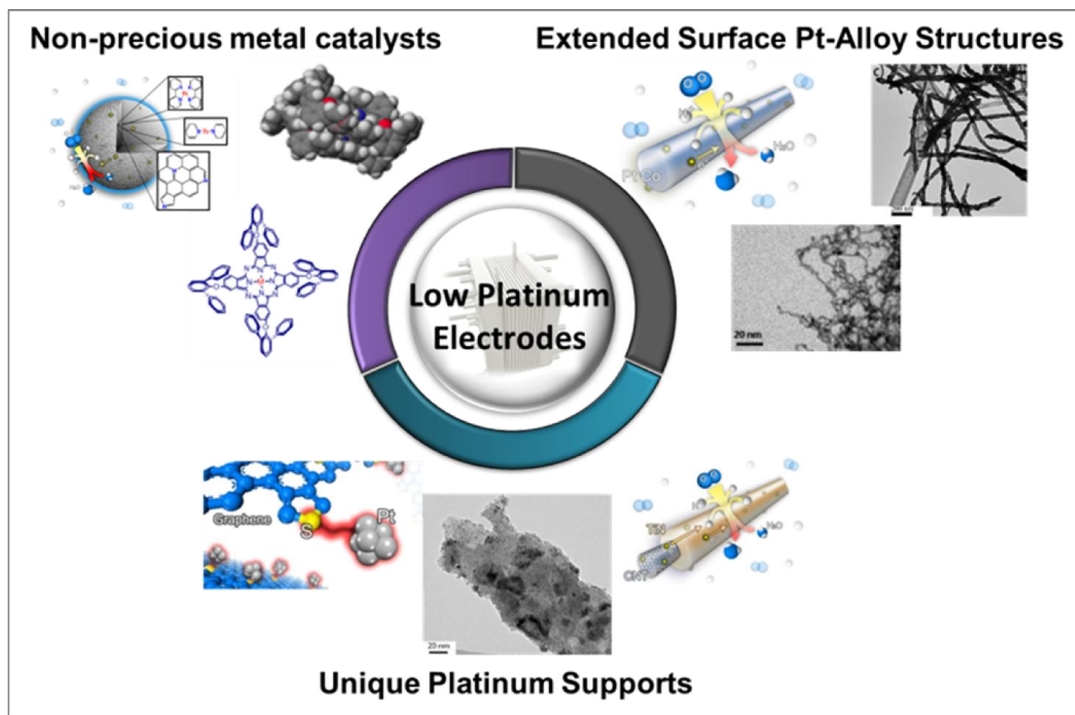
Figure 1-6: Schematic summary of the three primary approaches taken to develop reduced platinum catalyst and electrode structures. The assistance of Ja-Yeon Choi is gratefully acknowledged for his preparation of this (and many other) images.

1.4.1 Unique platinum nanoparticle supports

The selection of catalyst support materials can have a remarkable impact on the activity and durability of the resultant catalyst-support composites. An ideal catalyst support combined several properties, including: excellent electronic conductivity, high surface areas, electrochemical/corrosion resistance, favourable catalyst-support interactions and strong cohesive bonding to the catalyst nanoparticles.[45] The specific properties of the support will also affect interactions with the ionomer in the catalyst layer, along with impacting the resultant electrode architectures and properties. Beyond material selection, proper support nanostructure control to achieve favourable morphologies, three phase

15

boundary formation and mass transport conducive electrode architectures are of importance.[46] While there have been numerous investigations of unique support materials, the exact mechanistic nature of the impact on catalyst activity and stability is a subject of debate.

First, it is essential that the electrocatalyst support is able to provide good dispersion of uniformly sized nanoparticles. This is in order to achieve high utilization of the platinum materials and is directly influenced by the surface properties of the material being used. Platinum nanoparticle deposition is generally accomplished by a chemical reduction method, using a platinum salt (i.e. chloroplatinic acid hexahydrate) and a reducing agent such as ethylene glycol (EG) or sodium borohydride to form metallic platinum nanoparticles from platinum ion complexes.[17, 39] Surface anchoring sites are required to interact with the ions, followed by platinum nanoparticle nucleation and subsequent growth. It has been claimed that regions on carbon supports with π electron dense regions can serve as these anchoring sites.[47] The importance of appropriate surface species to act as anchoring sites has been successfully illustrated by several research groups, including our work in the case of nitrogen-doped carbon nanotubes.[17, 38] To this end, it was found that for undoped carbon nanotubes (CNTs), it was essential to functionalize them by a reflux technique using nitric acid in order to induce surface active species for successful platinum deposition. In the case of nitrogen doped carbon nanotubes however, no functionalization was required due to the presence of heteroatomic dopant species that could serve as anchoring sites.[17] Moreover, with increasing nitrogen sites, it was found that more uniform, well dispersed platinum nanoparticles could be achieved, which provided marked benefits in terms of

electrochemically active surface area availability and platinum utilization. This impact of catalyst support on morphology and dispersion of platinum nanoparticles is illustrated in **Figure 1-7**.
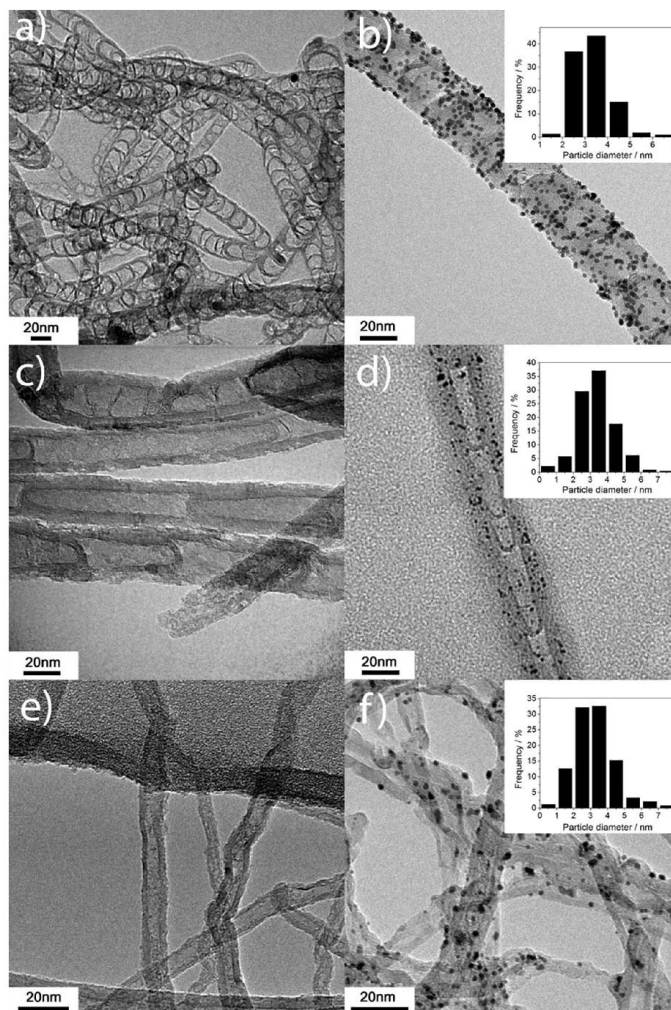
Figure 1-7: (a) Relatively high nitrogen content carbon nanotubes, (b) with platinum nanoparticles, (c) relatively low nitrogen content carbon nanotubes, (d) with platinum nanoparticles, (e) nitrogen free carbon nanotubes, (f) with platinum nanoparticles. The insets provide platinum nanoparticle size distributions, with reduced particle sizes, improved size uniformity, and better dispersion observed for materials with increasing nitrogen content. Reprinted with permission from [17]. Copyright 2010, American Chemical Society.

For well dispersed, uniformly sized platinum nanoparticles dispersed on various supports, there are several other factors that can influence the ORR activity and performance of these materials. These factors are primarily governed by the physicochemical properties of the support material and the corresponding interactions with the platinum nanoparticles. Primarily, these properties will modulate the electronic properties of the catalyst-support composites, altering the specific oxygen adsorption mechanisms, charge transfer characteristics and the reaction rate kinetics. These electronic modifications have been observed and reported by a variety of different analytical techniques including x-ray photoelectron spectroscopy (XPS), electron-spin resonance (ESR) and x-ray adsorption near-edge structure (XANES) characterization. For example, Lim et al.[48] prepared an array of TiO_2 nanotubes and deposited platinum on their surface by sputtering. Using XPS, they observed a 0.4 eV shift in the $Pt4f_{7/2}$ to higher binding energies of the Pt/TiO_2 sample in comparison with bulk platinum materials. The authors attributed this peak to the specific catalyst support-interactions, whereby the TiO_2 nanotubes can transfer electrons to the platinum, resulting in improved ORR rates. While it is very difficult to elucidate the exact nature of electron property modulation by the catalyst support interactions, it is clear throughout the literature that it can have a beneficial impact on the resulting electrochemical performance of catalyst materials.

As previously discussed, the current carbon supports used in Pt/C will not be sufficient to meet the demands of the PEFC market due significantly to stability limitations. The support material utilized has a significant impact on catalyst stability and therefore new and improved configurations require investigation. In order to address the issue of carbon

corrosion, materials with high electrochemical stability can be used including highly graphitic carbons (*i.e.,* carbon nanotubes or graphene)[38, 39, 49, 50] or transition metal oxides, nitrides or carbides.[16, 34, 35, 51-55] Selecting support materials that can combine excellent electrochemical stability during the harsh conditions encountered during PEFC operation with the other catalyst support requirements (i.e. electron conductivity, high surface area, etc.) can overcome the technical challenge of carbon corrosion.

Furthermore, the strength of the cohesive interaction between platinum and the support material will have a strong impact on the durability of the materials, hindering the occurrence of platinum dissolution, migration and agglomeration. It can be very difficult to predict the interaction strength between various support materials and the platinum nanoparticles, although some authors have resorted to computational studies in order to investigate this property. For example, Li *et al.*[56] found that the presence of nitrogen, or boron dopant atoms in carbon nanotubes could significant improve the adsorption strength and "tethering" of platinum nanoparticles in comparison to undoped carbon nanotubes. Expanding on this, several authors have successfully demonstrated improved durability of nitrogen doped carbon materials as platinum nanoparticle supports in comparison with similar, but undoped carbon support materials.[38, 57] Moreover, nitrogen doped carbon nanotubes with increased nitrogen contents retained higher electrochemically active surface areas (ECSAs) and hindered platinum nanoparticle agglomeration observed by TEM imaging of catalyst samples before and after half-cell accelerated durability testing (ADT).[38] Our group was also the first to ever report the use of sulfur-doped graphene as platinum catalyst supports[39, 50, 58] as shown in **Figure 1-8**. We found that, using

19

computational simulations liked with spectroscopic evidence, strong cohesive interactions would occur between sulfur dopants and the platinum nanoparticles.[39] This in turn led to unprecedented electrochemical stability of the resulting platinum/sulfur-doped graphene catalysts as measured by half-cell ADT protocols. Furthermore, the platinum mass activity of the newly developed catalysts was found to be 15% higher than that of commercial Pt/C, which was attributed to a shift in the d-band center of the platinum nanoparticles arising due to the electronic interactions with sulfur species.
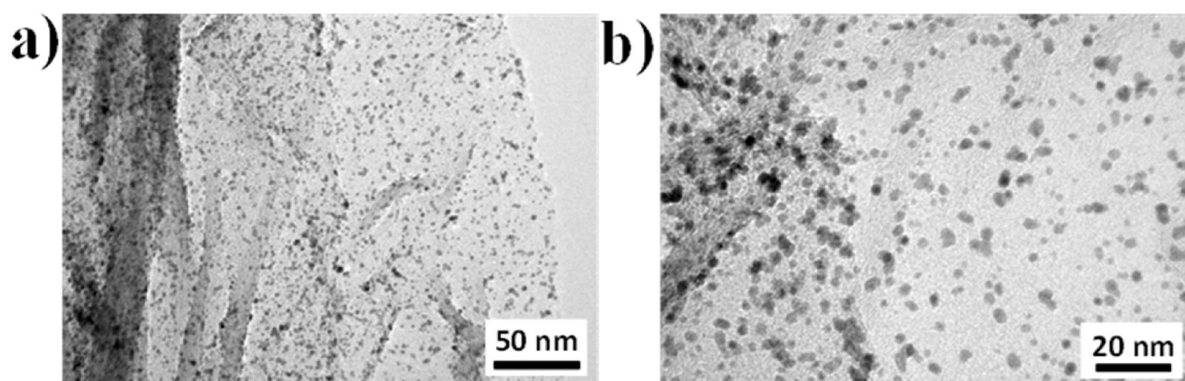
Figure 1-8: TEM images of platinum nanoparticles supported on sulfur-doped graphene. Reprinted from [39], with permission from Wiley.

Titanium dioxide materials have been considered promising as electrocatalyst supports because they can be synthesized by simplistic techniques, with highly variable and controllable nanostructures, and can moreover provide beneficial catalyst support-enhancements. For example, Huang et $al.$[35] synthesized mesoporous titanium dioxide using a templating technique. This Pt/TiO$_2$ composite obtained a maximum power density of 0.94 W/cm^2 in a single cell MEA, in comparison to 0.84 W/cm^2 for commercial Pt/C. The authors attributed this to the higher density of titanium dioxide, resulting in a thinner

catalyst layer than Pt/C with the same platinum loading. This thinner catalyst layer would then result in enhanced mass transport and higher catalyst utilization. Moreover, the durability was investigated by holding the cell potential at 1.2 V for varying time periods. After 200 hours, Pt/TiO$_2$ displayed only a negligible loss in performance, whereas commercial Pt/C los the majority of its performance after only 80 hours. The excellent stability of these materials was later confirmed further by these authors, employing a variety of accelerated stress and durability testing protocols.[34] Rajalakshmi et al.[59] prepared titanium dioxide nanoparticles by a sol-gel procedure and then deposited platinum on the surface using sodium borohydride as a reducing agent. While Pt/C demonstrated higher initial fuel cell performance, the Pt/TiO$_2$ materials provided promising stability capabilities through MEA cycling and durability testing.

Ultimately however, the poor inherent electronic conductivity of titanium dioxide may limit its practical applicability in PEFCs. To overcome this limitation, partially reduced Ti$_n$O$_{2n-1}$, also referred to as Magneli phase titanium oxide provides exemplary electronic conductivity, on the order of magnitude of carbon,[60] while retaining excellent electrochemical corrosion resistance.[61] To this end, Ioroi et al.[52] prepared Magneli phase supported Pt catalysts, which possessed very similar PEFC performance to that of commercial Pt/C, although significantly higher onset potential and lower magnitude of oxidation currents measured through cyclic voltammetry (CV) testing. This indicates the resiliency of these catalyst materials towards oxidation at elevated potentials. *Krishnan et al.*[62] prepared Magneli phase titanium oxide supported Pt, which was found to provide excellent electrochemical stability in the broad range of -0.25 to 2.75 V vs SHE; however

fuel cell performance was low in which the authors attributed to the low electronic conductivity of the specific phases synthesized and difficult preparing catalyst ink for MEA fabrication. It appears as if phase and morphology control are two important aspects of Magenli phase titanium oxide support developments. Interestingly, in a report published recently by Yao *et al.*[63], these researchers successfully prepared Ti_4O_7 fiber like nanostructures by a multi-step technique. First they fabricated titanium dioxide nanotubes, which were then coated with silicon oxide by a simple chemistry based procedure. Following that, conversion of the titanium dioxide to Ti_4O_7 was achieved by a high temperature (1050 ^{o}C) heat treatment in pure hydrogen, after which the silica shell was removed, preserving the one dimensional morphology. Upon deposition with platinum nanoparticles, Pt/Ti_4O_7 showed improved ORR kinetics through half-cell testing, along with dramatically improved stability following up to 3000 CV cycles from 0 to 1.4 V vs RHE.

1.4.2 Platinum alloy nanostructures

Parts of this section were reproduced in adapted form from [41], with permission of The Electrochemical Society.

D. C. Higgins, S. Ye, S. Knights and Z. Chen, "Highly Durable Platinum-Cobalt Nanowires by Microwave Irradiation as Oxygen Reduction Catalyst for PEM Fuel Cell" Electrochemical and Solid-State Letters, 2012, 15, B83-B85.

Alloying platinum based materials with other precious metals (Ru, Pd, etc.) or non-precious (Fe, Co, Ni, etc.) is a commonly reported approach in order to improve the

catalytic activity and stability. The latter configuration is favourable owing to the significantly lower cost of non-precious metals, with transition metals offering the most promising enhancements upon alloying. Alloying with inexpensive transition metals can effectively reduce platinum content in catalyst materials by replacing the platinum present in the core with alloying metals. Moreover, it has been consistently reported that alloying with transition metals can modulate the performance, providing specific activity and stability enhancements in comparison with pure platinum materials.[64, 65]

Numerous computational approaches and empirical investigations have been directed at gaining a theoretical understanding regarding the exact nature of performance enhancement. For example, Norskov *et al,.*[66] through computational calculations, highlighted that the electronic properties of the catalytically active platinum sites will govern the oxygen and hydroxyl bonding strengths. The corresponding ORR kinetics will be impacted by these adsorption energies, whereby if oxygen and hydroxyl are bonding too strongly, charge and proton transfer are impossible and the ORR will not proceed. Incorporating alloying transition metals into the materials can modify the electronic properties of the platinum species and by extension modulate the adsorption energies of ORR reactants and intermediates, thereby enhancing ORR activity. It has been well established that the surface bonding energies of reactants and intermediates can be directly linked to the average energy of the d states residing on the catalytically active surface atoms.[65] This is generally referred to as the d-band center, and by appropriate modification of this value performance enhancements are observed. Verifying this, Stamenkovic *et al.*[65] carried out experiments on polycrystalline alloy films with the composition of Pt_3M, where

M = Ni, Co, Fe and Ti. They observed a volcano trend of increasing catalytic activities towards the ORR with decreasing d-band centers (red lines in **Figure 1.9**), which were correlated closely with density functional simulations (black lines in **Figure 1-9**) that took into account the impact of d-band center on catalyst adsorption properties and subsequent rates of charge transfer and reactions. Strasser *et al.*[67] explained the distinct causes of these electronic d-band shifts upon alloying, dividing it up into three separate contribution. The first included geometric effects, or surface strain that implies differences in the atomic spacing of surface atoms due to interactions from the underlying layers. The second is ligand effects, involving two dissimilar surface atoms in the vicinity of each other partaking in electronic charge transfer and causing shifts in the electronic properties. The third is ensemble effects, whereby two different elemental surface atoms, or ensembles of atoms provide their own distinct and complementary functional mechanism. In platinum alloy catalysts for the oxygen reduction, it is generally geometric and ligand effects that have provided performance enhancements for platinum alloy ORR catalysts.[67, 68]
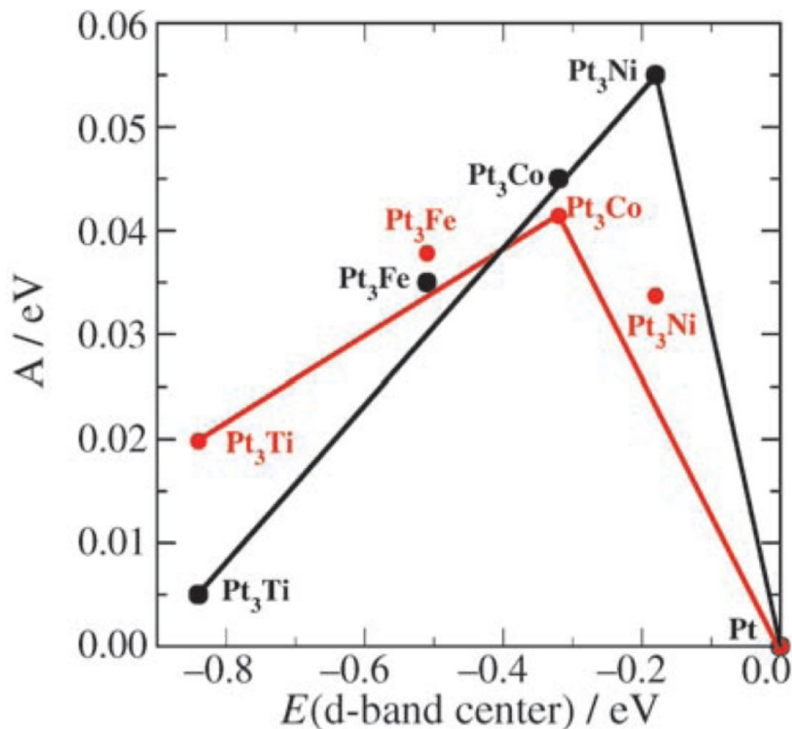
Figure 1-9: Catalytic activity versus d-band center position for pure Pt and a variety of Pt₃M alloys. Red line indicates results from experiments and black line indicates results from density functional theory simulations. Reprinted from [65], with permission from Wiley, copyright 2006.

During PEFC operation, dissolution of the transition metal components is a serious issue as the ions may transport through the catalyst layer and contaminate other component materials. Post treatment techniques applied to platinum alloy catalyst materials can be very effective at mitigating this occurrence by removing surface base metal species that are the most prone to leaching in PEFC systems. Acid washing[69, 70] or heat treatments in different environments[25, 53, 71] are the two most commonly reported techniques to accomplish this. Moreover, these post treatment techniques can also improve alloying, or provide atomic rearrangement in the alloy,[72, 73] where it is possible to segregate platinum near the surface

so it is accessible for the ORR, and the base metal in the core so it is less prone to leaching although can still have a beneficial impact on the ORR.[25]

With the issues associated with nanoparticle catalysts outlined, it is becoming increasingly clear that a fundamental shift from conventional zero-dimensional platinum nanoparticles to new catalyst designs and architectures may be necessary. This has been a focus of recent research endeavours.[74-79] One-dimensional platinum nanowire and nanotube composites have been investigated as ORR catalyst materials for fuel cell applications[27, 41, 50, 80-85] in an attempt to exploit the distinct advantages with respect to catalytic activity and stability arising from their unique morphology. The micrometer range length and unique morphology of one-dimensional nanostructure can provide high fuel cell performance and superior stability compared with commercial Pt/C (0D nanoparticles), primarily due to the anisotropic, self-supported nature. This can be attributed to: (i) high catalyst utilization due to enhanced reactant/product mass transport properties on nanowire configurations,[86] (ii) high surface aspect ratios,[87] (iii) lack of a carbon support eliminating the catalyst/support electron transport interface[88] and avoidance of carbon support corrosion, while (iv) their micrometer range length mitigates the occurrence of Pt dissolution and/or agglomeration when compared with high surface energy 0D Pt nanoparticles.[27] Commonly viewed as standalone catalyst materials, thereby eliminating the need for a carbon support and the impacts of corrosion, several researchers have also reported the fabrication of supported platinum nanowire catalysts[42, 43, 58, 85] by a simplistic room temperature techniques using formic acid as the platinum reducing agent. In terms of supportless platinum alloy nanowires and nanotubes, Chen e*t al.*[27] fabricated platinum and platinum palladium

nanotubes using a silver nanowire templating technique. These materials were found to provide both ORR activity and stability enhancements through half-cell testing in comparison to commercial Pt/C and platinum black. Zhang *et al.*[89] used a chemical based technique to synthesise ultra-thin PtFe nanowires. While the ORR activity of these materials was slightly lower than commercial Pt/C, following 1000 CV cycles, the ORR activity and ECSA retention of the PtFe nanowires was excellent, highlighting the promising durability of these materials. It should be noted however, that for the majority of platinum alloy nanowires and nanotubes reported in the literature, they are often synthesized by expensive and complex template-based procedures.[90-94] Furthermore, there is a lack of fundamental understanding regarding the impact of nanostructure control, alloying metal selection, atomic composition and atomic arrangement of platinum alloy nanowires that would provide immense benefits to the development of this class of electrocatalyst.

1.4.3 Non-platinum group metal catalysts

Parts of this section were reproduced in adapted form from [95], with permission from Wiley, and from [96], with permission from the Royal Society of Chemistry.

D. Higgins, Z. Chen, "Recent progress in non-precious metal catalysts for PEM fuel cell applications", *Canadian Journal of Chemical Engineering*, 91 (2013) 1881-1895.

Z. Chen, D. Higgins, A. Yu, L. Zhang, J. Zhang, "A Review on Non-precious Metal Electrocatalysts for PEM Fuel Cells", *Energy & Environmental Science*, 4 (2011) 3167-3192.

It would be ideal from a cost and manufacturing standpoint to completely replace platinum-based catalysts with non-platinum group metal (non-PGM) alternatives. Non-PGM research and development efforts have involved several different approaches, including the development of transition metal oxides, nitrides and/or carbides,[97-101] transition metal chalcogenides[102-106] and conductive polymers[107-110]. In terms of activity and stability, the most promising non-PGM catalysts have been a class of pyrolyzed transition metal-nitrogen-carbon complexes.[10, 96, 111-119] Despite their promise, these catalysts also have associated material challenges that must be addressed, or overcome by developing promising alternative non-PGM systems.

With the inherently minimal cost of non-PGM catalysts in comparison with platinum based materials, using very high catalyst loadings at the cathode is an economically viable approach. By extension, the activity of the relatively much thicker non-PGM catalyst layers (ca. 10 times thicker than Pt/C catalyst layers) have been traditionally evaluated on a volumetric basis as opposed to a precious metal loading basis. The DOE previously set volumetric activity targets of 300 Acm^{-3} at a PEFC voltage of 0.8 V (corrected for iR losses).[120] More recently however a shift in the fuel cell community has occurred, with more of an emphasis placed on areal performance owing to its more practical implications.[9] Catalyst activity on an areal basis (*i.e.,* working area of the electrode) is a product of several factors and can be defined as outlined in **Figure 1-10**. Ultimately, areal activity is a combination of the: (i) average active site turnover frequency (TOF), (ii) catalytically active site density, and (iii) catalyst layer utilization. Also shown in this Figure are three common approaches taken, focusing on each of the aforementioned

factors to improve overall activity. When evaluating the activity of non-PGM (or even platinum-based) electrode activity, cell voltages of 0.8 V are generally used. From a practical standpoint, non-PGM electrodes must also be capable of achieving high power densities at lower cell voltages, at which point catalyst layer utilization becomes an increasingly important consideration.

$$\underset{(A/cm^2_{elec})}{Activity} = \underset{(e^-/site.s)}{Turn\ over\ frequency} \times 1.6 \times 10^{-19} \times \underset{(site/cm^2_{elec})}{Areal\ active\ site\ density} \times \underset{(\%)}{Utilization}$$

		Specific active site $(site/cm^2_{cat})$	Catalyst surface area (cm^2_{cat}/cm^2_{elec})	
Kinetic activity		Active site size/distribution	Catalyst structure	Catalyst layer structure
	Active site optimization		Material Structure optimization	MEA optimization
	(1)		(2)	(3)
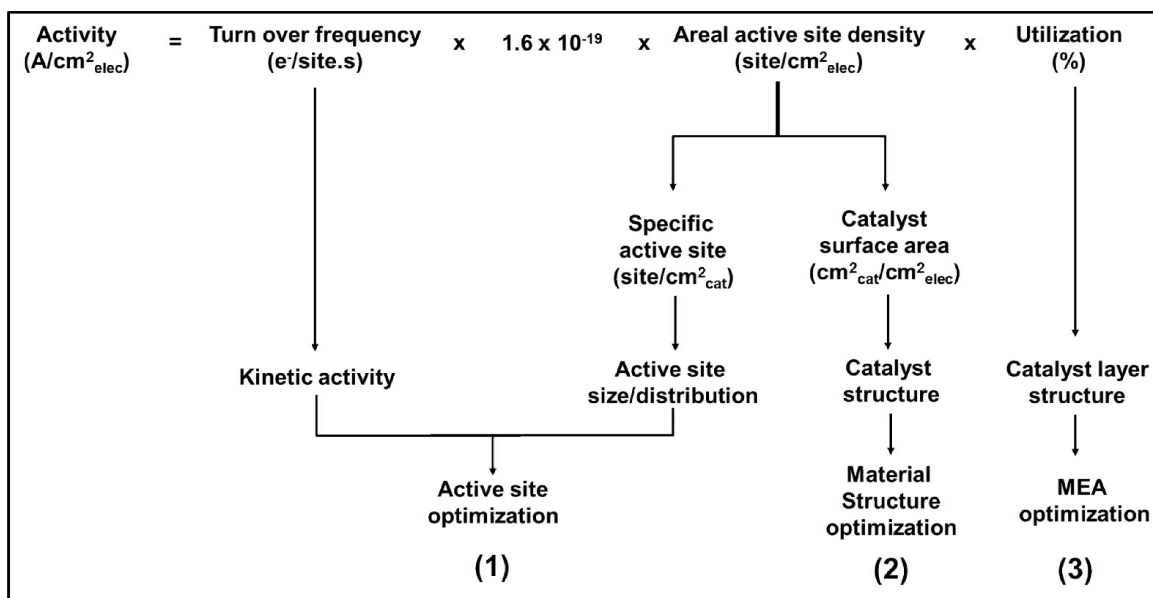
Figure 1-10: Practical approaches to improvements in non-PGM performance evaluated on an areal basis.

TOF relates to the number of electrons that are transferred at a single ORR active site per second. Catalyst TOFs are directly related to the kinetics of the ORR occurring at defined operating conditions, and are furthermore active site structure dependent, directly influenced by the exact nature and surrounding environment of the ORR active moieties present in the catalyst materials. For non-PGM catalysts, the average TOF takes into account all of the different active site structures that may be present in different forms and

quantities, possessing different site specific TOFs. The non-PGM catalyst active site density is a product of the concentration of active site structures per unit surface area, and the overall volumetric surface area of the catalyst materials. It is not dependent on the identity of the active site structure; however relies on the active site sizes, dispersion and overall catalyst morphologies. Dramatic improvements to non-PGM catalyst TOFs and active site densities have been realized over recent years by deliberate selection and modification of the particular synthesis and treatment techniques utilized. This has resulted in significant performance enhancements that have perpetuated non-PGM catalyst research and development efforts from a fundamental stage to its current status where it is considered extremely promising for practical PEFC applications, although still a long-term objective.[95, 96, 111, 121, 122] Limited operational stability is also a primary technical challenge facing non-PGM catalyst deployment,[10] owing to the harsh, oxidizing conditions encountered at the cathode of PEFCs during operation.

As mentioned previously, the most promising non-PGM catalysts to date are pyrolyzed transition metal-nitrogen-carbon complexes. This type of catalyst was first pioneered by Jasinski[123] who demonstrated that macrocyclic cobalt phtalocyanine (CoPc) was capable of facilitating the ORR in alkaline conditions. Years later, Alt *et al.*[124] expanded upon this study, demonstrating the potential of transition metal-N_4 chelates supported on carbon to facilitate the ORR in acidic solutions, albeit coupled with very limited stability. Through the years, many different transition metal macrocycle complexes have been investigated, including phtalocyanine and porphyrin structures, with a comprehensive review of the latter published recently to which the readers are referred for

detailed discussion.[125] It was eventually found that the stability limitations of these macrocycle cataysts could be effectively overcome by a heat treatment under inert environments at temperatures in the range of 400-1000 $^{\circ}$C.[126-128] These stability enhancements were furthermore accompanied by improved ORR activity of the pyrolyzed non-PGM catalysts, indicating that high temperature heat treatments induce favourable structural and atomic reconfigurations that have been the subject of extensive investigation and debate in the scientific community. Another breakthrough was realized by Gupta *et al.*[129] who demonstrated that non-PGM catalysts could be fabricated by the heat treatment of a simple mixture of carbon, nitrogen and transition metal sources. This provided significant economic advantages due to the relatively low cost of simple precursor materials in comparison with expensive macrocyclic complexes, along with providing a large degree of flexibility for non-PGM catalysts research and development efforts.

Although pyrolyzed transition metal-nitrogen-carbon catalysts are the best in class to date, a significant issue remains. This issue is the *lack of certainty regarding the exact active site structures* that are capable of facilitating the ORR. The elusive structural evolutions and morphological changes occurring during high temperature heat treatments lead to extremely heterogeneous structures with several different identities and phases of iron, carbon, nitrogen and sulfur species present,[130] as depicted in **Figure 1-11**. Coupled with limitations of existing structural and surface probing techniques, the exact identity and characterization of the particular ORR active moieties present in this class of catalyst material has been the subject of controversy in the literature. Specifically, several researchers insist that the ORR active site structures are metal-ion centered,[131-144] consisting

31

of either Fe or Co species coordinated by nitrogen species in various configurations and entrained in the matrix of the carbon support materials. Conversely, other researchers claim that the ORR active sites consist of carbon-nitrogen functionalities,[145-158] whereby the presence of transition metal species during NPMC synthesis is required only to catalyze the formation of these ORR active moieties. With a broad range of ORR active moieties proposed in the literature, it is highly likely that pyrolyzed NPMCs contain a variety of different active site structures, governed by the specific synthesis techniques employed (i.e. precursor selection, heat treatment conditions, post-treatment procedures). It is furthermore highly likely that each of these active site species is present in different amounts, possessing varying degrees of ORR activity; culminating in the overall sample dependent differences in NPMC activity observed at identical potentials.
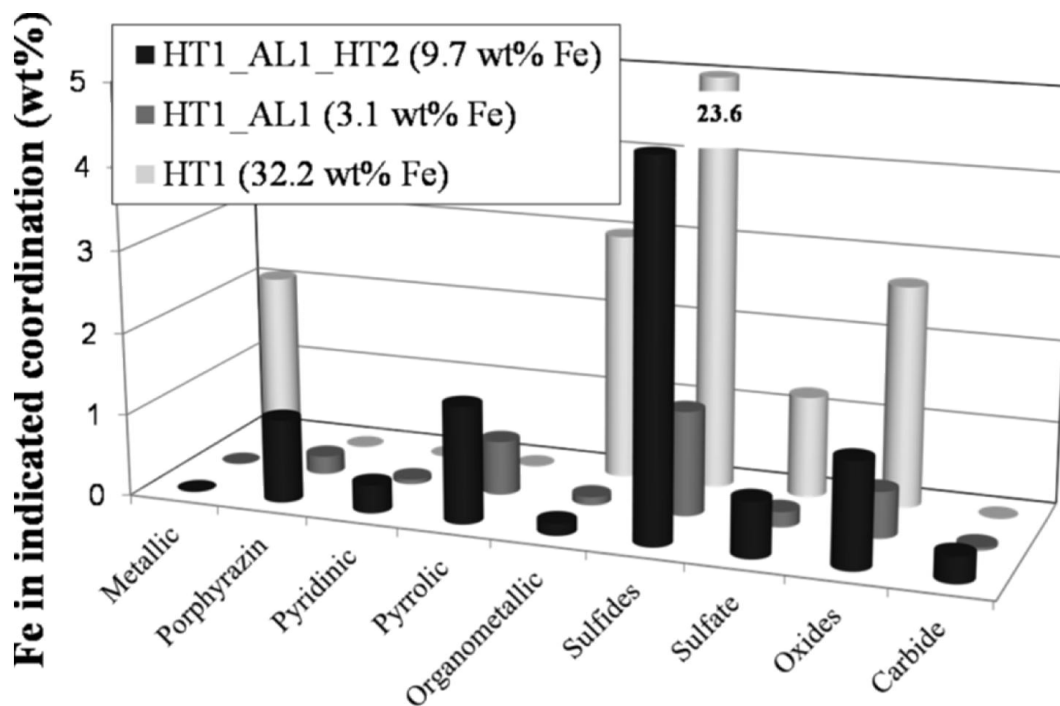
Figure 1-11: Bar graph depicting the weight percentage of different iron species in a polyaniline-iron-carbon derived catalyst at different stages of synthesis. HT refers to heat treatment, and AL refers to acid leaching. Reprinted from [130]. Copyright (2012) American Chemical Society.

It is therefore still prudent to investigate non-PGM catalysts that have well-defined active structures, so that researchers can employ a rational design approach, rather than the trial and error methods that have dominated pyrolyzed catalyst research for years. Transition metal chalcogenides are one group of ORR catalyst materials that can fulfill this criteria, and have been the subject of several studies in the last few decades. There are many reports about the high ORR catalytic activity of Mo-Ru-Se chalcogenide complexes, with performances approaching that of platinum.[159-166] However, Ru is considered a precious metal and its high cost and scarce availability hinder its potential application as

cathode catalysts in PEFCs. Thus, efforts have been directed at investigating non-precious transition metal chalcogenides, with some progress being made in recent years.

Behret *et al.*[102] initially demonstrated the potential application of non-precious transition metal chalcogenide materials as ORR electrocatalysts. These authors prepared various $M^{(a)}_z M^{(b)}_{3-z} X_4$ thiospinels, where $M^{(a)}$ = Mn, Fe, Co, Ni, Cu or Zn, $M^{(b)}$ = Ti, V, Cr, Fe, Co or Ni and X = S, Se or Te. A systematic study on ORR activity was carried out using these various thiospinels complexes in 2M H_2SO_4 vs a hydrogen electrode in the same solution. Co_3S_4 complexes synthesized by an aqueous precipitation reaction at moderate temperatures (~400-450°C) displayed the most promising ORR activity and performance with an open circuit voltage of ~800 mV vs RHE, and a current density of 20 mAcm^{-2} at 600 mV vs RHE. However, this activity was found to degrade rapidly when compared with other less active compounds synthesized at higher temperatures. Results from this investigation indicated that the ORR activity of the thiospinel compounds was directly related to the type of metal utilized, with an order of Co > Ni > Fe. Moreover, performance decrease was also observed when sulphur was partially replaced with O, Se or Te. This study provides insight into the activity of non-precious transition metal chalcogenides, initiating further investigations into these inexpensive materials as ORR catalysts several decades later.

This inspired theoretical investigations by Sidik *et al.*[167] in order to explain the exemplary activity of Co sulphide species, where three different Co_9S_8 surface structures were studied. It was determined that the partially OH covered surface of Co_9S_8 (202) should be active for ORR, with an onset potential of 0.74 V vs RHE. No investigations

were carried out with respect to ORR stability, thus experimental results would be needed in order to further characterize and optimize surface structures and properties. These interesting findings led to another similar theoretical investigation carried out on Co_9Se_8 phase structure, in an attempt to explain the inferior ORR activity of this complex compared with sulphur-based chalcogenides.[104] Results from this quantum computational approach indicated that Co_9Se_8 should in fact display a higher overpotential compared to Co_9S_8 (> 0.22 V), which was consistent with the experimental observations reported by Behret *et al.*[102] decades earlier. To supplement the theoretical investigation, the authors synthesized CoSe electrodes with unspecified stoichiometries by refluxing dicobalt octacarbonyl ($Co_2(CO)_8$) and selenium powder in a xylene solvent.[104] The synthesized compound displayed negligible ORR activity in 0.5 M H_2SO_4. However, after subjecting the CoSe complex to heat treatment at 900°C in an NH_3 environment, considerable ORR activity was observed, with an onset potential of 0.5 V vs RHE. While NH_3 pyrolysis of transition metals has been demonstrated to result in formation of active site structures (Section 2.2.4), in this study there is an absence of a carbon support to anchor these functional groups and XRD analysis indicated improved crystallization as opposed to ligand coordinated ion formation. Thus, the authors attributed this increase in ORR activity to the enhanced crystallization of nonstoichiometric CoSe as a result of heat treatment. The observed ORR activity however was still significantly lower than that of Pt-based electrodes.

At around the same time, Susac *et al.*[168] synthesized three thin films of CoSe with varying Co/Se ratios, using magnetic sputtering of different targets. For comparison, the

authors also developed an XC72 carbon supported CoSe powder (CoSe/C). The ORR activity of all materials was investigated in 0.1M H_2SO_4. Without any optimization to the surface structure or properties of the complexes, CoSe/C displayed an open circuit potential of 0.78 V vs RHE, slightly higher than the most active CoSe thin film (0.74 V vs RHE). CV was carried out on these materials, and the results indicated that after initial CV sweeps, some surface Co was leached out, leaving a chalcogen rich active surface. The authors proposed that the ORR active sites consisted of a Co deficient form of CoSe surrounded by chalcogen atoms. It was also noted, that during electrochemical testing, some Se-S exchange occurred between the surface of the thin films and the H_2SO_4 electrolyte, however the exact effects of this occurrence are still unknown. Due to the fundamental differences between the CoSe/C and Pt/C materials, specifically the unknown CoSe/C surface area, the authors argued that appropriate comparison with platinum based catalysts is obscured. The CoSe/C particles were also very large and non-uniform (ca. 10-100 nm) with numerous agglomerates observed, thus development of carbon supported CoSe nanoparticles with uniform size and proper dispersion could potentially increase the applicability of this class of catalyst.

A year later, Susac *et al.*[103] expanded on their investigations, preparing FeS_2 and $(Fe/Co)S_2$ thin films by a similar magnetic sputtering procedure. The synthesized FeS_2 thin films were found to display higher ORR activity compared to naturally occurring mineral FeS_2 (pyrite), which had previously been shown to possess ORR activity in acidic conditions.[169] The variation in ORR activity of these two materials was attributed to differing surface sulphur contents, however the exact mechanism of the activity

enhancement is still unknown. In addition, the ORR activity of the synthesized thin films were compared with the ORR activity of a thin film of Pt, allowing adequate comparison based on similar reaction surface areas. Unfortunately, this FeS_2 thin film displayed a much lower open circuit potential of 0.78 V vs RHE than that of the Pt electrode which had an open circuit potential of 1.02 V vs RHE. Moreover, in terms of catalytic current density at 0.6 V vs RHE, the Pt electrode had a current density three orders of magnitude larger than that of the FeS_2 electrode. In addition, the cobalt containing $(Fe/Co)S_2$ thin film displayed a slightly higher open circuit potential (0.8 V vs RHE) and enhanced catalytic current densities than that of FeS_2 thin film electrode. Despite performance still significantly lower than a Pt thin film electrode, this work indicated the possibility of combining transition metal species for improved ORR activity and performance. Whether the observed ORR enhancement arises due to a complementary reaction mechanism occurring between Fe and Co or simply due to the addition of Co sulphide species with a higher activity is unknown. Elucidating this relationship, along with investigating other binary transition metal catalysts could provide valuable information and progress towards the development of transition metal chalcogenide catalysts.

Feng *et al.*[105] used a Vulcan XC-72 carbon as a dispersing agent and support material in preparing Co_3S_4 and $CoSe_2$ carbon supported chalcogenides (Co_3S_4/C and $CoSe_2/C$, respectively). Co_3S_4/C (20% wt.) complexes were synthesized by three different reflux methods using cobalt carbonyl and sulphur dispersed in p-xylene, followed by a heat annealment at 250°C in pure nitrogen. The two samples synthesized by in-situ surfactant free methods displayed promising ORR activity with onset potentials of ~0.66-0.68 V vs

RHE in 0.5 M H_2SO_4. This activity was significantly higher than that of the third Co_3S_4/C material synthesized by a surfactant based method (onset potential of ~0.3 V vs RHE). This poor activity was attributed to the presence of surfactants blocking the ORR active sites. These materials were shown to have electrochemical stability below 0.8 V vs RHE,[170] however a later report by these authors suggested that these compounds were unstable under long term exposure to air, where phase conversion from Co_3S_4 to $CoSO_4$ was observed by XRD analysis.[171] In addition, the $CoSe_2$/C compounds developed in this study were also synthesized by a similar organic solvent based reflux procedure.[105] After slight modification of these materials, an onset potential of ~0.70 V vs RHE and an open circuit potential of 0.81 V vs RHE were observed through electrochemical testing.[172] These methods led to more uniform sized particles dispersed on the carbon support and minimal agglomerates observed compared with the work of Susac *et al.*;[168] however these particles were still relatively large (> 50 nm). Development of synthesis procedures to load carbon support materials with smaller transition metal chalcogenide nanoparticles with controlled surface morphologies and properties could provide valuable ORR activity enhancements and should be a focus of future investigations.

In summary, non-precious transition metal chalcogenides have displayed some promise as alternative catalyst materials for PEFCs, however ORR activity and electrochemical stability still requires improvements to meet practical targets. Therefore, developing novel non-precious chalcogenides (including new phases) along with the optimization of bulk and surface properties should be on the forefront of research in this area. The use of a carbon supports, such as doped graphene and carbon nanotubes could

also serve to improve the dispersion and reactive surface area of transition metal chalcogenide particles and is an attractive approach. Future work is still required directed at reducing particle sizes while enhancing their surface properties, particle morphologies and dispersion on the carbon support.

2. Thesis objectives and approach

The ultimate objective of this thesis is to develop and deliver new catalyst technologies that are capable of improving the performance of PEFCs, while simultaneously reducing the platinum loading. To accomplish this, a new strategy will be pursued that combines high activity platinum-based catalysts with non-PGM catalysts in a hybrid configuration. This new approach is being taken to investigate the feasibility of this configuration. The hypothesis is as follows. High activity platinum catalysts (either extended surface platinum-alloy nanostructures, or platinum deposited on unique catalyst supports) will be capable of reducing the activation potential loss of the PEFC (**Figure 2-1**, region A). This can be accomplished even at sufficiently low platinum loadings, provided the developed catalyst can provide increased activity in comparison to conventional Pt/C on a *platinum mass basis*. These high activity catalysts will be integrated with high surface area, non-PGM catalysts into new electrode configurations. Although the non-PGM catalysts will inherently possess lower intrinsic ORR activity in comparison to platinum, its primary contributions will be twofold. First, it will provide supplementary ORR active sites that will play a promotional role in achieving higher current densities at reduced electrode potentials (**Figure 2-1**, region B) that could not be achieved due to the low loading of platinum, as the electrochemical surface area of platinum as opposed to ORR kinetics will be the limiting factor under these conditions. Achieving high current densities and improved power output at these reduced cell voltages is very important for practical applications, such as fuel cell vehicles. The second role of the non-PGM catalyst is to provide a microstructure "scaffold" that is conducive to reactant transport through the

electrode, and provide excellent dispersion and connectivity of the high activity platinum materials throughout the catalyst layer.
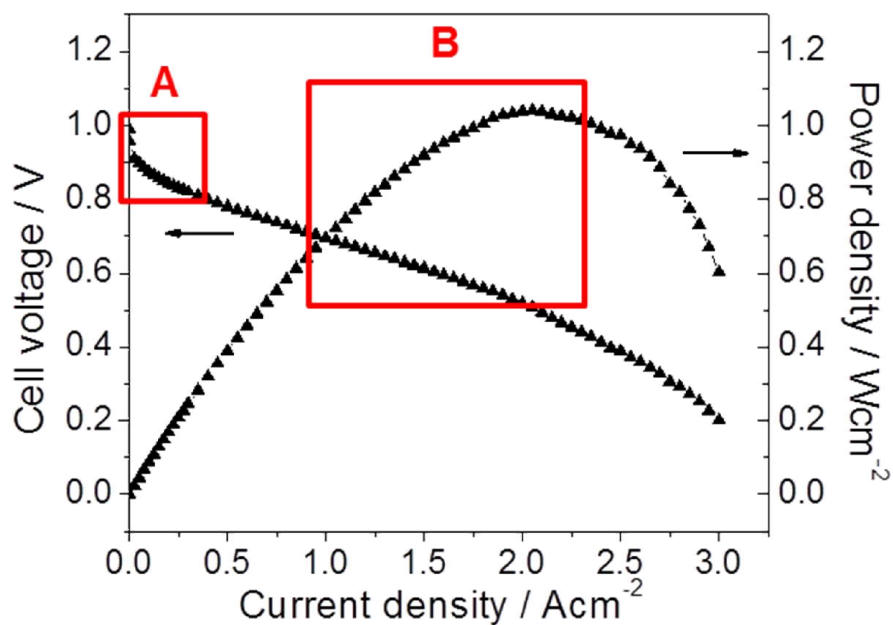
Figure 2-1: Typical PEFC polarization and power density curves showing the areas of primary contribution for high activity platinum catalyst (region A) and non-PGM catalyst (region B).

This thesis comprises the first important step of this long-term approach, and includes the design, development and optimization of novel ORR electrocatalysts. The specific objectives include:

- Design, development and optimization of unique platinum catalyst support materials, or nanostructured platinum alloy nanowire catalysts with high stability and improved ORR activity on a platinum mass basis in comparison to conventional Pt/C.

41

- Design and synthesis of non-PGM with well-defined active site structures and nanostructures conducive for excellent reactant transport through catalyst layers.

- Physicochemical and electrochemical characterization of developed materials, including analysis of ORR activity in acidic electrolytes and stability investigations involving accelerated durability testing protocols.

- Delivery of both high activity platinum and non-PGM catalyst technologies prepared by reliable and simplistic procedures for electrode integration and fuel cell performance investigations.

This project is iterative in nature and branches several important areas of electrocatalyst research and development. **Figure 2-2** depicts a simplified breakdown of the project tasks conducted throughout this thesis.
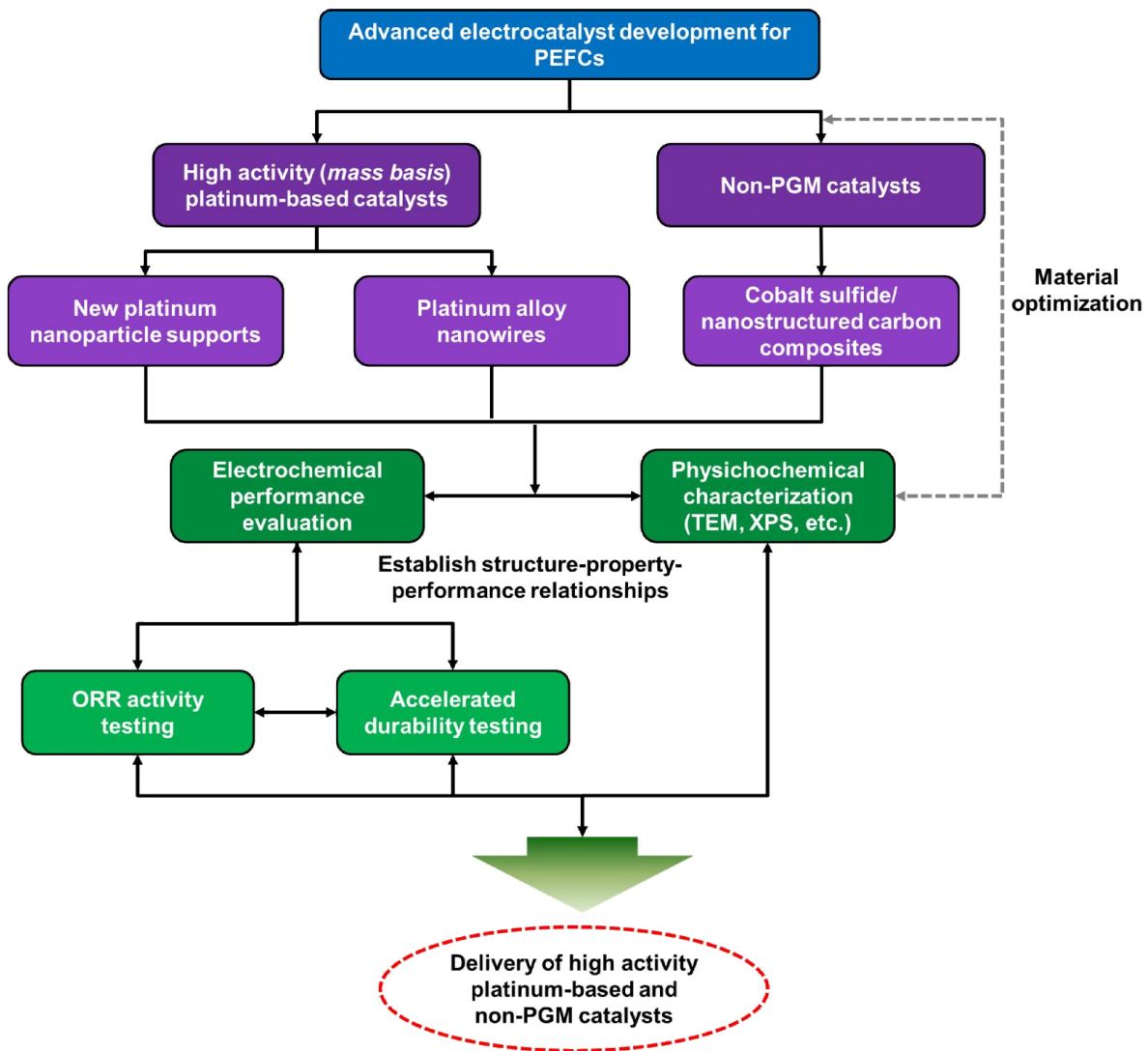
Figure 2-2: Schematic of the project work flow.

2.1 Thesis outline

As already seen, Chapter 1 consists of background information relevant to the thesis work and Chapter 2 provides a description of the overall project objectives and task organization. The preceding chapters will provide details, results and discussion about the specific work conducted throughout the entire project. Chapter 3 provides an introduction to the experimental procedures used throughout the project, with in depth details and task

specifics provided within subsequent chapters. Chapter 4 will introduce the reader to the development of unique titanium nitride coated carbon nanotubes and their use as platinum nanoparticle supports. Chapter 5 will highlight the development of platinum cobalt nanowires by a microwave assisted solvothermal technique. The structure and electrochemical activity of these materials are carefully elucidated, with further challenges clearly outlined. These challenges are addressed by the content of Chapter 6, which is the development of morphology and composition controlled platinum-cobalt nanowires by electrospinning. The electrospinning procedure is rigorously investigated, and performance capabilities of the resulting nanowires carefully elucidated. Chapter 7 focuses on the development of non-PGM catalysts, and in particular the development of graphene/carbon nanotube composite supported cobalt disulfide octahedral nanoparticles. The beneficial impact of the controlled surface structure of these nanoparticles, in addition to the effect of the nanostructured carbon support are carefully investigated and reported. Finally, Chapter 8 provides conclusions and summary of all the results reported within the thesis, along with recommendations for future work that can translate the progress made throughout this thesis into practical PEFC performance improvements.

3. Experimental methods and techniques

This section will provide general details and fundamental principles regarding the experimental techniques (synthesis, characterization, electrochemical evaluation) used throughout the thesis. For more specific details and experimental parameters, the reader should refer to the experimental section within the preceding Chapters.

3.1 Nanostructured catalyst synthesis

Throughout this thesis, several different techniques were used to prepare nanostructured catalyst materials. These techniques, to name a few, include wet chemical techniques (Chapter 4), microwave assisted solvothermal treatments (Chapter 5), electrospinning (Chapter 6) and solvothermal induced reduction and nanocrystal deposition (Chapter 7). An emphasis was placed on adopting and developing procedures that are simple, inexpensive, scalable and environmentally friendly. This ensures that the catalysts can be reliably prepared in sufficient quantities for subsequent electrode and MEA integration work. Please refer to the respective chapters for detailed descriptions of the synthesis and processing techniques used within those particular tasks.

3.2 Physichochemical characterization techniques

Developed electrocatalysts are extensively characterized by a variety of physichochemical techniques to understand the structure and property of the materials. The obtained insight is correlated to electrochemical performance evaluation to establish fundamental synthesis-structure-performance relationships that can be applied into the project feedback loop. In this way, elucidating the important factors governing

electrochemical properties and catalytic activity, improved catalysts can be rationally designed and synthesized. Details of the commonplace physicochemical characterization techniques used throughout this thesis are provided within this section.

3.2.1 Scanning electron microscopy

Scanning electron microscopy (SEM) is a powerful imaging tool used to investigate morphology and topological features of micro and nanostructured materials. It involves illuminating the sample with a powerful beam of electrons, and projecting images based on collected secondary or backscattered electrons.[173] The image resolution is similar to the size of the utilized electron beam and can be on a nanometer or micrometer scale. In the proposed project, SEM will be utilized to investigate the distinct nanostructures of the fabricated electrocatalyst materials. Preparation of samples for SEM imaging involves spreading the powder sample onto carbon tape that is secured to a sample holder stub. This stub can then be placed into the SEM machine, followed by evacuation of the sample chamber and subsequent imaging.

3.2.2 Transmission electron microscopy

Transition electron microscopy (TEM) allows high resolution imaging of samples on the nanometer scale, whereby high resolution TEM imaging can approach the atomic scale. Samples are illuminated by an electron beam with constant current density, generally produced by field emission techniques and passed through several condensers to focus it upon a very small site of interest. When the electrons come in contact with the sample, they will be scattered either elastically or inelastically and collected. Based on electron diffraction theory, the signals from the collected diffracted electrons can be processed in

order to produce an image. With such high resolution, TEM is effective in determining nanostructures, atomic arrangements, exposed crystal facets and defects within the structure. **Figure 1-5b** provided typical TEM images of commercial Pt/C catalyst.

3.2.3 Energy dispersive x-ray spectroscopy

Energy dispersive x-ray spectroscopy (EDX) capabilities are commonly incorporated into SEM and TEM devices, and can be carried out concurrently with common imaging techniques. EDX involves bombardment of electrons onto a materials surface which results in the emission of x-rays collected by a detector. The energy of the emitted x-rays and their corresponding intensity are characteristic of certain elements, allowing their appropriate identification and quantification in the sample being investigated. Elemental mapping is also an interesting technique that can be utilized and involves analyzing the x-rays emitted from localized positions on the sample. Variations in the emitted x-ray intensities will indicate variations in the specific atomic contents at those locations and can be used to map the concentration of different elements over the entirety of the sample being investigated.

3.2.4 X-ray diffraction

X-ray diffraction (XRD) is a prevalent characterization tool in materials science and engineering, used to identify materials upon comparison with diffraction pattern databases and to investigate particular crystal arrangements. X-ray beams are emitted from a source, and then interact with the atoms in the materials being investigated. As the x-rays have wavelengths similar to the distance between atoms in crystalline and polycrystalline samples, a diffraction pattern will occur characteristic of the present crystal phases. In the

present study, XRD is used to identify crystal phases, determine average platinum nanoparticle sizes and calculate the lattice spacing. For example, commercial Pt/C will display the characteristic fcc platinum diffraction peaks.

3.2.5 X-ray photoelectron spectroscopy

XPS is a surface specific characterization technique that allows probing of the composition and identity of atoms in the top ca. 0.5 to 5 nm of a sample.[174] The materials under investigation are exposed to x-ray photons with a known energy. These x-rays, upon interaction with the materials, will cause the emission of electrons. The emitted electrons are counted, along with their kinetic energies being measured. By determining the differences between the initial x-ray energies and those of of the emitted electrons, the electron binding energy within the materials can be determined. Electron binding energies are characteristic of several factors, including the type of atom, the chemical state and the empirical state that can be inferred from the obtained spectra. In the field of electrocatalysis, XPS is very commonly conducted on nitrogen-doped graphitic carbon structures, such as carbon nanotubes or graphene.[175-180] High resolution N1s (*i.e.,* nitrogen) spectra is commonly the most analyzed and interpreted component of the overall XPS signal. By deconvoluting the overall spectra into distinct contributions, the quantity of various nitrogen functionalities (*i.e.,* pyrollic, pyridinic, graphitic nitrogen) can be determined. This same approach is also very applicable to numerous other elements and bonding configurations.

3.3 Electrochemical characterization and performance evaluation

To understand the electrochemical properties and activity of the various catalyst technologies developed through this thesis work, different electrochemical characterization techniques were employed. This section provides an introduction and background information regarding these techniques. It should be noted that the ideal parameters for electrochemical testing (*i.e.*, electrode preparation technique, electrode loading, ionomer to catalyst contents, catalyst ink solvent type) are material specific. Therefore readers should refer to the appropriate chapters within this thesis for information regarding the preparation and testing parameters used for different catalysts.

3.3.1 Rotating disc electrode testing

Half-cell rotating disc electrode (RDE) testing is a well-established technique in order to screen the electrochemical activity of various catalyst materials.[181] It is ideal because it is simplistic and timely, allowing a high throughput of catalyst materials to be investigated. Half-cell testing uses an electrolyte filled electrochemical glass cell and three electrodes as shown in **Figure 3-1a**. Throughout the present project, 0.1 M $HClO_4$ was used as the electrolyte to simulate the acidic conditions encountered during PEFC operation at the cathode. The electrolyte is saturated with oxygen during ORR activity testing in order to ensure a consistent supply of oxygen for diagnostic purposes. The working electrode, also known as the RDE, is a glassy carbon disc, upon which the catalyst materials under investigation are deposited (**Figure 3-1b**). Working electrode preparation first consists of creating a catalyst ink by ultrasonically dispersing the catalyst materials in a solvent (*i.e.,* ethanol, methanol or isopropanol). This catalyst ink is then dropcasted onto the electrode

using a pipette, with the volume of ink deposited carefully controlled to achieve a desirable electrode loading. After drying, the entire electrode surface area should be uniformly coated with the catalyst materials. Nafion can either be incorporated directly into the catalyst ink, or deposited afterwards onto the prepared electrode. The role of Nafion through these experiments is to serve as both a binder and proton conducting ionomer. During testing, this electrode will be immersed into the oxygen saturated electrolyte solution. The potential is then swept in the ORR relevant range, and currents measured. A counter electrode is used to complete the circuit, and is generally either a platinum wire (for platinum catalyst investigations) or a graphite rod (for non-PGM experiments) immersed in the electrochemical cell. The third electrode is a reference electrode and allows for electrode potential measurement and control versus a standard electrode potential. Generally for acidic ORR evaluation, a Ag/AgCl, $Hg/HgSO_4$ or reversible hydrogen electrode (RHE) is utilized.
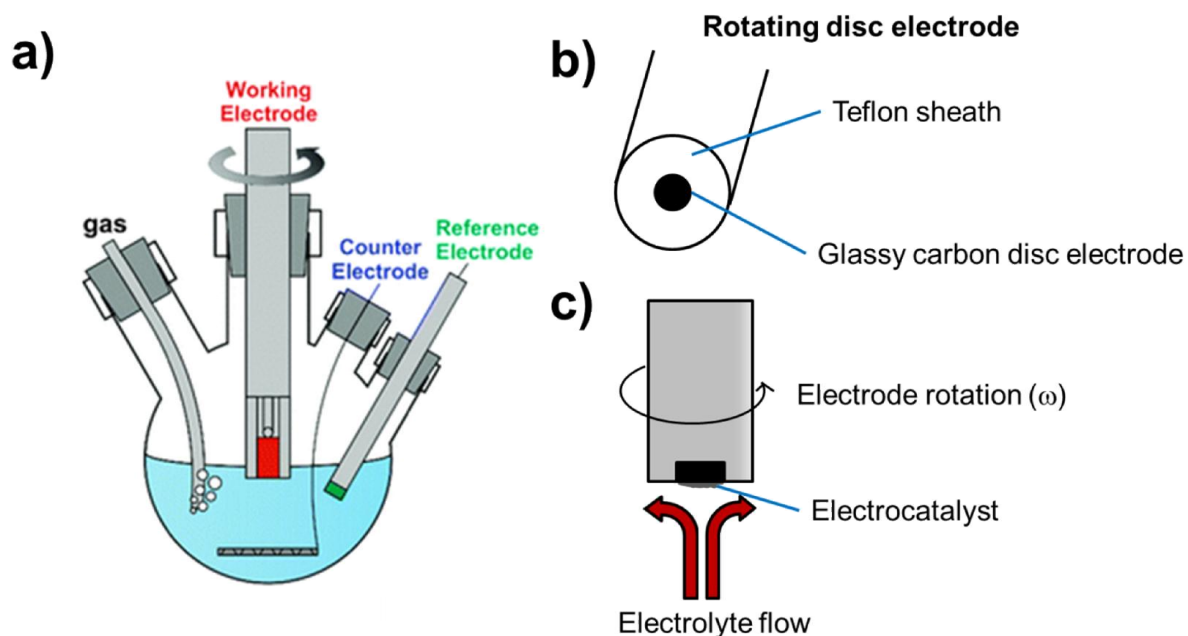
Figure 3-1: (a) Standard three electrode cell used for RDE measurements, reprinted in adapted form from [182], with permission from the Royal Society of Chemistry. (b) Rotating disc electrode upon which the catalyst is deposited, and (c) schematic of electrode rotation to induce convective electrolyte flow.

In a typical measurement of ORR activity, the potential of the electrode is swept from *ca*. 1.1 to 0 V *vs*. RHE at 10 mV/s, while measuring current under oxygen saturated electrolyte conditions. The electrode is continuously rotated (*i.e.,* at 900 rpm) to induce convective electrolyte flow that ensures a steady supply of oxygen saturated electrolyte to the catalyst layer (**Figure 3-1c**). Background (capacitive) currents obtained under nitrogen saturated conditions will be removed in order to only account for the Faradaic ORR. This will result in a typical ORR polarization curve as illustrated in **Figure 3-2a**. From this data, ORR electrokinetics occurring on the catalyst materials can be evaluated, whereby increased onset potentials for the ORR and higher current densities indicate improved activity. Platinum catalysts are generally evaluated based on their ORR activity (both on a

platinum mass and a surface area basis) at an electrode potential of 0.9 V *vs.* RHE. For non-PGM catalysts, the primary activity metric employed is referred to as the half-wave potential ($E_{1/2}$). This is the potential at which the current density reaches exactly half that of the mass transport limited current. Half-wave potential thereby provides indication of intrinsic ORR activity, along with mass transport and catalyst utilization in the electrode.

CV cycling under nitrogen saturated conditions is utilized to investigate the electrochemical signatures of catalyst materials under investigation. For platinum catalysts, ECSAs can be determined using this technique. To accomplish this, the electrode potential is cycled (*i.e.,* at 50 mV/s), resulting in a typical CV curve such as that illustrated in **Figure 3-2b**. ECSA values can be calculated using the hydrogen adsorption/desorption region observed below ca. 0.35 V vs RHE. In this figure, areas Q' and Q'' represent the charge transfer/current generated for the adsorption and desorption of hydrogen, respectively. The shaded region represents the capacitive current generated by the carbon support or in the catalyst materials. Catalyst ECSAs can then be calculated based on Equation 3-1:[17, 183, 184]

$$ECSA = \frac{Q}{mc} \qquad (3\text{-}1)$$

Here, Q is the charge transfer for hydrogen adsorption/desorption (mC/cm^2 electrode), m is the mass loading of platinum (mg$_{Pt}$/cm^2 electrode) and c is the charge required to oxidize a monolayer of hydrogen on a platinum surface (0.21 mC/cm$_{Pt}$^{2}). ECSA provides an indication of platinum accessibility/utilization in the catalyst and can also be utilized to calculate specific ORR activity (activity per unit of platinum surface area).
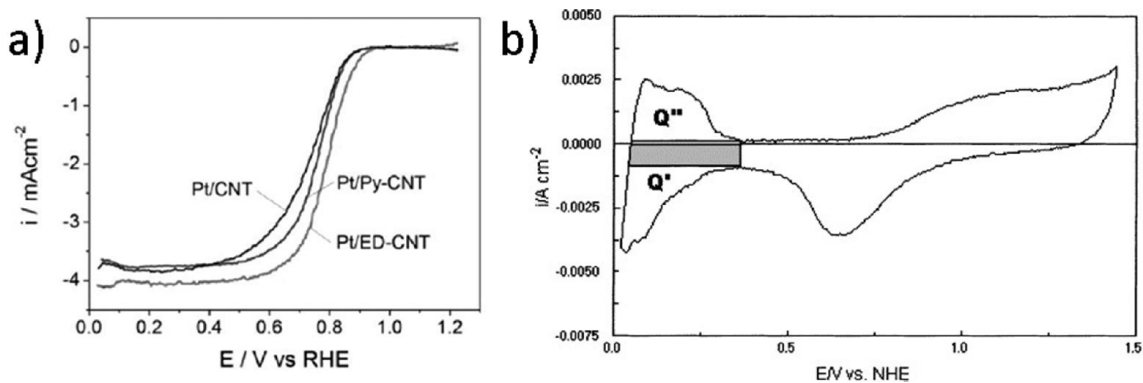
Figure 3-2: (a) Typical ORR polarization plot obtained from half-cell ORR activity investigations. Reprinted with permission from [17]. Copyright 2010, American Chemical Society. (b) Typical CV curve for platinum based materials, indicating areas used to calculate ECSA values. Reprinted from [184], Copyright 2002 with permission from Elsevier.

3.3.2 Half-cell accelerated durability testing

The durability of catalysts can be investigated by applying what is referred to as a half-cell ADT. These experiments are done using the same setup as that described in the previous section on rotating disc electrode testing. ADT protocols typically involve subjecting catalyst materials to repeated cycles (typically several thousand at least). These transient conditions will induce catalyst deactivation faster than what might be encountered under normal operative conditions. ORR activity, ECSAs and electrochemical signatures can be compared both before and after ADT. This will provide indication of the electrochemical stability of the developed catalysts, in addition to understanding the physical changes that may occur as a result of extended potential cycling. During a Department of Energy – Fuel Cell Technologies Office webinar, typical guidelines regarding experimental conditions that can be used for testing have been published.[185] Parameters can be modified during testing to simulate different conditions, or to induce

different catalytic degradation mechanisms. For example, higher electrode potentials will result in more rapid corrosion of carbon support materials, and a potential ranges that spans the oxidation/reduction platinum surface redox couple will result in accelerated platinum particle degradation. Many different ADT protocols are used throughout the literature, and conditions must be designed and applied according to the objectives of the current project.

4. Titanium nitride coated carbon nanotubes as platinum supports

This chapter is reprinted in adapted form from [16], with permission from the Royal Society of Chemistry.

D. C. Higgins, J.-Y. Choi, J. Wu, A. Lopez and Z. Chen, "Titanium nitride-carbon nanotube core-shell composites as effective electrocatalyst supports for low temperature fuel cells" Journal of Materials Chemistry, 2012, 22, 3727-3732.

4.1 Introduction

Platinum catalyst supports are utilized to achieve excellent dispersion of nanosized particles for the pertinent electrochemical reactions. For ORR electrocatalysis, it is well known that the activity and stability of platinum nanoparticle catalysts can be tuned by the specific type of support material used.[45, 186] Additionally, by using more corrosion resistant supports, the detrimental impact of carbon corrosion can be mitigated or even eliminated. numerous alternatives have been investigated including various carbon morphologies such as carbon nanotubes[187-189] and graphene,[190, 191] or transition metal based oxides, nitrides and oxynitrides.[35, 192, 193] Particularly, titanium nitride (TiN) has recently been investigated as electrocatalyst support materials for both the cathodic ORR[194] and anodic methanol oxidation reaction (MOR),[195-197] owing to its exemplary chemical and thermal resistance combined with high electronic conductivity. These investigations are generally limited to pure TiN in nanoparticle or thin film morphologies.

The present chapter highlights the development of novel coaxial TiN coated (CNTs) formed by a simplistic two step approach. In the first step, CNTs are utilized as a substrate

for the deposition of a layer of titanium dioxide (TiO_2) by refluxing the appropriate precursors. After annealing in argon, the second step involved heat treatment of the TiO_2 coated CNTs under flowing ammonia, resulting in TiN coated CNTs (TiN-CNTs) composites. These newly developed materials were used as electrocatalyst supports for PEFC applications by depositing platinum nanoparticles on their surface (Pt/TiN-CNTs). The advantages of using TiN-CNT nanocomposites as electrocatalyst supports for fuel cell reactions are immense. The CNT core structure can effectively provide interconnected electronically conductive pathways[198, 199] during fuel cell operation. They also possess a one-dimensional anisotropic morphology that has been shown to result in enhanced electron transport properties for electrocatalyst materials,[200] can serve to enhance mass transport properties[27] and can easily be arranged into porous, interconnected electrode structures.[201, 202] The TiN coating can further provide a protective barrier in order to hinder the rates of carbon corrosion during fuel cell operation and upon compositing with CNTs has also been shown to result in dramatically enhanced electronic properties compared with pure TiN.[203, 204] Moreover, and most notably, TiN has been found to offer advantageous catalyst-support interactions, including enhanced electrocatalytic activity,[194-197] along with markedly improved CO tolerance.[196, 197] Therefore, in the present study, coaxial TiN-CNT composites are developed in order to exploit the distinct advantages of utilizing this novel nanocomposite arrangement as electrocatalyst supports. Using these Pt/TiN-CNT materials, promising ORR performance and electrokinetics were observed, superior to state of the art carbon supported platinum (Pt/C) catalyst.

4.2 Specific materials and experimental methods

Carboxylic acid (0.5 %) functionalized CNTs were purchased from a commercial supplier for use in this study. The first step of TiN-CNT synthesis involved the deposition of a TiO_2 layer onto CNT substrates by a simple chemical method modified from a procedure reported previously.[205] Briefly, the commercial CNTs were refluxed in 6M HNO_3 solution for 5 hours to further oxidize the surface of the CNTs in order to provide facile precursor adsorption, remove any amorphous impurities and allow for easier dispersion in solution during processing. Following filtration and washing, 50 mg of the acid treated CNTs were ultrasonically dispersed in 60 mL of ethanol for several hours. The mixture was then transferred to a stir plate and 500 uL of titanium butoxide was added and allowed to mix constantly for approximately 30 minutes, upon which 500 uL of DDI water was added and allowed to mix for another 30 minutes. The entire mixture was then refluxed for 6 hours where deposition of the TiO_2 precursors occurred on the surface of the CNTs. After cooling, the products were filtered, washed and annealed under nitrogen protection at 400^oC for 4 hours. Heat treatment in ammonia gas was then carried out in order to allow the conversion of TiO_2 to TiN.[195, 203, 204] The temperature was ramped up to 800^oC over 45 minutes under nitrogen protection. After reaching the desired reaction temperature, ammonia was emitted to the system (100 sccm) where the reaction was carried out for 4 hours. After completion, the system was purged with nitrogen and allowed to cool and the TiN-CNT composites could be collected.

Pt nanoparticle deposition onto the surface of TiN-CNTs was carried out by the well-established EG reduction method.[48, 183, 188, 192] Specifically, TiN-CNTs were

ultrasonically dispersed in EG solvent, followed by the addition of the required amount of Pt (20 wt. %) in the form of a H_2PtCl_6/EG mixture (5 mg Pt/mL). Under constant stirring, a 2.5 M NaOH/EG solution was added to increase the pH of the solution to ca. 13 and then reduction was carried out by refluxing the solution at 140 ^{o}C for 3 hours. After cooling the mixture, 1M aqueous HCl solution was added to reduce the pH to ca. 5, followed by filtration and washing of the resulting products.

For testing, thermogravimetric analysis (TGA) was carried out under a steady flow of N_2/air (50/50), where the temperature was maintained at 60°C for thirty minutes in order to remove any water products followed by increasing the temperature from 60 to 900°C at a steady rate of 20 ^{o}C/min. All electrochemical characterization was carried out using a three neck glass cell using a CHI electrochemical workstation potentiostat and a Pine electrode rotator. A glassy carbon disk working electrode, platinum wire counter electrode and dual chamber Ag/AgCl reference electrode were utilized for all testing. Where appropriate, electrode potentials were converted to RHE for ease of comparison. Catalyst ink was prepared by mixing 4 mg of catalyst sample into 2 mL of an ethanol/water solution. The sample was ultrasonicated for one hour in order to ensure good dispersion, upon which a 20 uL aliquot was deposited onto the glassy carbon working electrode. After drying, 10 uL of a 0.05 wt. % Nafion solution was coated onto the electrode in order to ensure adequate adhesion of catalyst sample. CV and ORR testing were carried out in 0.1 M $HClO_4$. CV was carried out under nitrogen saturation between 0.05 and 1.25 V vs RHE at a scan rate of 50 mV/s and no electrode rotation. ORR linear potential sweeps were carried out under oxygen saturated electrolyte conditions at a scan rate of 10 mV/s at various electrode

rotation speeds (100, 400, 900 and 1600 rpm) in order to provide insight regarding the electrokinetics of the ORR occurring on the catalyst samples. Background currents obtained under nitrogen saturation were removed in order to eliminate capacitance and redox contributions.

4.3 Results and discussion

The structural evolutions occurring during synthesis of the TiN-CNT composite materials is summarized by the TEM images displayed in **Figure 4-1**. **Figure 4-1a** demonstrates the standard one-dimensional morphology of the acid treated CNTs utilized as substrates for TiN coating. The deposition of TiO_2 on the surface of the CNTs was found to be very uniform as displayed in **Figure 4-1b**, with some small portions of the CNT surface exposed. The polycrystalline TiO_2 shell structure was observed to have a thickness of ca. 15-30 nm. Following heat treatment in ammonia, **Figure 4-1c** displays the one-dimensional TiN-CNT coaxial core shell structure arrangement that is pertinent to this work. A distinct structural transformation was observed for the TiN-CNT composite materials resulting from the conversion of TiO_2 to TiN. The coating layer maintained its thickness and uniformity; however, it exhibited a polycrystalline morphology with larger crystallite sizes compared with the TiO_2 coating layer.
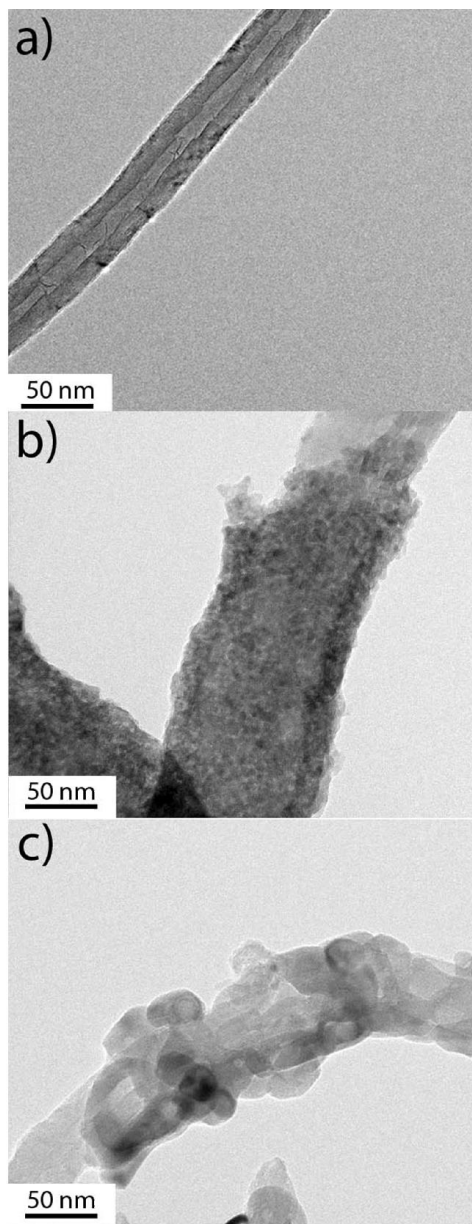
Figure 4-1: TEM images of (a) acid treated CNTs, (b) TiO$_2$-CNT and (c) TiN-CNT composite materials. Reproduced in adapted form from [16], with permission from the Royal Society of Chemistry.

XRD patterns were obtained to provide further insight regarding the structural transformations occurring during the material synthesis and are displayed in **Figure 4-2a**. TiO$_2$-CNT displayed characteristic TiO$_2$ peaks containing primarily the anatase phase, with

a diffraction pattern almost identical to that reported previously for similar materials.[205] After heat treatment in ammonia, conversion of TiO_2 to TiN is exclusively confirmed by the distinct shift observed in the diffraction patterns. The peaks are characteristic for TiN materials located at 2θ values of ca. 36.7, 42.7, 62.0, 74.8 and 78.0^o and can be attributed to the (111), (200), (220), (311) and (222) hexagonal TiN crystal phases, respectively. XRD also indicated preservation of the CNT core structure, where the sharp graphitic peak observed at 26° is maintained, corresponding to the (002) plane structure.
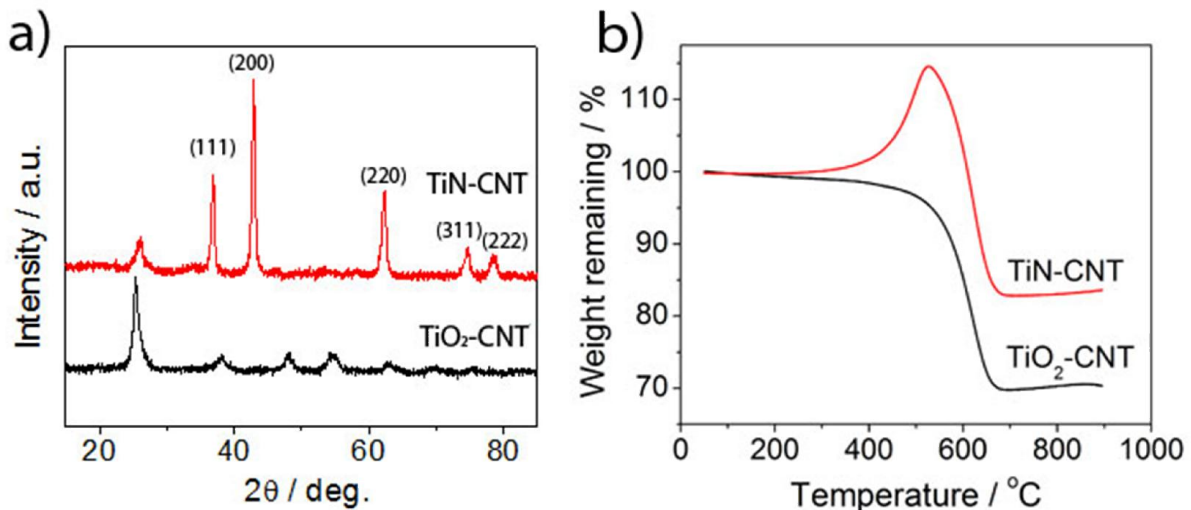
Figure 4-2: (a) XRD patterns and (b) TGA profile obtained for TiO_2-CNT and TiN-CNT composite materials. Reproduced in adapted form from [16], with permission from the Royal Society of Chemistry.

TGA profiles obtained for TiO_2-CNTs and TiN-CNTs and are displayed in **Figure 4-2b**. For the TiO_2-CNT materials, the TiO_2 shell was determined to comprise ca. 70 wt. % of the overall composite materials based on the residual mass from TGA testing. Assuming stoichiometric TiO_2, this represents a very high (> 90 %) product yield of titanium from the precursor solution, most likely attributed to the high concentration of CNTs present in the

reflux mixture and the high degree of functional groups on their surface to readily facilitate precursor adsorption. Mass loss was observed to occur beginning at ca. 350 $^{\circ}$C, attributed at first to combustion of any amorphous carbon species followed by the CNT core structures. The TGA profile of TiN-CNTs displayed a weight increase initiating at ca. 350 $^{\circ}$C and reaching a maximum of 114.6 wt. % at 525 $^{\circ}$C. This increase in weight can be directly attributed to the oxidation of TiN and is in direct agreement with previous reports.[206] The weight gain resulting from TiN oxidation is well below the theoretical value of 29.1 wt. % assuming complete conversion of stoichiometric TiN to TiO_2. Non-stoichiometric TiN and TiO_2 offers reasonable explanation for this observation along with the onset of CNT oxidation occurring at these excessive temperatures. The residual mass remaining after completion of the temperature ramping was higher for TiN-CNTs compared with TiO_2-CNTs, with 83.6 and 70.4 wt. % remaining, respectively. Non-stoichiometric TiN and TiO_2 will most likely contribute to this observation; however, it is most likely that the increased residual weight remaining for TiN-CNTs is due to the etching of carbon from the CNTs occurring during ammonia treatment.[33, 207]

Following Pt deposition by a modified ethylene glycol reduction method, TEM imaging (**Figure 4-3**) confirmed the successful deposition of well dispersed Pt nanoparticles with an average diameter of ca. 2.9 nm and the majority of nanoparticles possessing diameters between 1 and 4 nm. This positively indicates that the ethylene glycol method is effective for deposition onto TiN based supports; however, some larger Pt nanoparticle agglomerates were observed, possibly due to the lack of surface functional groups such as the ones on carbon based supports in order to facilitate Pt ion nucleation and

subsequent particle growth.[208, 209] The structural morphology of the TiN-CNTs is maintained, with Pt nanoparticles observed on the surface, along with Pt deposition onto the exposed CNT surfaces adjacent to the termination sites of the TiN coating.
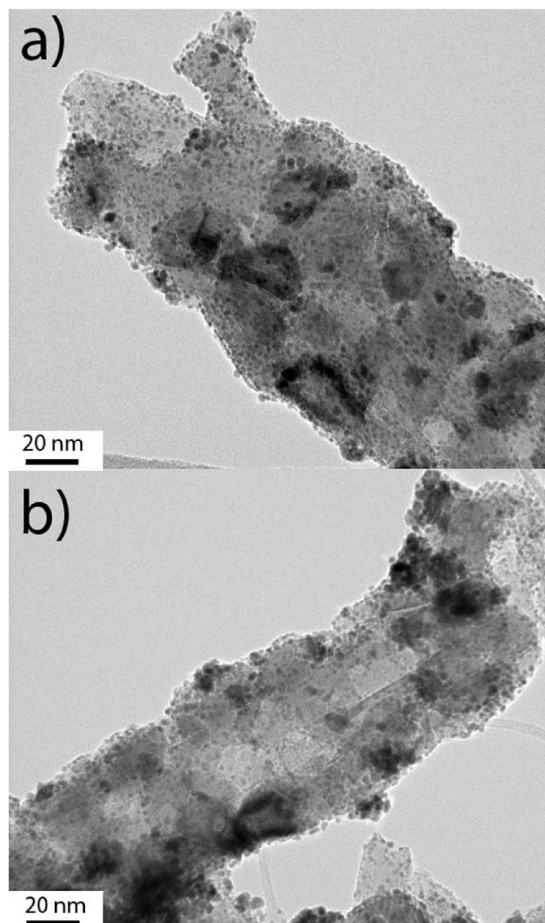
Figure 4-3: TEM images of Pt/TiN-CNT composite materials. Reproduced in adapted form from [16], with permission from the Royal Society of Chemistry.

CV curves are presented for Pt/TiN-CNTs along with state of the art commercial Pt/C for comparison in **Figure 4-4a**. As expected, both samples display the characteristic platinum oxidation/reduction peaks at higher electrode potentials and the hydrogen adsorption/desorption peaks at lower potentials. The charge transfer for hydrogen

desorption was used to calculate the ECSA of each material. Based on these calculations, the ECSA of Pt/TiN-CNT was found to be 109.75 m^2/g_{Pt}, comparable to 104.37 m^2/g_{Pt} determined for commercial Pt/C.
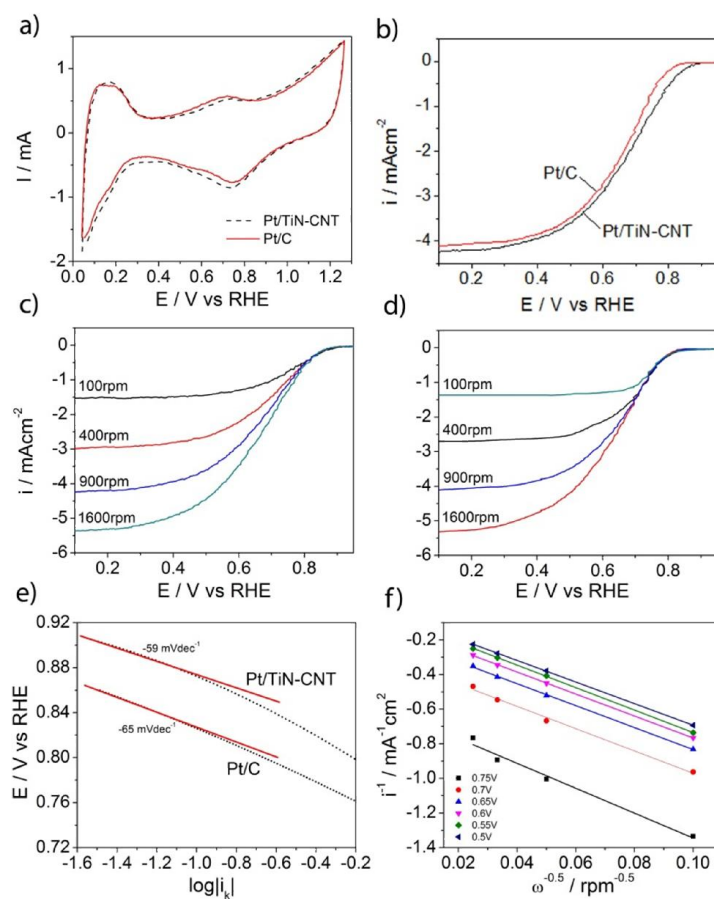
Figure 4-4: (a) CV curves for Pt/TiN-CNT and Pt/C obtained in 0.1 M HClO$_4$ at a scan rate of 50 mV/s under nitrogen saturation and (b) ORR polarization curves obtained at a scan rate of 10 mV/s and electrode rotation rate of 900rpm under oxygen saturation, with background currents obtained under nitrogen saturation removed. Polarization curves at various rotation rates for (c) Pt/TiN-CNT and (d) Pt/C. (e) Tafel plots for Pt/TiN-CNT and Pt/C (900rpm) and (f) Koutecky-Levich plots for Pt/TiN-CNTs at various potentials. Reproduced in adapted form from [16], with permission from the Royal Society of Chemistry.

64

ORR polarization curves obtained in oxygen saturated 0.1M HClO$_4$ are provided in **Figure 4-4b** comparing Pt/TiN-CNTs and commercial Pt/C, along with full polarization curves provided in **Figure 4-4c** and **4-4d**, respectively. It is apparent that utilizing TiN-CNTs as a catalyst support material enhances the ORR electrokinetics compared with the benchmark state of the art Pt/C electrocatalyst. Improved onset potential and current densities were obtained over the potential range investigated, with a slightly higher mass transport limited current observed. The latter can most likely be attributed to reduced peroxide byproducts released from the carbon support materials due to the TiN shell coating. This higher diffusion limited current density is in contrast to results reported previously indicating a lower diffusion limited current reported for Pt supported on TiN particles compared with Pt/C,[194] indicating a potential influence induced by the 1D anisotropic morphology of the TiN-CNTs, or a potential composite interaction with the highly graphitic CNT core supports. Regardless, the improved on-set potential obtained with TiN based catalyst supports is consistent with this previous report, rendering these materials as promising electrocatalyst support materials. Kinetic controlled current densities were determined and Tafel plots of Pt/TiN-CNTs and Pt/C are provided in **Figure 4-4e**. In the low current density region, Tafel slopes of -59 mV/dec and -65 mV/dec were observed for Pt/TiN-CNT and Pt/C respectively. This analysis indicates the enhanced ORR electrokinetics occurring on the surface of Pt/TiN-CNTs and the values obtained are very similar to the theoretical low current density Tafel slope of -60 mV/dec commonly reported for platinum materials.[210, 211] At higher current density values, a shift in the slope is observed to more negative values commonly attributed to altered adsorption isotherms and reaction mechanisms.[212, 213] **Figure 4-4f** exhibits Koutecky-Levich plots for Pt/TiN-CNTs

65

at various potentials in the mixed mass transport-kinetic current density regime. Parallel, linear behaviour is observed which confirms first order reaction kinetics with respect to oxygen concentration occurring on the Pt/TiN-CNT electrode.[214] It has however recently been demonstrated that upon immersion in acidic solutions and exposure to potential cycling over long periods of time the surface of TiN will be passivated, ultimately resulting in drastic performance loss.[215] It is unknown how this reported phenomena will behave under actual fuel cell conditions and remains to be investigated; however, this surface passivation is an implicit drawback of TiN based support materials that must be overcome in order to exploit their significant electrokinetic enhancements as ORR electrocatalyst supports.

The performance enhancement observed for Pt/TiN-CNTs can most likely be attributed to the specific properties of the TiN-CNT composites and the catalyst-support interactions present in these materials. The possible interactions occurring between TiN-CNTs and the active Pt nanoparticles remain elusive and further investigations are required; however, it has been proposed that there may exist a synergistic mechanism that occurs. In one instance, a shift in the electron binding energy of Pt supported on TiN species has been demonstrated by x-ray photoelectron spectroscopy.[195] These modified electron properties could potentially account for improvements in the electrokinetics observed on Pt/TiN-CNTs in comparison to commercial carbon supported Pt. It is also likely that the improved electronic properties obtained upon compositing TiN materials with CNTs, along with the distinct advantages of using electrocatalysts possessing unique, one dimensional morphologies will provide electrocatalytic improvements. While the exact nature of the

enhancements reported herein requires stringent investigations, the promise of utilizing TiN-CNTs as electrocatalyst support materials is apparent.

4.4 Conclusions

Unique TiN-CNT core-shell nanocomposites were developed by a simplistic fabrication procedure and were characterized by XRD, TGA and TEM techniques. These materials were then utilized at platinum nanoparticle supports for the ORR fuel cell reaction. Improved ORR activity was obtained for Pt/TiN-CNTs compared with commercial state of the art Pt/C electrocatalysts. These performance enhancements were attributed to the specific properties of the TiN-CNT nanocomposites, particularly their one-dimensional anisotropic morphology and improved electronic properties. In terms of activity, TiN-CNTs are presented as promising electrocatalyst support materials for low temperature fuel cell applications. A challenge however remains due to passivation of a thin surface layer of the titanium nitride. This thin layer of oxide species with poor intrinsic conductivity may serve to limit the electrochemical stability of these catalyst materials.

5. Microwave assisted solvothermal preparation of platinum cobalt nanowires

This chapter is reprinted in adapted form from [41], with permission of The Electrochemical Society.

D. C. Higgins, S. Ye, S. Knights and Z. Chen, "Highly Durable Platinum-Cobalt Nanowires by Microwave Irradiation as Oxygen Reduction Catalyst for PEM Fuel Cell" Electrochemical and Solid-State Letters, 2012, 15, B83-B85.

Parts of the introduction for this chapter is printed in adapted form from [83], with permission of Elsevier.

D. Higgins, R. Wang, A. Hoque, P. Zamani, S. Aburedcn, Z. Chen, "Morphology and composition controlled platinum-cobalt alloy nanowires prepared by electrospinning as oxygen reduction catalyst", *Nano Energy*, 10 (2014) 135-143.

5.1 Introduction

The occurrence of support corrosion for nanoparticle catalysts is well acknowledged,[37] and its implications such as those discussed in the previous chapter are detrimental to the practical application of these catalyst systems in PEFCs. To this end, one-dimensional (1D) Pt and Pt-alloy catalysts are considered promising cathode catalysts for PEFC technologies.[27, 43, 216-219] Increased activity is commonly observed on this new paradigm of nanostructured catalysts,[58, 220, 221] owing to the relatively smooth surfaces on the atomic scale that consist of Pt atoms with high coordination numbers. This effectively weakens the adsorption strengths of oxygen species on Pt, thereby reducing overpotentials

for the ORR. These smooth Pt surfaces also have reduced surface energies, rendering them less prone to activity loss by dissolution and agglomeration during PEFC operation; and their self-supported nature can eliminate the detrimental impact of carbon corrosion. Even further activity enhancements can be realized by effectively coupling 1D nanostructure control strategies with Pt-alloying using relatively inexpensive transition metals such as Fe, Co and Ni.[41, 89, 222, 223] Cobalt was used in the present work as the transition metal of choice. This is because polycrystalline platinum-cobalt alloys commonly outperform other platinum-transition metal combinations.[224] Traditionally however, Pt nanowires and nanotubes are synthesized by expensive and complex template-based procedures,[90-94] or require long processing times due to conventional heating methods.[225, 226] Furthermore, the activity and long-term stability of 1D Pt based materials has still not met the requirements for fuel cell application.

In the present work, we report a unique microwave assisted synthesis of 1D Pt-Co alloy nanowires (Pt-Co-NWs) for use as highly active, durable ORR electrocatalyst materials. This distinct approach allows for exploitation of the specific ORR activity and stability enhancements consistently demonstrated on Pt-Co alloys,[227-231] generally attributed to the modified structural and electronic properties arising due to the binary alloy nature of these materials. Furthermore, microwave-irradiation through dielectric heating provides a simple, rapid and energy efficient synthesis method [225, 232, 233]. The facile temperature controlled microwave heating method utilized herein provides a hard-template free synthesis procedure that is timely, inexpensive and provides uniform volumetric heating [234, 235], ideal for up-scalability to meet the demands of a potential fuel cell market. Notably, we

demonstrate that Pt-Co-NWs possess substantial ORR activity and exemplary stability through ADT in 0.1 M HClO$_4$.

5.2 Specific materials and experimental methods

Platinum acetylacetonate (0.001 mol) and cobalt carbonyl (0.001 mol) were completely dissolved in ethylenediamine solvent under nitrogen protection and transferred to an autoclave reactor where the reaction was carried out at 160°C for 1 hour with a maximum power setting of 600W. After completion, the Pt-Co-NWs were collected by filtration and washed thoroughly with DI water and ethanol, followed by annealing at 600°C in Ar for 1 hour.

Electrochemical testing was done by depositing Pt-Co-NW catalyst ink onto a glassy carbon rotating disk electrode. Testing and ADT was carried out in 0.1 M HClO$_4$, maintained at 50 ^{o}C. Commercial 20 wt. % platinum on Vulcan-XC (BASF, 0.1 mgcm^{-2}) and platinum black (Pt-B, Sigma-Aldrich, 0.2 mgcm^{-2}) were tested for comparison. ADT consisted of 1000 CV cycles (0 to 1.5 V vs RHE, 50 mVs^{-1}) in order to simulate the broad range of potentials that can be encountered at the cathode during transient PEFC operation. ORR and CV polarization curves were measured to determine catalytic activity and provide ECSA estimates based on hydrogen desorption charge transfer [236] before and after ADT, respectively.

5.3 Results and discussion

Formation of high purity 1D Pt-Co-NWs was confirmed by SEM) imaging (**Figure 5-1a, b**) and TEM imaging (**Figure 5-1c**). XRD patterns are presented in **Figure 5-1d**,

along with commercial Pt/C for comparison. As expected, commonly reported diffraction peaks for Pt-Co alloy materials were observed for Pt-Co-NWs, with a shift to higher reflection angles due to alloy formation and lattice contraction.[237]
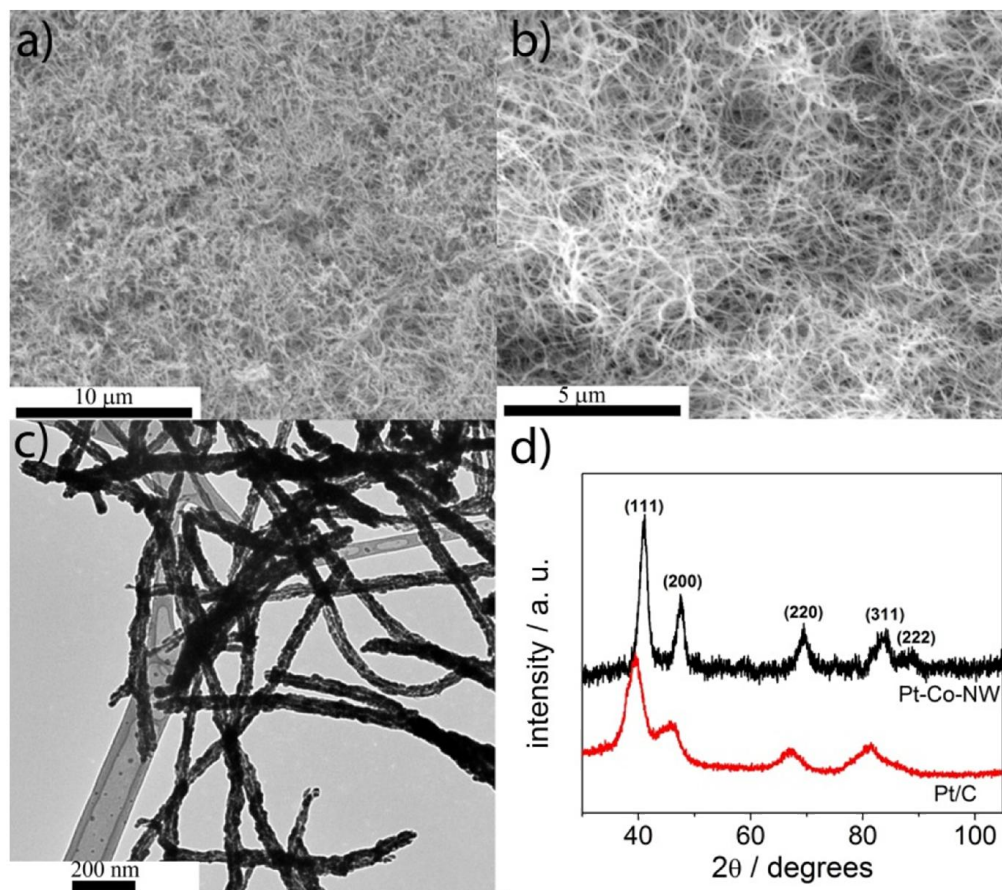
Figure 5-1: (a, b) Low resolution SEM and (c) TEM image for Pt-Co-NWs and (d) XRD pattern for Pt-Co-NWs and commercial Pt/C. Reprinted in adapted form from [41], with permission from the Electrochemical Society.

ORR polarization curves are provided in **Figure 5-2**. For Pt-Co-NWs, 200 CV cycles (0 to 1.2 V vs RHE) were applied prior to ECSA and ORR testing for catalyst conditioning, where a distinct increase in ORR performance occurred. This activity

increase was attributed to Pt-Co-NW activation, in which surface Co species were preferentially leached out, resulting in a Pt-rich surface phase.[72, 224, 238, 239] Pt-Co-NWs displayed high ORR activity and exemplary stability, where almost identical polarization curves were observed before and after ADT (**Figure 5-2a**). Conversely, Pt/C (**Figure 5-2b**) and Pt-B (**Figure 5-2c**), which was tested in addition to Pt-Co-NWs in order to eliminate the effects of carbon support corrosion, displayed significant ORR activity loss after ADT. Half-wave potentials and overall current density losses were observed at all electrode potentials investigated. It should be noted that diffusion limited current densities for Pt/C were lower than those of Pt-Co-NWs and Pt-B, most likely due to the existence of a 2 electron ORR occurring on carbon supported Pt catalysts[240] resulting in the formation of some hydrogen peroxide by-products. Pt-mass based kinetic current densities were calculated at an electrode potential of 0.85 V vs RHE (**Figure 5-2d**) in order to provide a gauge of the ORR activity of these materials. Pt/C initially demonstrated higher Pt mass based activity compared with Pt-Co-NWs and Pt-B due to the uniform size and high dispersion of Pt nanoparticles facilitated by the carbonaceous support. However, following ADT Pt-Co-NWs maintained their ORR activity, with a Pt mass based kinetic current density four times higher than that of Pt/C and over twenty times higher than Pt-B. Moreover, ECSA retention of the Pt-Co-NWs (59.5%) was superior to that of Pt/C and Pt-B, which retained 4.9% and 48.9% of their original ECSA, respectively. These results indicate that despite ECSA loss, Pt-Co-NWs maintained their ORR activity, indicative of an increase in their specific activity which could be attributed to the specific physical properties of the materials after ADT including surface chemistry, electronic properties, exposed crystal facets, etc.
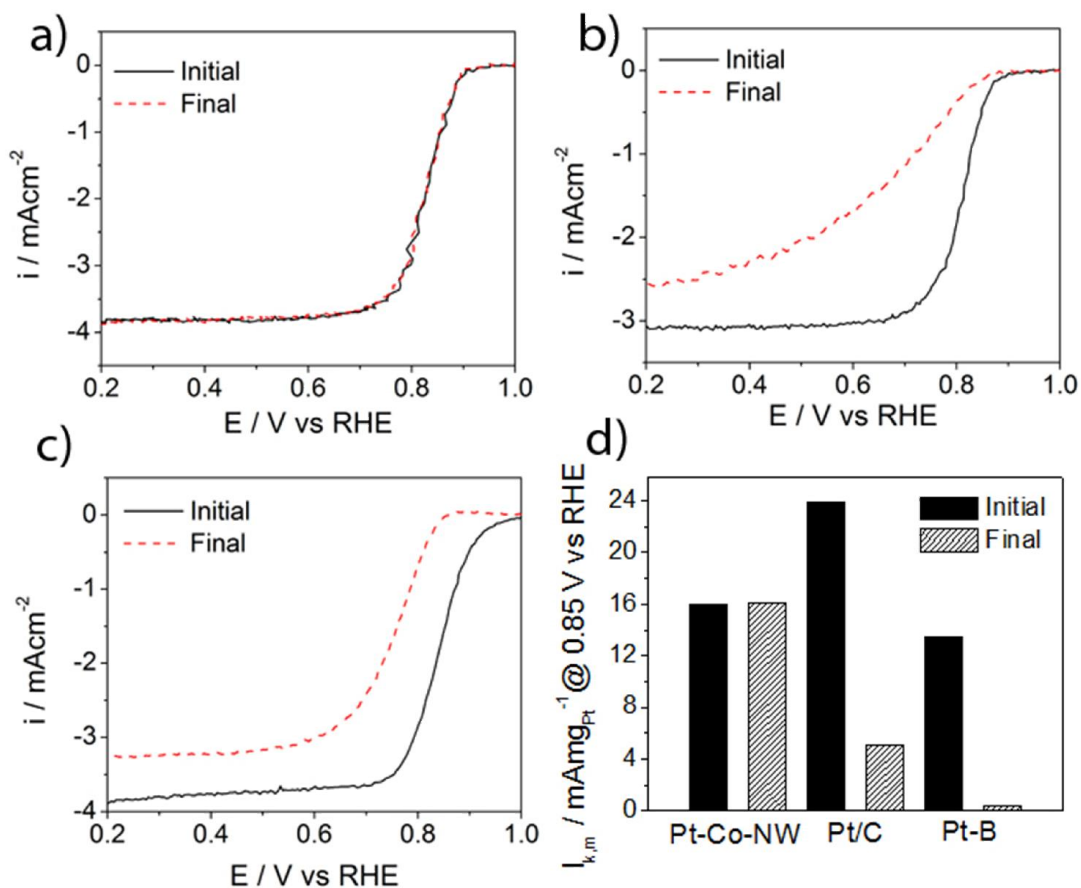
Figure 5-2: ORR current-potential curves prior to and after ADT obtained at a scan rate of 10 mVs⁻¹ and an electrode rotation of 900 rpm in oxygen saturated 0.1M HClO₄ for (a) Pt-Co-NW, (b) Pt/C and (c) Pt-B, (d) kinetic platinum mass-based current densities calculated at an electrode potential of 0.85 V vs RHE. Reprinted in adapted form from [41], with permission from the Electrochemical Society.

In order to provide insight regarding the exact nature of catalyst degradation, TEM images were obtained prior to and after ADT. Initially, Pt-Co-NWs (**Figure 5-3a**) displayed diameters in the range of 40-70 nm, with varying lengths. After ADT, Pt-Co-NWs (**Figure 5-3b**) displayed reduced nanowire diameters (25-45 nm). This could result from Co dissolution and moderate Pt loss, providing explanation for the ECSA decrease observed. By electron dispersive x-ray spectroscopy, the Pt:Co atomic ratio was found to change from

48:52 to 81:19 through catalyst conditioning and ADT. Thus, the increase in the specific activity of the Pt-Co-NWs is attributed to modification of the alloy's electronic structure, resulting in enhanced adsorption and catalytic properties induced by Co depletion.[224] High resolution TEM imaging and the corresponding electron diffraction pattern indicated that the crystallinity of the Pt-Co-NWs was preserved through ADT (not shown). Prior to ADT, Pt/C (**Figure 5-3c**) displayed relatively uniform Pt nanoparticles (ca. 2-3 nm), evenly dispersed on the carbon black support. After ADT, Pt nanoparticle agglomeration is apparent, with large, non-uniform Pt particles (ca. 9 nm) unevenly dispersed on the carbon support material. This is a commonly reported degradation mechanism for Pt/C,[6] attributed to Ostwald ripening and agglomeration due to surface-energy minimization. This phenomenon, coupled with carbon corrosion which is likely perpetuated at the high potentials encountered during ADT can contribute to the performance loss observed. Prior to ADT, relatively small (ca. 6 nm) uniform nanoparticles were observed for Pt-B (**Figure 5-3e**). After ADT, similar particle growth and agglomeration to Pt/C was observed (**Figure 5-3f**), providing reasonable explanation for the loss in ORR activity and ECSA displayed.
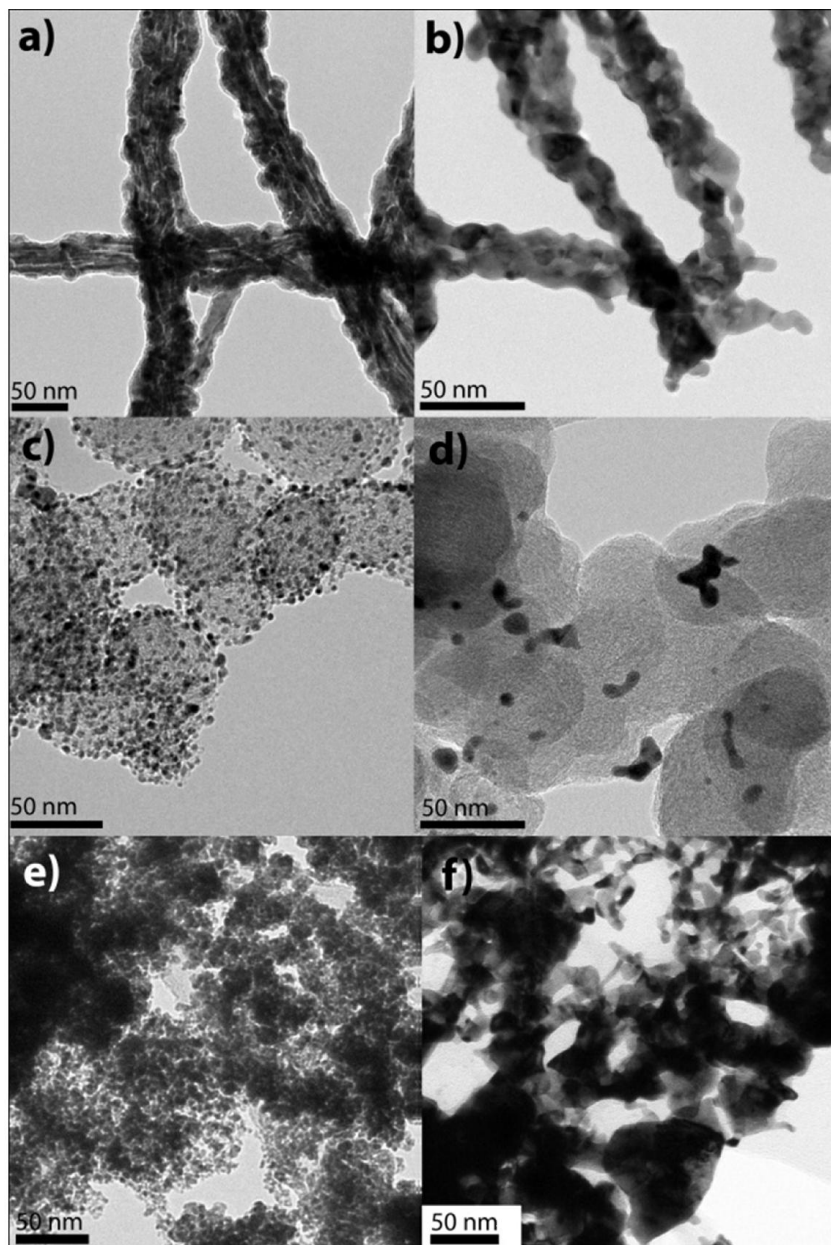
Figure 5-3: TEM images obtained (a, c, e) prior to and (b, d, f) after ADT for Pt-Co-NWs, Pt/C and Pt-B, respectively. Reprinted in adapted form from [41], with permission from the Electrochemical Society.

5.4 Conclusions

In summary, a simple, unique microwave based solvothermal procedure was employed for the inexpensive, timely synthesis of Pt-Co-NWs. These 1D Pt-Co-NW

demonstrated activity towards ORR through half-cell testing. Moreover, exemplary stability was demonstrated through ADT, where Pt-Co-NWs exhibited negligible ORR performance loss, rendering the stability of these materials superior to that of Pt/C and Pt-B. Thus, Pt-Co-NWs are presented as active, highly stable electrocatalyst nanostructures for potential replacement of Pt/C as cathode catalyst materials for fuel cell applications. Future investigations will focus on increasing the mass activity of Pt-Co-NWs to reduce cost, as the nanowires are relatively thick (40-70 nm) resulting in inaccessible platinum atoms within the bulk.

6. Morphology and composition controlled platinum cobalt nanowires by electrospinning

Please note, to differentiate these materials from the Pt-Co-NWs reported in the previous chapter, the platinum cobalt nanowires prepared by electrospinning are referred to as PtCoNWs.

This chapter is reprinted in adapted form from [83], with permission from Elsevier.

D. Higgins, R. Wang, A. Hoque, P. Zamani, S. Abureden, Z. Chen, "Morphology and composition controlled platinum-cobalt alloy nanowires prepared by electrospinning as oxygen reduction catalyst", *Nano Energy*, 10 (2014) 135-143.

6.1 Introduction

A fundamental shift from conventional zero-dimensional Pt nanoparticle based systems to new catalyst designs and architectures has been a focus of recent research endeavours.[74-79] In the previous chapter, platinum cobalt nanowires were developed using a microwave assisted solvothermal process. Despite promising activity and excellent electrochemical stability, this technique unfortunately provided very little versatility during synthesis, and resulted in relatively thick (ca. 40-70 nm) nanowires. Therefore, understanding, controlling and optimizing the exact structural and compositional factors underlying the performance of 1D Pt-alloy catalysts still remains a challenge,[241] yet holds promise to generate improved catalysts that can perpetuate the technological advancement of PEFC systems. Establishing reliable techniques in order to prepare Pt and Pt-alloy nanowires with readily controllable diameters and atomic compositions is desirable, and

would provide a versatile platform for both fundamental and practical investigations in order to develop unique catalyst systems with excellent activity and stability towards the ORR.

Electrospinning has been used as an effective technique to prepare a wide array of nanowire and nanofiber structures including metal oxides,[242] non-precious metal ORR catalysts[243, 244] and Pt-based materials.[70, 243] In the present study, using Co as the choice alloying element owing to the high activity of Pt_3Co surfaces towards the ORR,[245] we report the first development of PtCo nanowires (PtCoNW) by the electrospinning technique. PtCoNWs with near unity stoichiometric ratios were investigated for ORR activity by half-cell electrochemical evaluation, and were found to provide significantly improved Pt-mass and surface area specific activities in comparison to commercial Pt/C and pure PtNWs. Catalyst surface area retention of PtCoNWs during electrochemical cycling was also improved in comparison to commercial Pt/C, highlighting their promise as ORR electrocatalysts for PEFC applications. We furthermore demonstrate the versatility of the electrospinning process in order to prepare PtCoNWs with varying Pt:Co stoichiometric ratios and nanowire diameters, providing a valuable platform for future studies in order to elucidate and optimize the effects of 1D nanostructure, chemical composition and atomic distributions on ORR activity.

6.2 Specific materials and experimental methods

Platinum-cobalt nanowires (PtCoNW) were prepared by electrospinning a methanol/water solution of polyvinylpyrrolidone (PVP, MW = 1,300,000), hexachloroplatinic acid hexahydrate and cobalt acetate tetrahydrate. The use of cobalt

acetate tetrahydrate could also be substituted for cobalt nitrate with no changes observed to the nanofiber morphology. In a typical process, 34.9 mg of PVP was dissolved in 0.9 mL of methanol, and 18.75 mg of hexachloroplatinic acid hexahydrate and 8.15 mg of cobalt acetate tetrahydrate were dissolved in 0.1 mL of DDI water. These values correspond to a precursor solution containing 4 wt. % PVP, 3 wt. % metal salts, and a Pt to Co molar ratio of 53:47 that were used as the standard in the present study. It was necessary to use water as a co-solvent to eliminate precipitation of PVP in methanol solution upon addition of the metal precursor salts. The prepared DDI water solution was then added to the methanol/PVP solution, and the entire mixture was stirred magnetically for 1 hour. This solution was then loaded into a syringe with a stainless steel tip for subsequent electrospinning.

The electrospinning process was carried out inside an acrylic chamber, and in order to ensure successful nanofiber formation, it was necessary to decrease the relative humidity to below ca. 40% by introducing dry nitrogen gas. The syringe tip was stationed 6 cm from the aluminum foil collection substrate and the power source was set to 6 kV. The solution flow rate was set to 0. 25 mLh^{-1}, during which time a beige film formed on the aluminum foil surface. After completion, the electrospun film was peeled off the aluminum foil and loaded into a 0.5 inch diameter quartz tube. This tube was then loaded into a large tube furnace and the temperature was increased to 480 ^{o}C at a heating rate of 0.5 ^{o}Cmin^{-1}. After removal of PVP, the resultant black materials were collected, and subjected to hydrogen treatment in a tube furnace at 150 ^{o}C for 2 hours, and the resultant PtCoNWs were collected for subsequent characterization. Inductively coupled plasma (ICP) spectroscopy was

conducted using a Teledyne Leeman Labs Prodigy High Dispersion ICP system. Atomic concentrations were evaluated by digesting PtCoNW powder in an aqua regia solution. Measurements were done in triplicates, and the obtained spectra were calibrated with respect to two separate commercial standard solutions to ensure accuracy.

PtCoNW catalyst ink was prepared by mixing 3 mg of PtCoNWs and 3 mg of Vulcan XC-72 carbon black in 2 mL of ethanol containing 4 uL of 15 wt. % Nafion solution. 10 uL of the prepared catalyst ink solution was then deposited onto a polished glassy carbon disc electrode (geometric surface area of 0.19635 cm^{-2}) leading to a loading of 59.9 $ug_{Pt}cm^{-2}$, and allowed to completed dry under ambient conditions. The electrode was them immersed into 0.1 M $HClO_4$ maintained at 30 ^{o}C by a circulating water bath, and all electrochemical testing was carried out using a RHE. In order to evaluate ORR activity, the potential of the electrode was scanned at 10 mVs^{-1} in the positive direction under oxygen saturated electrolyte conditions and at electrode rotation rates varying from 100 to 1600 rpm. In order to remove capacitive contributions, background currents obtained under the same conditions except for with nitrogen saturation were removed, and the resultant ORR current densities were corrected for uncompensated electrolyte resistances using a technique reported previously [246]. ADT was conducted by repeatedly cycling the electrode potential from 0.05 to 1.3 V vs RHE at a scan rate of 50 mVs^{-1}. Commercial carbon supported platinum (Pt/C, TKK) was tested for comparison using an electrode loading of 20 $ug_{Pt}cm^{-2}$, a commonly utilized value for high surface area commercial Pt catalysts.[181]

6.3 Results and discussion

PtCoNWs were prepared by electrospinning a solution containing PVP as the carrier polymer, owing to its ability to complex with metal salt precursors. Several parameters can have an effect on the properties of the prepared nanowires. This includes properties of the precursor solution, including polymer concentration, metal species concentration, solution viscosity, and electronic conductivity; or preparation parameters, including electrospinning distance, applied voltage, humidity, needle tip gauge size and the solution flow rate. Some of these parameters were investigated through this study, whereas others (such as solution flow rate or needle gauge size) were found to not have a significant effect. To produce long, uniform nanofibers, the metal salt concentration was maintained at 3 wt. % and an optimal PVP concentration of 4 wt. % was determined systematically through SEM imaging of the prepared materials (**Figure 6-1**).
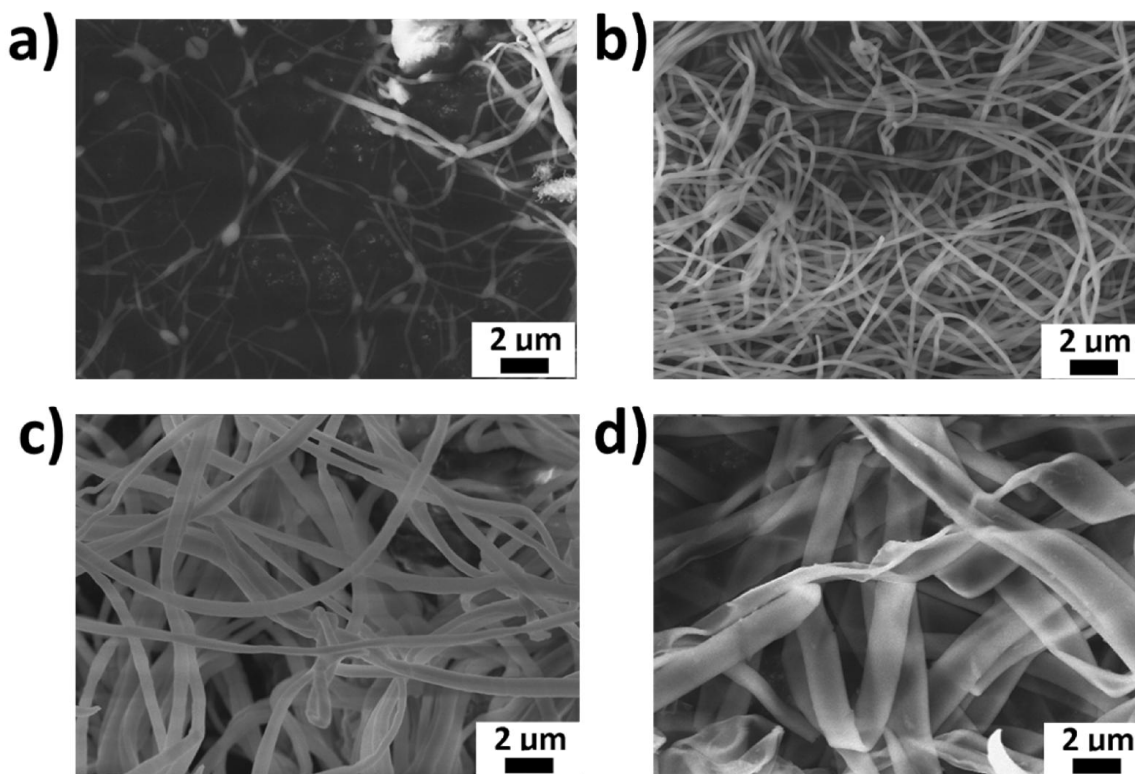
Figure 6-1: Effect of PVP concentration in the electrospinning solution. SEM images of PtCo-PVP nanofibers prepared with (a) 2, (b) 4, (c) 6 and (d) 10 wt. % PVP precursor solution. Reproduced in adapted form from [83], with permission from Elsevier.

We found that by varying the concentration of metal salts added into the solution between 1 and 5 wt. %, no changes to the as prepared PtCo-PVP nanofibers were observed (**Figure 6-2**); however after PVP removal, significant variations in the average PtCoNW diameters occurred (**Figure 6-3**). At 1 wt. % metal salt, no nanowires were obtained (not shown), indicating that the concentration of Pt and Co in the PtCo-PVP nanofibers was too low to achieve good interconnectivity during heat treatment. Increasing the metal salt concentration from 2 to 5 wt. % resulted in an increase in the average nanowire diameters from 24 to 41 nm, in a near linear fashion (**Figure 6-3c**, inset). Unless specified otherwise, as the standard for subsequent investigations, PtCoNWs were prepared with a metal salt

concentration of 3 wt. %, PVP concentration of 4 wt. % and a Pt:Co atomic ratio of 53:47. Additionally, a sufficiently slow rate of temperature increase (0.5 °C/min) for PVP removal was necessary, as higher rates of temperature increase would result in the nanowires melting together into 3-dimensional agglomerate structures (**Figure 6-4**).
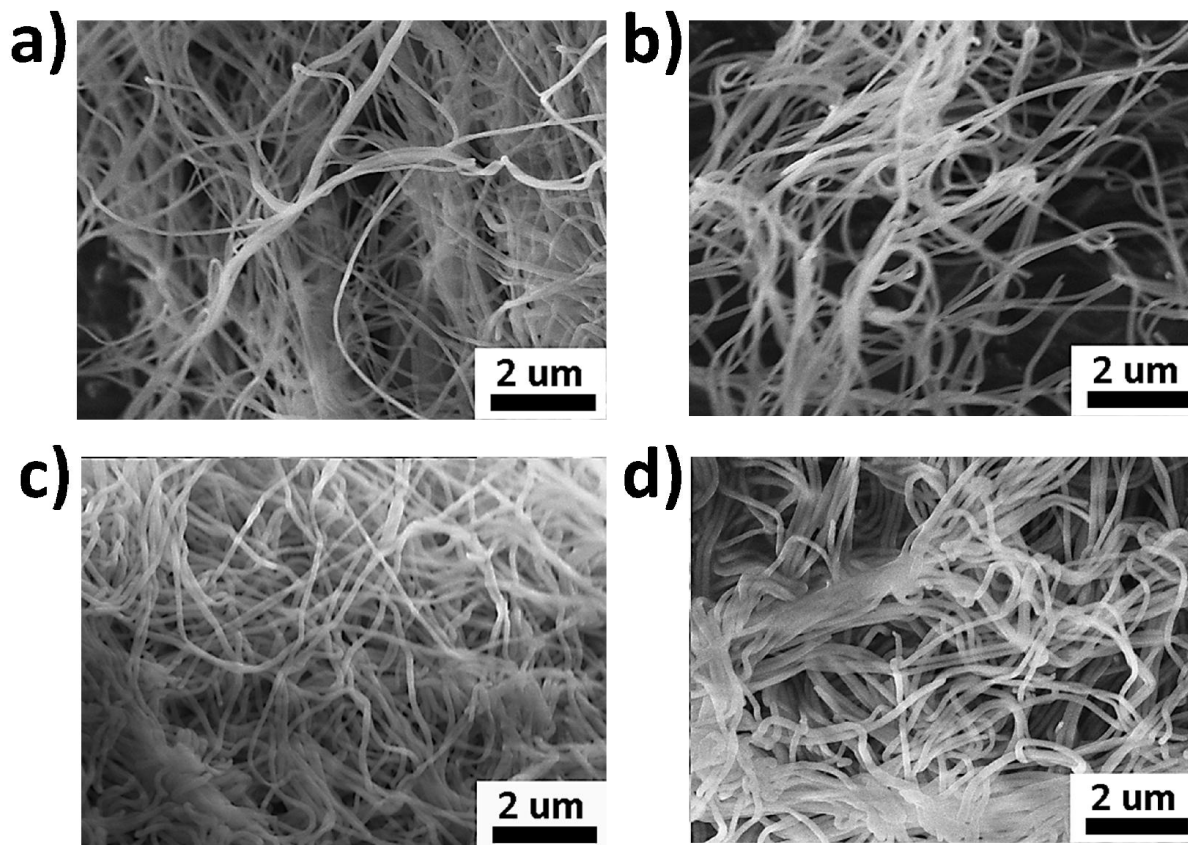
Figure 6-2: SEM images of PtCo-PVP nanofibers prepared with (a) 1, (b) 2, (c) 4 and (d) 5 wt. % metal salts in the precursor solution. For PtCo-PVP nanofibers electrospun with 3 wt. % metal salt precursor solution please refer to Figure 4b. Reproduced in adapted form from [83], with permission from Elsevier.
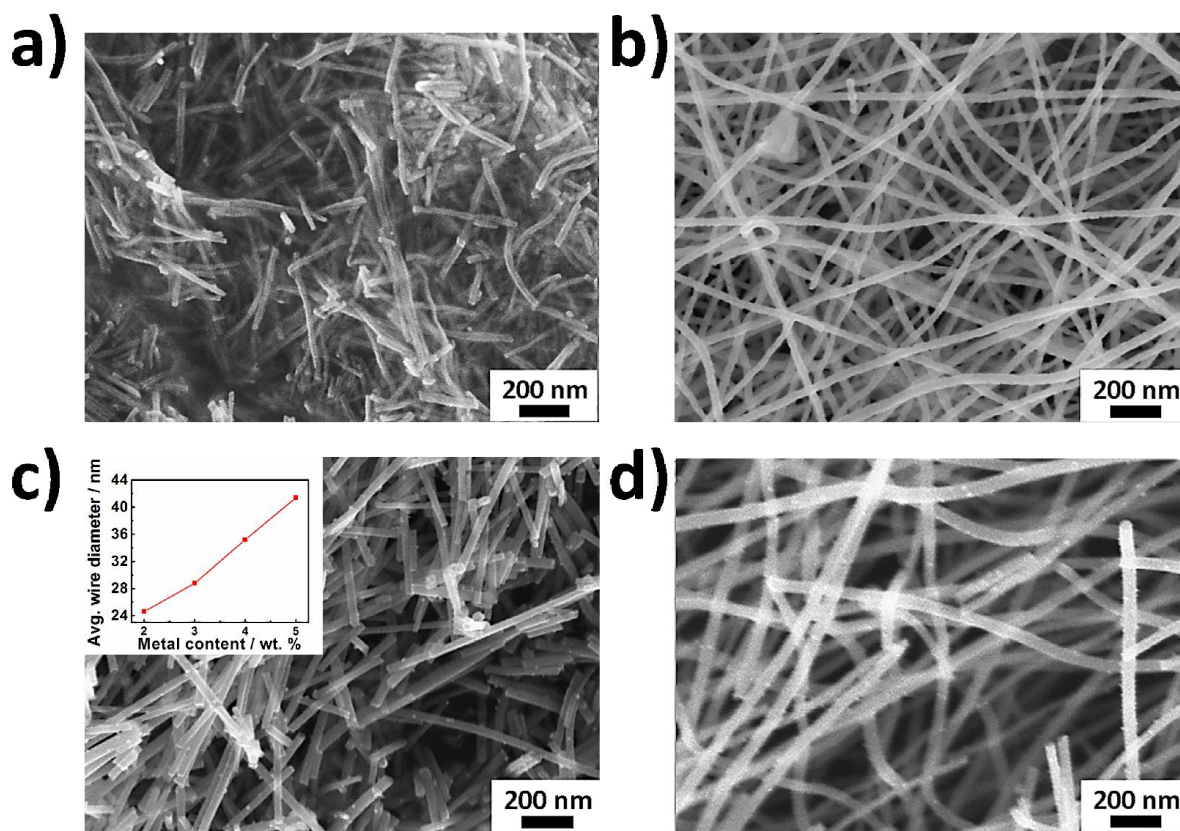
Figure 6-3: SEM images of PtCoNWs prepared using metal salt concentrations in the precursor solution of (a) 2, (b) 3, (c) 4 and (d) 5 wt. %. (c-inset) Plot of average nanowire diameter versus metal content of precursor solution. Reproduced in adapted form from [83], with permission from Elsevier.
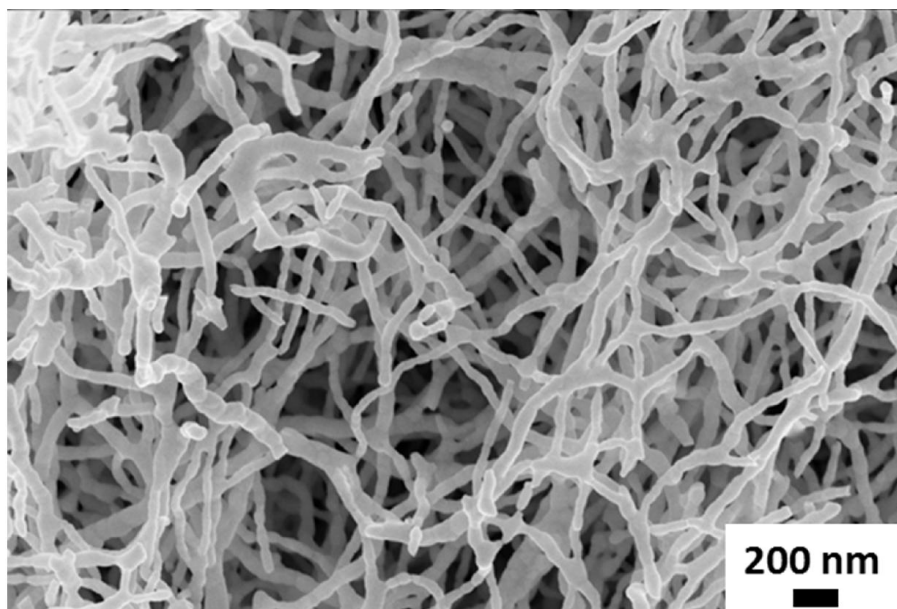
Figure 6-4: SEM image of PtCoNWs displaying a 3-dimensional agglomerated nanostructure resulting from using a heating rate of 5 ^{o}Cmin^{-1} in air during PVP removal. Reproduced in adapted form from [83], with permission from Elsevier.

TEM images of PtCoNWs after PVP removal and hydrogen reduction are displayed in **Figure 6-5a** and **b**. Nanowires with micrometer scale length and an average diameter of ca. 28 nm are clearly observed, and a polycrystalline structure was indicated by the select area electron diffraction (SAED) patterns (**Figure 6-5b**, inset) and high resolution TEM (**Figure 6-5c**). After PVP removal, both Pt (fcc) and Co_3O_4 (cubic) crystalline phases were observed by XRD (**Figure 6-5d**). After hydrogen treatment at 150 ^{o}C, disappearance of the Co_3O_4 peaks was observed and the Pt(fcc) peak locations were shifted to higher diffraction angles indicating the successful incorporation of Co into the Pt-alloy phase structure.[247, 248] Both Pt and Co were well distributed throughout the entirety of the PtCoNWs evidenced by electrode dispersive x-ray (EDX) colour mapping (**Figure 6-5e**).
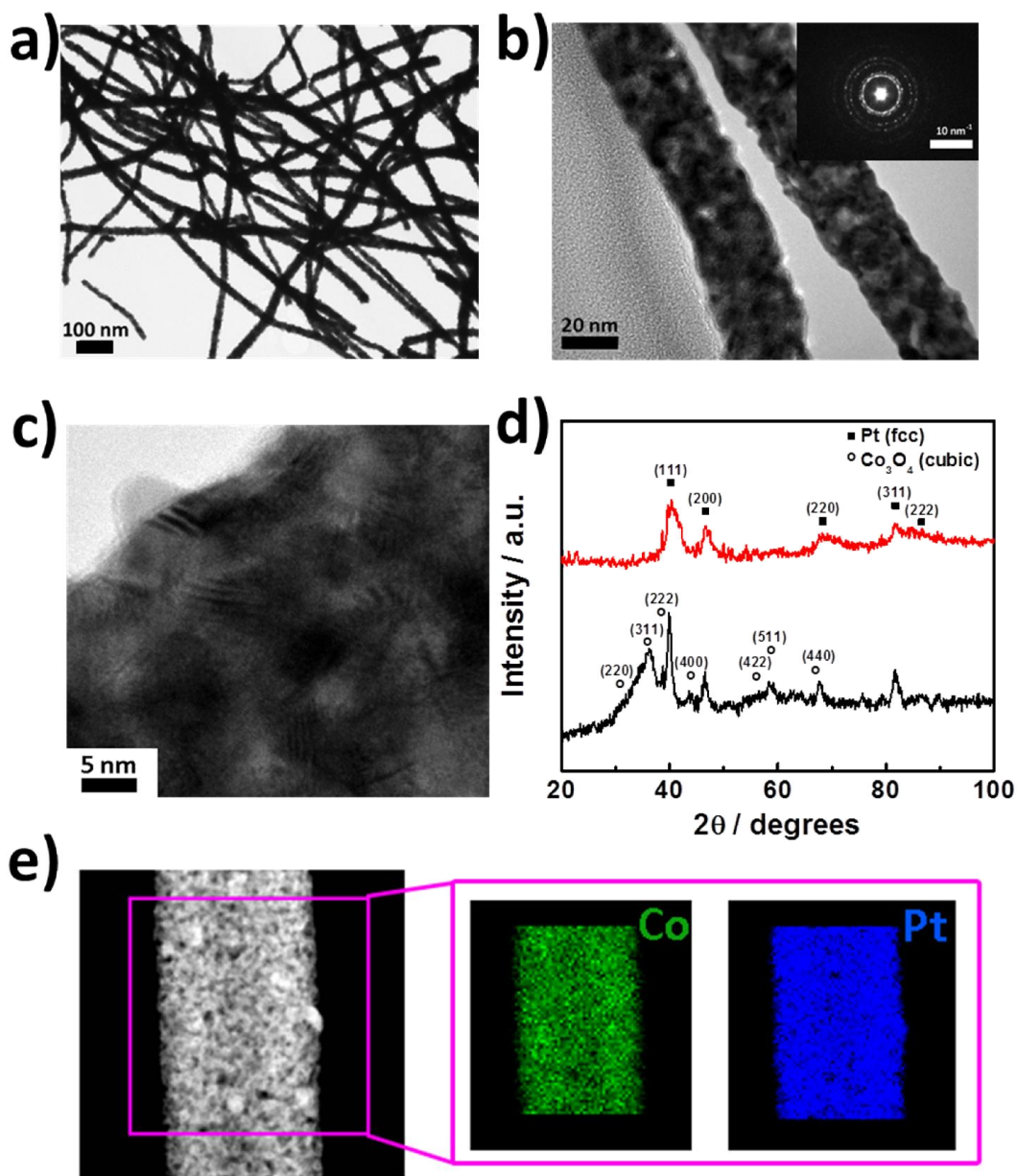
Figure 6-5: (a,b) TEM, (c) high resolution TEM images and (b-inset) SAED patterns of PtCoNWs. (d) XRD diffraction pattern of (black) PtCoNWs before and (red) after reduction in hydrogen at 150 °C. (e) EDX colour map of PtCoNWs. Reproduced in adapted form from [83], with permission from Elsevier.

The overall EDX spectra is displayed in **Figure 6-6**, indicating a Pt:Co ratio of approximately 54:46, in close agreement with the 53:47 ratio used in the electrospinning

solution. ICP analysis on a bulk sample of nanowires confirmed these results, showing that the PtCoNWs are composed of 52.96 at. % Pt and 47.04 at. % Co.
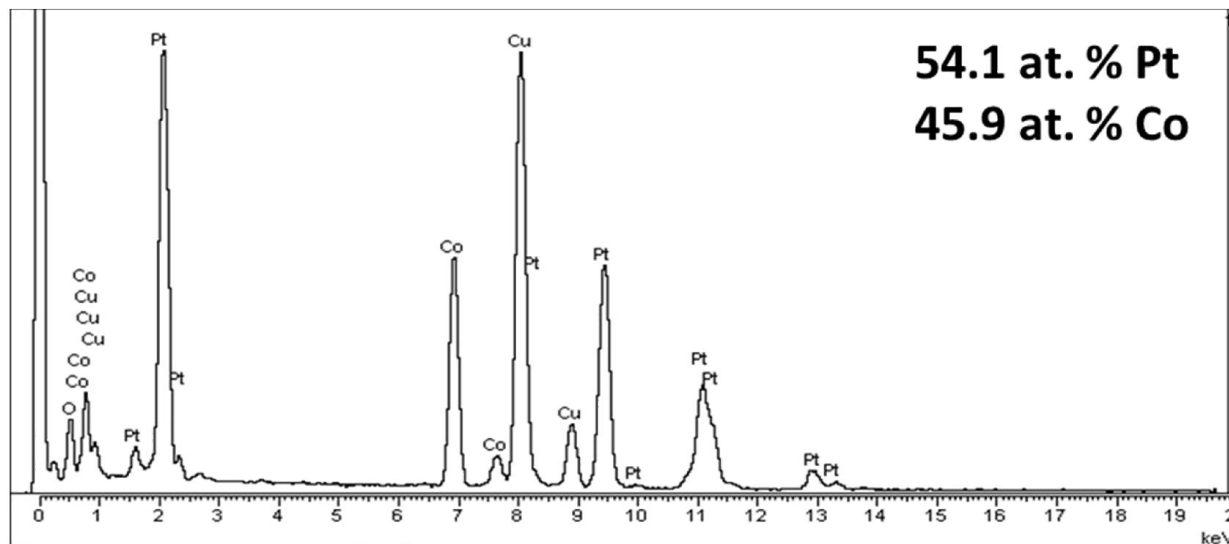
Figure 6-6: Energy dispersive x-ray spectra and associated atomic contents of PtCoNWs. Reproduced in adapted form from [83], with permission from Elsevier.

It was also possible to prepare PtCo-PVP nanofibers with readily tunable Pt:Co atomic contents, along with pure Pt-PVP nanofibers. SEM images of Pt-PVP, $Pt_{53}Co_{47}$-PVP, $Pt_{36}Co_{64}$-PVP and $Pt_{27}Co_{73}$-PVP nanofibers are displayed in **Figure 6-7a, b, c** and **d**, respectively. Consistent nanofiber morphology, diameters and uniformity are observed, highlighting once again the versatility of the PtCoNW electrospinning process. Drawing on this, the Pt-PVP nanofibers were heat treated in air to produce pure PtNWs for comparative purposes, with TEM and high resolution TEM images provided in **Figure 6-7e** and **f**, respectively. Like PtCoNWs, PtNWs displayed a polycrystalline structure as highlighted by the SAED pattern provided in **Figure 6-7e** (inset).
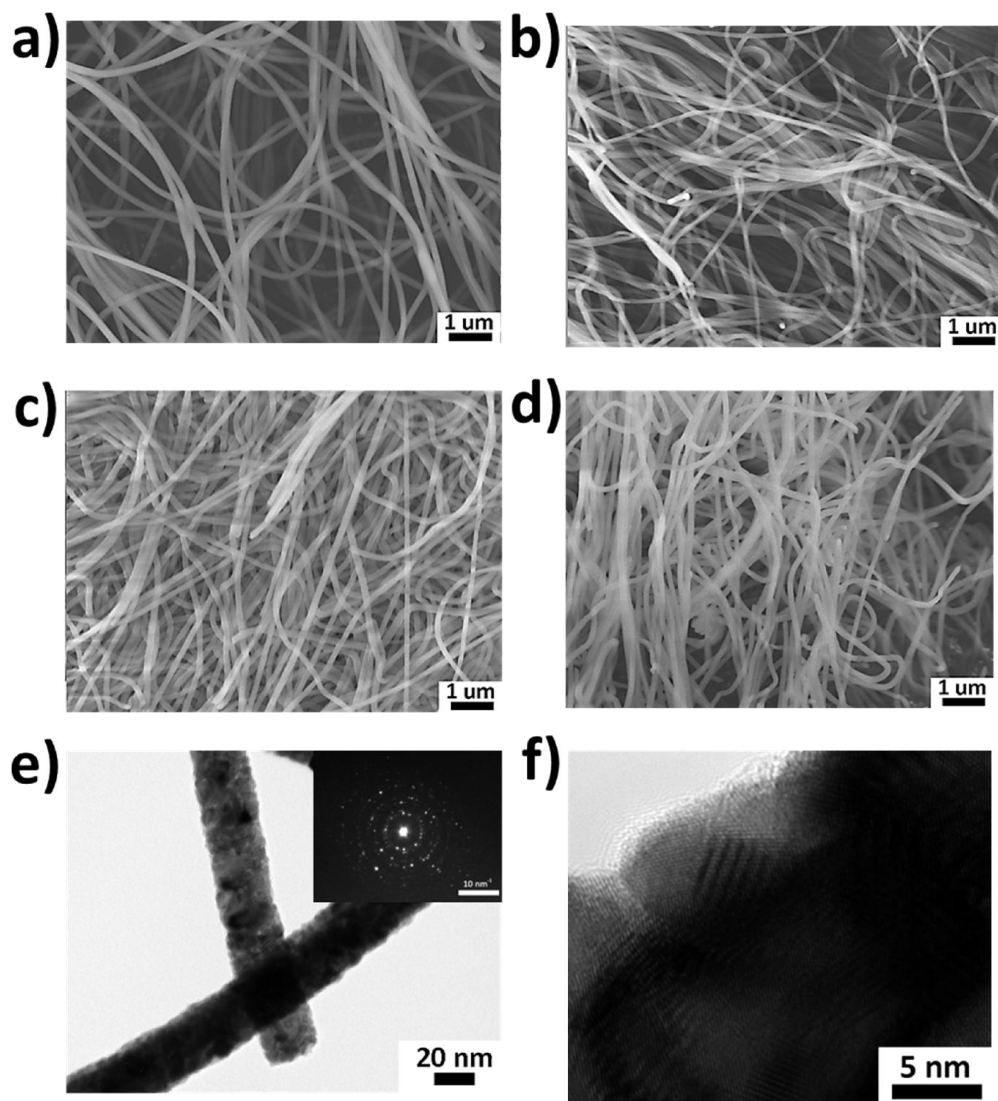
Figure 6-7: SEM images of (a) Pt-PVP, (b) Pt$_{53}$Co$_{47}$-PVP, (c) Pt$_{36}$Co$_{64}$-PVP and (d) Pt$_{27}$Co$_{73}$-PVP

nanowires. (e) TEM and (f) high resolution TEM images of PtNWs, with (e-inset) SAED pattern.

Reproduced in adapted form from [83], with permission from Elsevier.

The EDX spectra (**Figure 6-8**) indicated the atomic purity of the PtNWs. It should also be noted that for pure PtNWs, a relatively lower heat treatment temperature of 450 ^{o}C was used to remove PVP. In the case of PtCoNWs however, at this slightly lower temperature, residual PVP remained on the surface of the nanowires as evidenced by TEM

imaging (**Figure 6-9**) and large oxidative currents observed during electrochemical testing at potentials above ca. 0.6 V vs RHE. This indicates some sort of interaction occurring between PVP and the cobalt precursors, and is also evidenced by the thermogravimentric analysis (TGA) where a very minor weight loss is observed for the Co containing samples in this 400-480 $^{\circ}$C temperature range (**Figure 6-10**). To overcome this challenge, a slightly increased PVP removal temperature of 480 $^{\circ}$C was utilized for PtCoNW preparation.
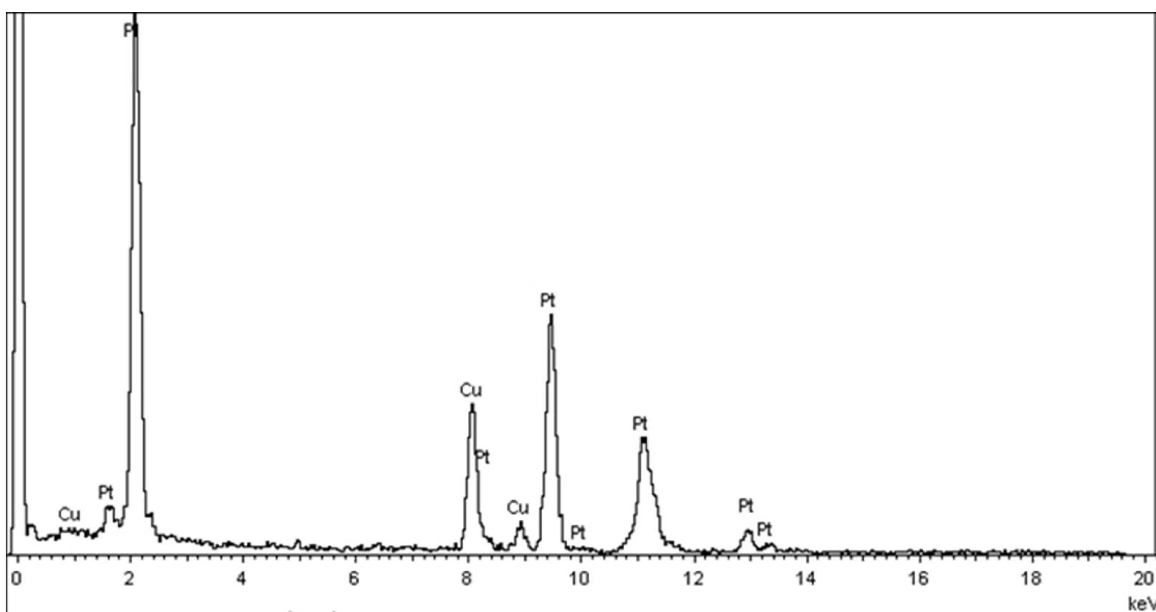
Figure 6-8: Energy dispersive x-ray spectra of PtNWs indicating atomic purity. Reproduced in adapted form from [83], with permission from Elsevier.
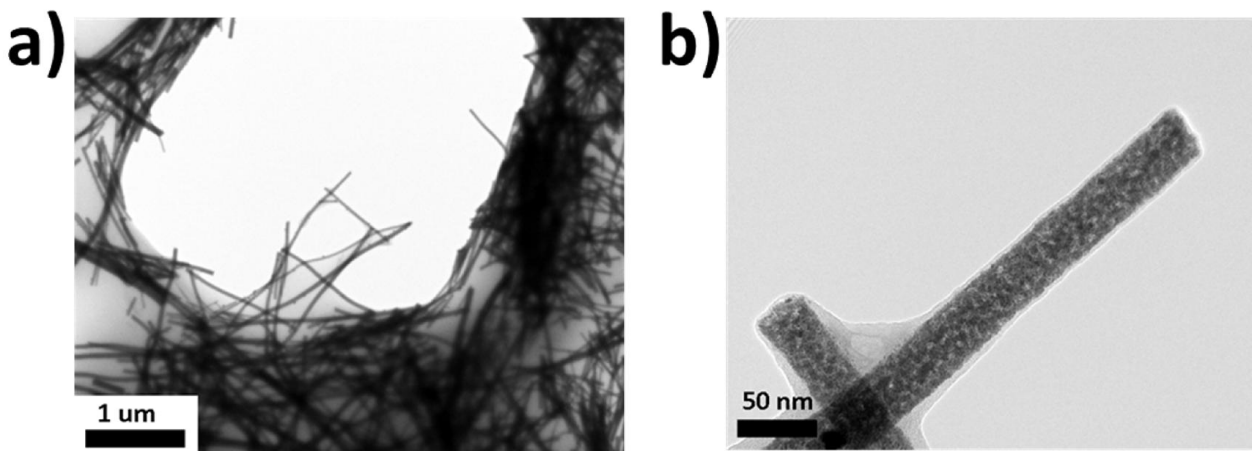
Figure 6-9: Residual PVP observed by TEM on PtCoNWs when only heat treating in air at a temperature of 450 ^{o}C. Reproduced in adapted form from [83], with permission from Elsevier.
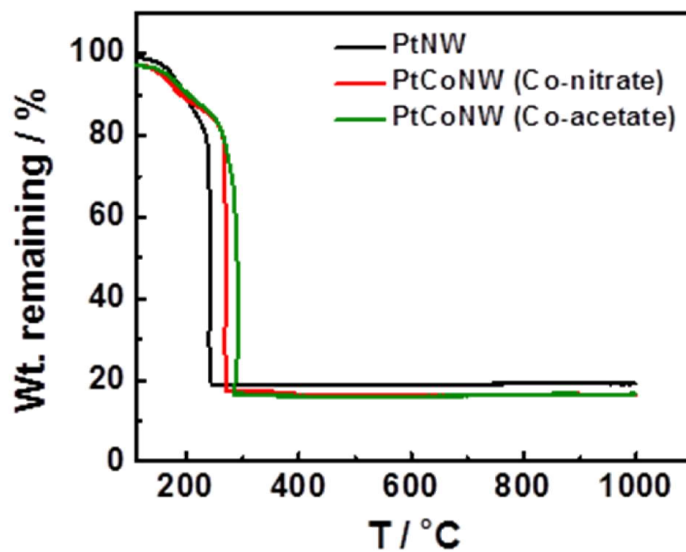
Figure 6-10: TGA curves of Pt-PVP and PtCo-PVP nanofibers prepared using either cobalt nitrate or cobalt acetate tetrahydrate. TGA was conducted in air, and began with maintaining the sample temperature at 100 ^{o}C for one hour in order to remove residual moisture. The temperature was increased at 5 ^{o}Cmin^{-1} up to 1000 ^{o}C. Reproduced in adapted form from [83], with permission from Elsevier.

ORR activities of the nanowire samples were investigated by electrochemical half-cell testing in 0.1 M HClO$_4$ at 30 ^{o}C. The PtCoNW electrode preparation process was investigated and optimized, whereby **Figure 6-11** provides insight into the various parameters (electrode loading, carbon incorporation) that must be considered when dealing with extended surface Pt nanostructures.[249]
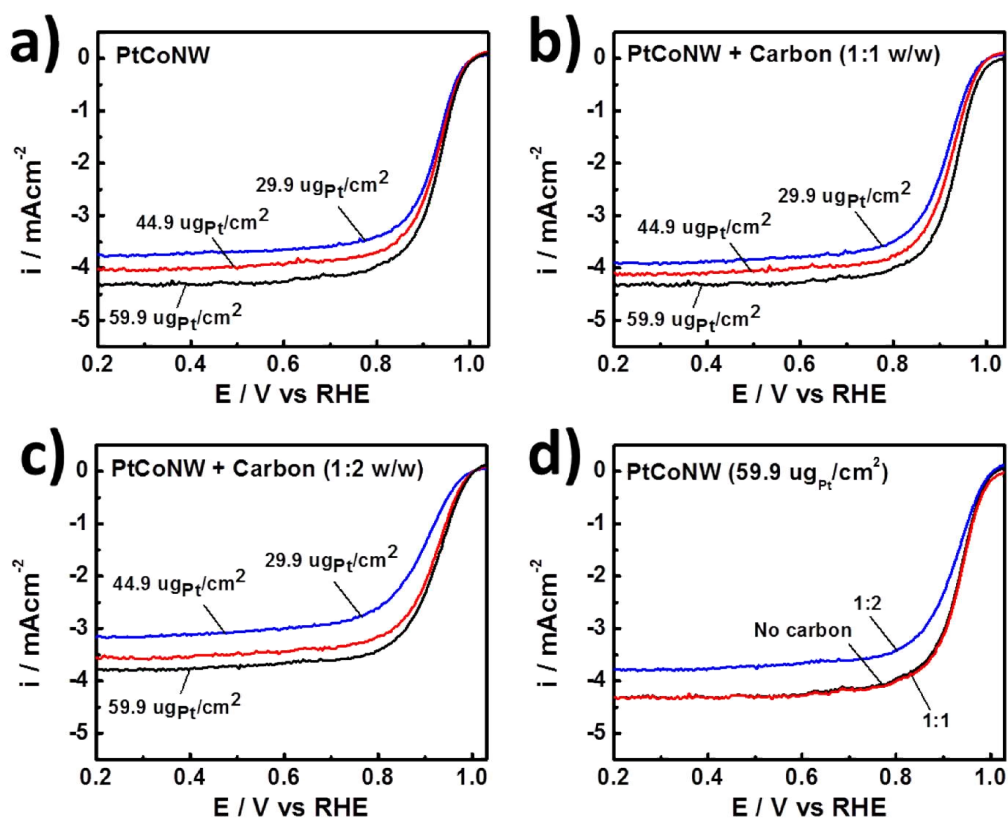
Figure 6-11: Optimization of the electrode fabrication process for PtCoNWs. Polarization curves obtained at 900 rpm in 0.1 M HClO$_4$ for (a) different electrode loadings of PtCoNWs, (b) different electrode loadings of PtCoNWs with carbon black in a 1:1 wt. ratio, (c) different electrode loadings of PtCoNWs with carbon black in a 1:2 wt. ratio, and (d) the impact of PtCoNW:carbon weight ratios on polarization curves. Reproduced in adapted form from [83], with permission from Elsevier.

Following background current and uncompensated electrolyte resistance correction [246], **Figure 6-12a** provides performance evaluation of PtNW and PtCoNW at electrode metal loadings of 76.4 ugcm^{-2} and catalyst to carbon black weight ratios of 1:1 (morphology depicted in **Figure 6-13**). Notably, PtCoNWs demonstrate an on-set potential and half-wave potential of 1.01 and 0.92 V vs RHE, respectively, representing 40 mV increases over that of PtNW. These activity enhancements are observed despite a lower overall Pt electrode loading for PtCoNW (59.9 ug$_{Pt}$cm^{-2}), highlighting the dramatic activity gains realized by alloying Pt with Co atoms. The increase in ORR activity of the PtCoNWs can most likely be attributed to the modified electronic and structural properties of alloy surfaces in comparison to pure Pt.[250] These modulated features in turn tune the adsorptive properties of the catalytically active surface structure, weakening the binding with spectator oxygen containing species (*i.e.*, OH$_{ad}$), thereby freeing up more active sites for the ORR and enhancing the reaction kinetics.[245] Additional ORR activity improvements for PtCoNWs are realized by the partial replacement of expensive Pt atoms in the nanowire core, reducing the catalytically active Pt content that is not accessible to reactant oxygen species. ORR polarization plots for PtCoNWs and PtNWs at electrode rotation rates varying from 100 to 1600 rpm are also provided in **Figure 6-14**.
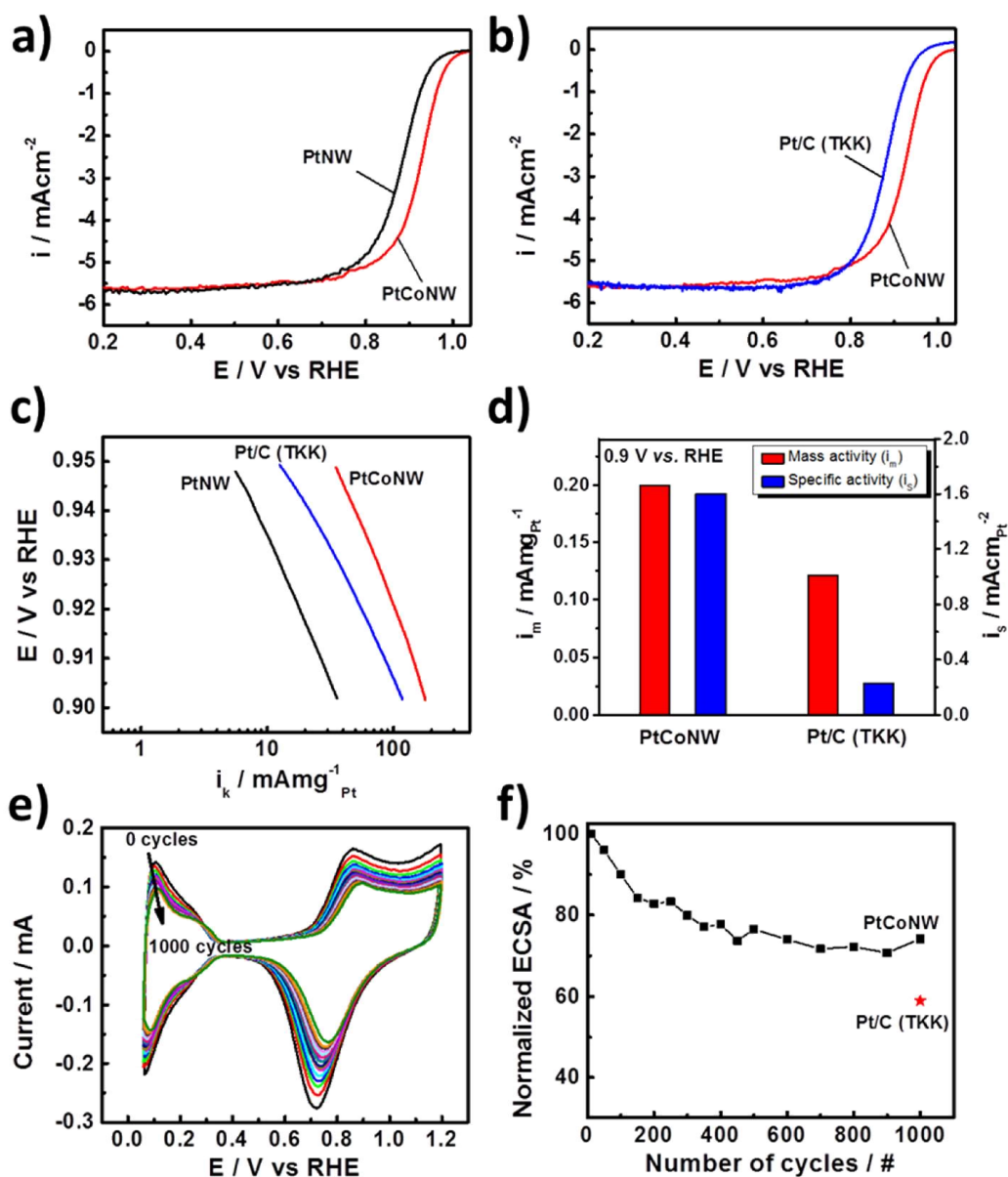
Figure 6-12: RDE polarization curves for **(a)** PtCoNW and PtNW and **(b)** PtCoNW and commercial Pt/C in 0.1 M HClO₄. **(c)** Mass-transport corrected Tafel plots for all materials on a Pt-mass basis and **(d)** determined Pt-based mass and specific based activities at 0.9 V vs. RHE for PtCoNW and Pt/C. **(e)** CV polarization data collected intermittently during ADT for PtCoNWs. **(f)** Normalized ECSA values remaining for PtCoNW during ADT with commercial Pt/C provided for comparison. Reproduced in adapted form from [83], with permission from Elsevier.

93
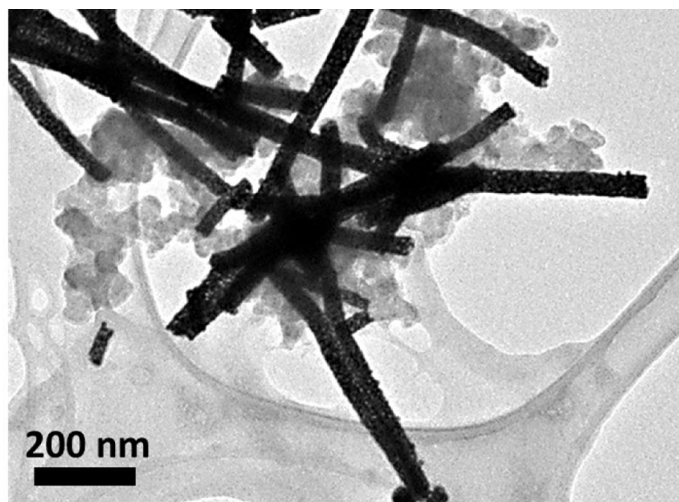
Figure 6-13: TEM image of the PtCoNW and carbon black mixture prepared for electrochemical activity evaluation. Reproduced in adapted form from [83], with permission from Elsevier.
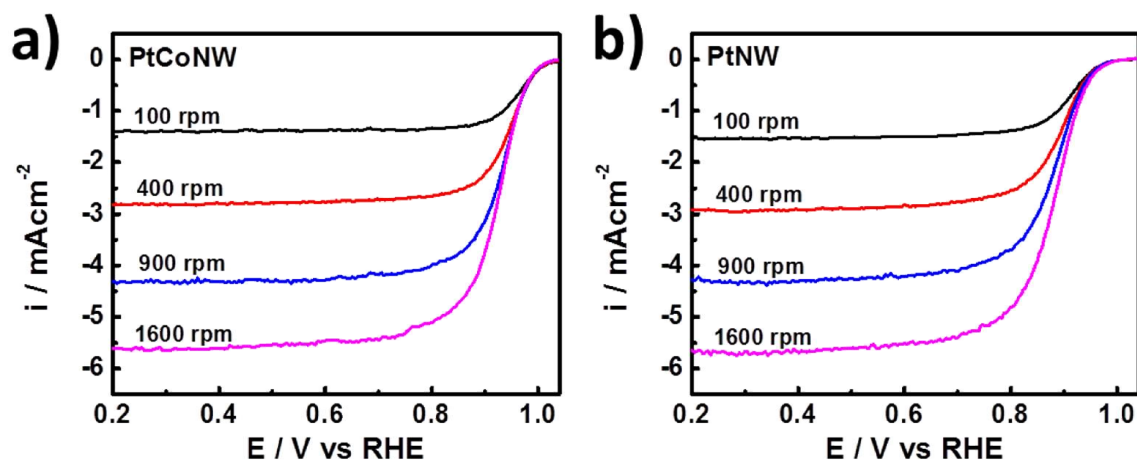
Figure 6-14: ORR polarization curves for (a) PtCoNW and (b) PtNW obtained at varying electrode rotation rates in 0.1 M HClO$_4$ at a scan rate of 10 mV s^{-1} and temperature of 30 °C. Electrode loadings were 59.9 ug$_{Pt}$ cm^{-2} and 76.4 ug$_{Pt}$ cm^{-2} for PtCoNW and PtNW, respectively. Reproduced in adapted form from [83], with permission from Elsevier.

Figure 6-12b provides the ORR performance of PtCoNWs in comparison to commercial Pt/C with a lower electrode loading of 20 ug$_{Pt}$cm^{-2}, a value typically used for

94

commercial catalyst testing.[181] To account for different mass loadings of Pt on the electrode

and provide quantitative evaluation, Tafel plots displaying mass-transport corrected kinetic

current densities (i_k)[251] on a Pt mass basis are provided in **Figure 6-12c**. **Figure 6-12d** also

provides the calculated Pt-based mass and specific activities of PtCoNWs and Pt/C

evaluated at 0.9 V *vs*. RHE. Notably, PtCoNWs demonstrate a specific activity of 1.6

$mAcm_{Pt}^{-2}$, an almost 7-fold improvement in comparison to commercial Pt/C (0.23 $mAcm_{Pt}^{-2}$). In addition to these significant specific activity improvements arising from the

previously discussed alloy configuration, it is highly likely that the anisotropic

nanostructure of the PtCoNWs provides distinct performance advantages as well. Extended

surface structures such as nanowires have a larger portion of high coordination number

surface atoms in comparison to zero-dimensional nanoparticles with numerous low

coordinated surface atoms and defects. The elongated nanowire structure therefore provides

a relatively smooth surface that can mimic the extended surface structure of bulk

polycrystalline films, enhancing the ORR kinetics of the catalyst by supressing the

adsorption of active site blocking spectator species.[223, 241] At all current densities evaluated,

PtCoNWs also provide higher Pt mass based activities than commercial Pt/C, including a

65% improvement at 0.9 V *vs*. RHE (200 $mAmg_{Pt}^{-1}$ versus 121 $mAmg_{Pt}^{-1}$, respectively). It

should also be noted that using lower electrode loadings of PtCoNW could result in higher

Pt-mass based activities. Performance as high as 260 $mAmg_{Pt}^{-1}$ was obtained at an electrode

loading of 29.9 $ug_{Pt}cm^{-2}$ (900 rpm, **Figure 6-11a**), most likely due to increased catalyst

utilization under these conditions. Achieving the theoretical mass-transport limited current

densities predicted by the Levich equation (ca. 4.3 at 900rpm, 5.7 at 1600rpm) were

however not possible at lower catalyst loadings owing to incomplete electrode coverage, an

observation consistent with previous findings[252] and inherent with relatively low surface area catalysts.

The stability of PtCoNW was investigated by electrochemical accelerated degradation testing (ADT). The potential of the electrode was swept 1,000 times between 0.05 and 1.3 V vs RHE at 50 mVs^{-1} with the electrolyte temperature maintained at 30 ^{o}C (**Figure 6-12e**). ECSAs were determined by measuring the charge transfer for hydrogen adsorption/desorption.[17] **Figure 6-12f** provides the normalized ECSA remaining as a function of cycle number. After 1,000 cycles, PtCoNWs retained 75 % of the initial ECSA, compared to 59% for commercial Pt/C. This indicates that the extended surface mimetic structure of PtCoNWs can potentially mitigate Pt dissolution and agglomeration in addition to overcoming the detrimental impact of carbon corrosion owing to the their self-supported nature.

6.4 Conclusions

In summary, PtCoNWs were prepared by electrospinning and found to provide excellent activity and stability towards the ORR in acidic electrolytes. The benefits of alloying were demonstrated by comparing the activity of PtCoNWs with that of pure PtNWs, whereby over a 4x improvement in Pt mass-based activities at 0.9 V vs. RHE was achieved with the incorporation of Co into the 1D Pt nanostructure. An almost 7-fold improvement in specific activity was observed for PtCoNWs in comparison to commercial Pt/C, along with improved ECSA retention (75% versus 59%, respectively) measured through ADT cycling. A 65 % increase in Pt mass based activity was also obtained for PtCoNWs in comparison to Pt/C, despite the relatively low surface area arising from the

thick diameter of these nanowire catalysts. It is expected that further mass activity improvements can be achieved by careful control of the morphology (i.e. diameter) and atomic compositions of the PtCoNWs, capabilities that have been demonstrated herein by the versatile electrospinning technique. This provides a valuable platform for systematic structure-property investigations and optimization in order to combine the specific activity enhancements observed for extended Pt-alloy surfaces with increased Pt utilization by nanostructure control strategies, with the ultimate goal of preparing highly active, operationally stable 1D Pt-alloy nanowires to potentially replace conventional nanoparticle catalysts.

7. Heteroatom doped graphene-carbon nanotube composite supported cobalt disulfide octahedral nanoparticles

This chapter is reprinted in adapted form from [253], with permission of the Royal Society of Chemistry.

D. Higgins, F. Hassan, M. Seo, J. Choi, A. Hoque, D. Lee, Z. Chen, "Shape-controlled octahedral cobalt disulfide nanoparticles supported on nitrogen and sulfur-doped graphene/carbon nanotube composites for oxygen reduction in acidic electrolyte", *Journal of Materials Chemistry A*, 3 (2015) 6340-6350.

The computational simulations reported in this chapter were done by Dr. Min Ho Seo.

7.1 Introduction

The development of suitable non-PGM catalysts to composite with high activity platinum in a hybrid electrode configuration is the objective of this chapter. There have been significant non-PGM ORR catalyst research efforts in recent years, with several promising replacements including transition metal chalcogenides and oxides, or high temperature heat treated transition metal-nitrogen-carbon complexes (dubbed "M-N-C", where M is generally Co, or Fe) demonstrated.[96, 111, 254] The M-N-C systems remain the most extensively investigated class of non-PGM catalyst to date, with significant improvements to ORR activity and operational durability realized in recent years.[113, 117, 255-257] Despite this, very rarely are they prepared without a heat treatment.[258, 259] By extension, the multi-step fabrication process, including high temperature (i.e. > 800 °C) heat treatment(s) invariably results in highly heterogeneous, multi-component structures. This

leads to extensive debate over the identity and nature of the ORR active site structures present in these catalysts, even after over two decades of research activities, rendering the rational design of improved performance M-N-C catalysts a very challenging endeavour. It is therefore of interest to develop and investigate alternative non-precious ORR catalyst technologies, prepared by simplistic, energy efficient and scalable techniques that can provide highly homogeneous active phase structures. This will provide opportunity for researchers and scientists to understand and improve the ORR kinetic processes occurring on these well-defined nanostructured surfaces, in an attempt to ultimately eliminate the dependence on Pt-based catalysts.

One interesting type of non-PGM material is nanostructured metal chalcogenides that have emerged on the forefront of materials science and technology research as promising functional materials for application in a variety of energy technologies.[260] Cobalt sulfide, exhibiting interesting phase-dependent electronic, magnetic and catalytic properties,[261, 262] boasts great potential for application in energy conversion and storage technologies, including fuel cells,[263-268] supercapacitors,[269-271] lithium ion batteries[272-274] and photoelectrochemical dye-sensitized solar cells.[275-277] The controllable synthesis of highly crystalline and mono-phase nanostructures of cobalt sulfide is however very challenging, yet desirable from an application standpoint. This is owing to the highly oxophilic nature of cobalt and the complicated stoichiometry of cobalt sulfide that consists of various phases, all with different physicochemical properties.[262] Using cobalt sulfide nanoparticles in conjunction with high surface area nanostructured carbon supports, such as graphene or CNTs, can also be highly advantageous. These supports in particular provide

interconnecting mesostructured scaffolds that can facilitate good nanoparticle dispersion and electron transport. The structural, surface and electron properties of graphene or CNTs can furthermore be modulated through doping with various heteroatoms, such as nitrogen or sulfur.[278-282] In addition to inducing unique functionality, these dopant species can also provide beneficial carbon support-nanoparticle interactions.[279, 283-285]

In this work, the unique solvothermal preparation of shape controlled, single crystal cobalt disulfide (CoS_2) octahedron particles supported on nitrogen and sulfur doped CNT/graphene composites (CoS_2-CG) is reported. This single step, relatively low temperature (220 ^{o}C) approach offers several notable advantages, including an inexpensive, low-energy consuming and one-pot scalable synthesis, along with excellent CoS_2 shape control and facet exposure achieved without the addition of any template or surfactant species. With excellent phase purity, the prepared CoS_2-CG nanostructures are demonstrated to provide the highest performance towards the ORR in acidic electrolyte (0.1 M $HClO_4$) reported to date for non-precious metal chalcogenide materials. Through careful investigation, the CoS_2 octahedron formation process is elucidated and a growth mechanism proposed. Additionally, the performance advantages of using CNT/graphene composites as supports for the octahedron nanoparticles is demonstrated, and the nature of nitrogen and sulfur doping into the graphitic lattice of the nanostructured carbon materials rigorously probed. Nitrogen and sulfur co-doped graphene materials are generally prepared by high temperature heat treatment approaches, and this work highlights successful double-doping by a solvothermal process, providing practical implications for various applications such as ORR catalysis in alkaline conditions.[280, 282, 286]

7.2 Specific materials and experimental methods

Graphene oxide (GO) was used as the starting material and was prepared by a modified Hummer's method as reported previously.[287] Commercial CNTs were functionalized by refluxing in 6M HNO_3 for 6h (HNO_3-CNT)[16] to improve the dispersion in EG solvent and interactions with ionic precursor species. In a typical synthesis, 15 mg of GO and 15 mg of HNO_3-CNTs were well-dispersed in 11 mL of EG by ultrasonication for 4 h. Meanwhile, two separate aqueous solutions containing 150 mg/mL of thiourea and 10 mg/mL of cobalt acetate tetrahydrate were prepared and mixed thoroughly by magnetic stirring. Using a pipette, 2 mL of each aqueous precursor solution was then added to the GO/HNO_3-CNT/EG solution, and the total volume of the mixture was increased to 20 mL by the addition of EG. This solution was then ultrasonicated for an additional 30 min to ensure adequate precursor mixing, and was then transferred to a 25 mL Teflon-lined autoclave and tightly sealed. The solvothermal synthesis was carried out by heating the mixture to 120 ^{o}C and holding it for 10 h, and then further increasing the temperature to 220 ^{o}C, where it remained for an additional 10 h. After cooling, the product was separated by centrifugation, washed thoroughly with DDI water and acetone, and collected by lyophilization. CoS_2 octahedrons supported on just CNTs (CoS_2-C) or graphene (CoS_2-G) were prepared by the same procedure, however using 30 mg of HNO_3-CNT or 30 mg of GO as the nanostructured carbon precursor, respectively. Pure CoS_2 was also prepared in the absence of any nanostructured carbon supports.

In these experiments, all XRD patterns were obtained using cobalt radiation (wavelength = 1.789 Angstroms). Raman spectra was carried out on a Bruker Senterra

Raman Microscope operating with a wavelength of 532 nm. The BET surface areas were determined by N_2 adsorption at 77 K (Micromeritics ASAP 2020). Prior to the BET analysis, catalyst samples were degassed by helium for at least 2 h at 473 K to remove any impurities.

All electrochemical testing was carried out in a conventional three-electrode glass cell in 0.1 M $HClO_4$. Catalyst ink was prepared by ultrasonically dispersing 4 mg of catalyst in 1 mL of isopropanol containing 0.05 wt. % Nafion ionomer. 30 uL of catalyst ink was then micro-pipetted onto the surface of the glassy carbon working electrode by sequential 10 uL depositions, leading to an overall electrode loading of ca. 0.6 mgcm^{-2}. ORR activity was measured under oxygen saturated electrolyte conditions by sweeping the electrode potential from 1.05 to 0.05 V *vs*. RHE, at a scan rate of 10 mVs^{-1}. Capacitative contributions were eliminated by subtracting background currents obtained under the same testing conditions, although under nitrogen saturated electrolyte. All ORR polarization curves were corrected for uncompensated electrolyte resistance.[246]

For computational simulations, the total energies of CoS_2 were calculated using the Vienna *ab initio* simulation package (VASP) program[288] with the implemented DFT method.[289, 290] The electron exchange-correlation energy was described by the Perdew, Burke and Ernzerhof (PBE) functional,[291] which employs the spin-polarized generalized gradient approximation (GGA).[292,293] The core electrons were replaced by projector augmented wave (PAW) pseudo-potentials.[294, 295] The valence electrons were described by Kohn-Sham wave functions, which were expanded with a plane-wave basis set. A cutoff energy of 520 eV was used. All ions were fully relaxed during the structural optimization

until the total energy was converged within 10^{-4} eV. A gamma point mesh with ($15 \times 15 \times 15$) k points was used for the CoS_2 (1×1) unit cell to sample the Brillouin zone for bulk calculation. Periodic boundary conditions were imposed on the CoS_2 unit cell in terms of each surface direction of (111), (110) and (001), and a vacuum space of 20 Å was employed to avoid interactions between top and bottom surface. To calculate the total energies of CoS_2 on different surface directions, we only used a gamma point mesh of ($5 \times 5 \times 1$), and utilized the Methfessel-Paxton smearing method.[296]

7.3 Results and discussion

Three primary materials were developed in this work by a single-step solvothermal approach using different nanostructured carbon supports, including CoS_2 supported on graphene (CoS_2-G), CNTs (CoS_2-C) and a CNT/graphene composite (CoS_2-CG). TEM images of each of these materials are provided in **Figures 7-1a**, **b** and **c**, respectively. Consistent with results from SEM imaging that show the overall homogeneous morphology (**Figure 7-2**), it was observed that regardless of the nanostructured carbon support type, shape controlled octahedral CoS_2 particles were grown on the carbon surface, with no unsupported particles formed in solution. For CoS_2-CG (**Figure 7-1c**, **Figure 7-2c**), octahedral nanoparticles were clearly intermixed with CNTs that had assembled on the sheet-like surface of graphene. This CNT assembly likely arises from the amphiphilic surfactant-like nature of GO, consisting of hydrophilic oxygen-containing surface species that render it highly dispersible in aqueous solutions, along with basal plane aromatic regions[297]. When dispersed in solution with CNTs, the aromatic groups present in each component can provide a strong attachment through π-π interactions,[298, 299] resulting in the

observed assembly of CNTs on the surface of graphene sheets, and no free CNTs observed on the TEM grid. A high resolution TEM image of a shape controlled nanoparticle from the CoS_2-CG sample is provided in **Figure 7-1d**, consisting of a single crystal with an octahedral morphology. The lattice space measurement of 0.318 nm is in close agreement with the theoretical {111} spacing of CoS_2 (0.319 nm), indicating that the crystalline octahedral particle is encased by the {111} facets. This observation is consistent with the results of Bao *et al.*,[300] who demonstrated the biomolecule-assisted hydrothermal preparation of free-standing microscale Co_3S_4 octahedrons enclosed by the {111} surfaces.
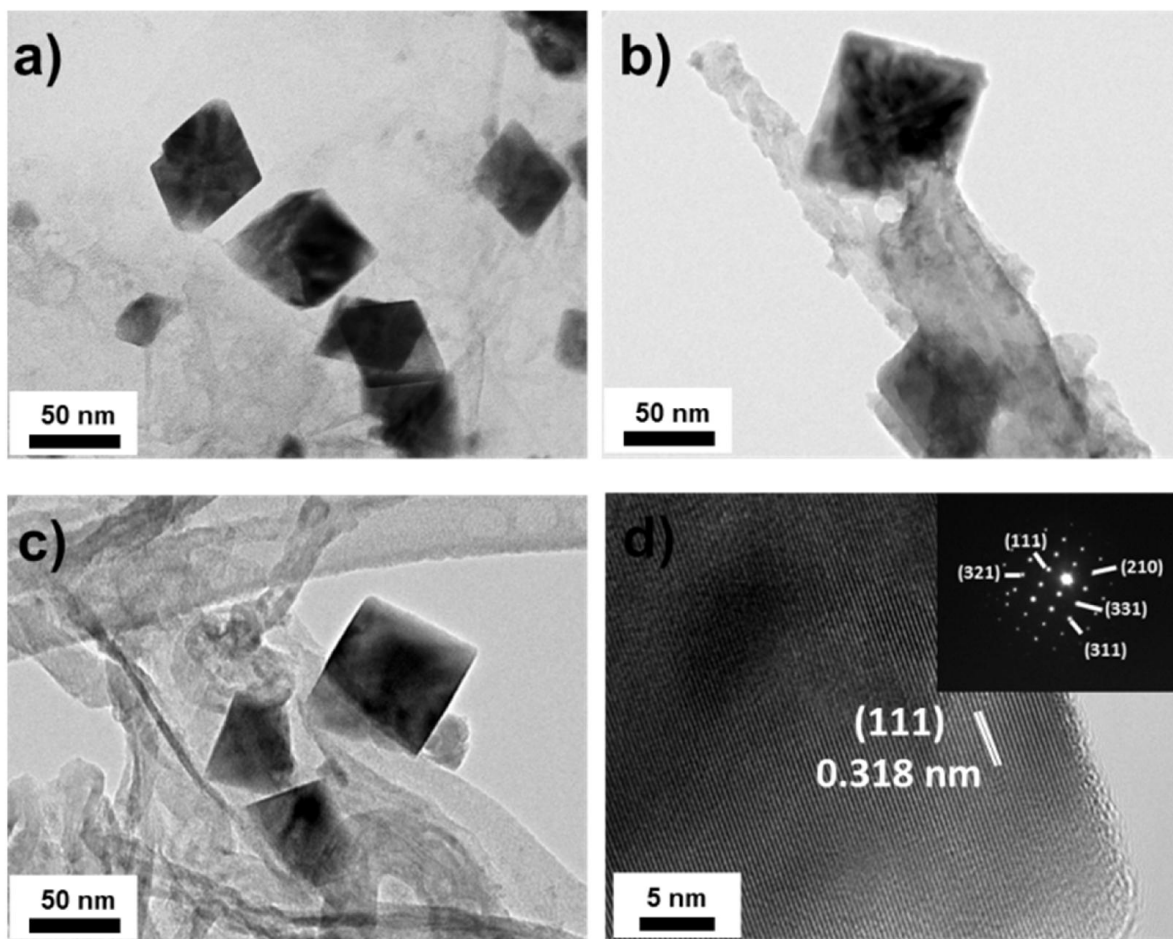
Figure 7-1: TEM images of (a) CoS$_2$-G, (b) CoS$_2$-C and (c) CoS$_2$-CG. (d) High resolution TEM image of a single crystal CoS$_2$ octahedron particle along with (inset) SAED pattern. Reproduced in adapted form from [253], with permission of the Royal Society of Chemistry.
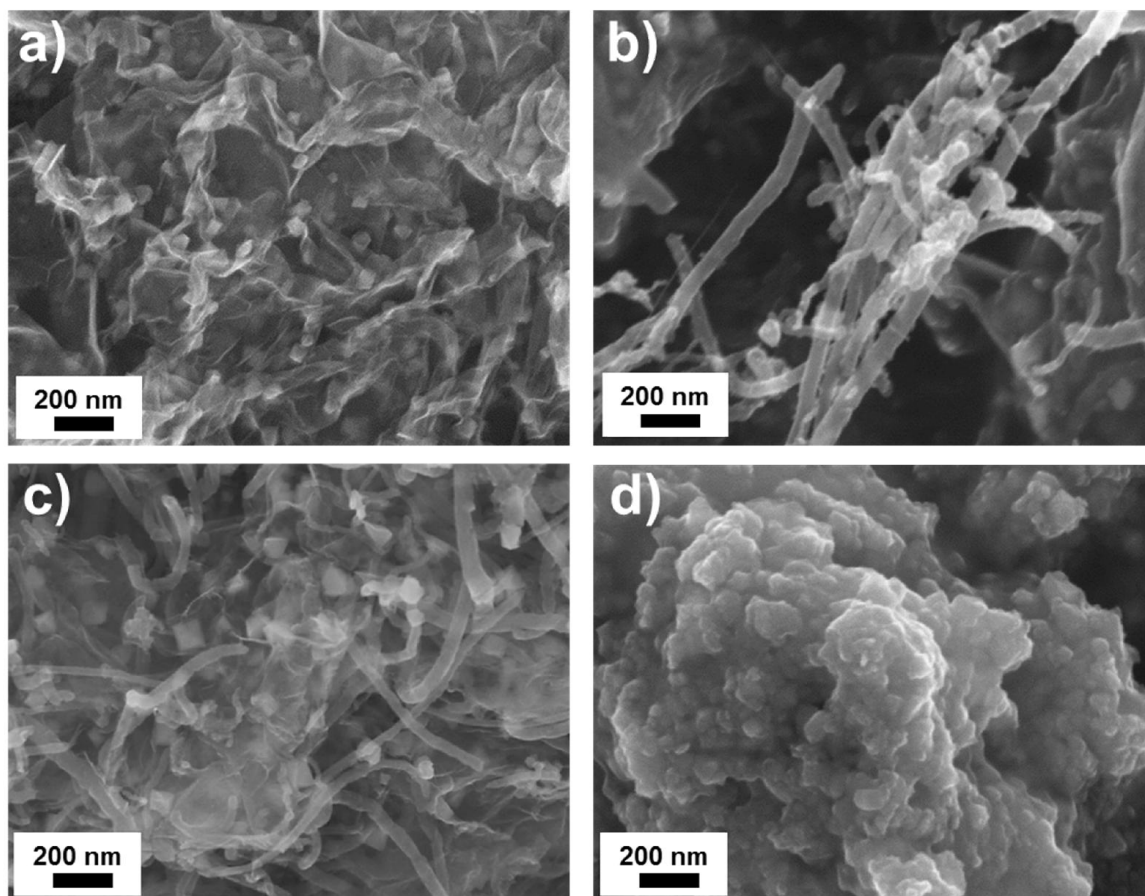
Figure 7-2: SEM images of (a) CoS$_2$-G, (b) CoS$_2$-C, (c) CoS$_2$-CG and (d) as-prepared, unsupported CoS$_2$. Reproduced in adapted form from [253], with permission of the Royal Society of Chemistry.

Interestingly, when only CNTs were used as the nanostructured carbon support, the distribution of CoS$_2$ particles on CoS$_2$-C was reduced, with larger average crystallite sizes observed. This indicates that the high concentration of surface functional species on the GO starting materials provides a beneficial impact in terms of providing nucleation and anchoring sites for well distributed nanoparticles.[283] The impact of support selection was also indicated by the results of carrying out the solvothermal process in the absence of any

nanostructured carbon support. Only large particle agglomerate structures were obtained (**Figure 7-2d**), with no evidence of octahedron nanostructure formation.

Operating in scanning transmission electron microscopy (STEM) mode, EDX atomic mapping was carried out on a bundle of octahedral particles of varying size in order to determine the atomic content and distributions of the CoS_2-CG materials. With colour mapping images provided in **Figure 7-3a**, the octahedron particles consist of concentrated regions of both cobalt and sulfur, with some sulfur species observed throughout the CNT/graphene supports, indicative of sulfur doping into the graphitic structures during solvothermal processing. The atomic composition of a single octahedral particle was investigated by carrying out EDX analysis, with the obtained spectra (**Figure 7-4**) indicating a Co:S ratio of 36.3 to 63.4 at. %, in close agreement with the expected atomic content of the CoS_2 phase.
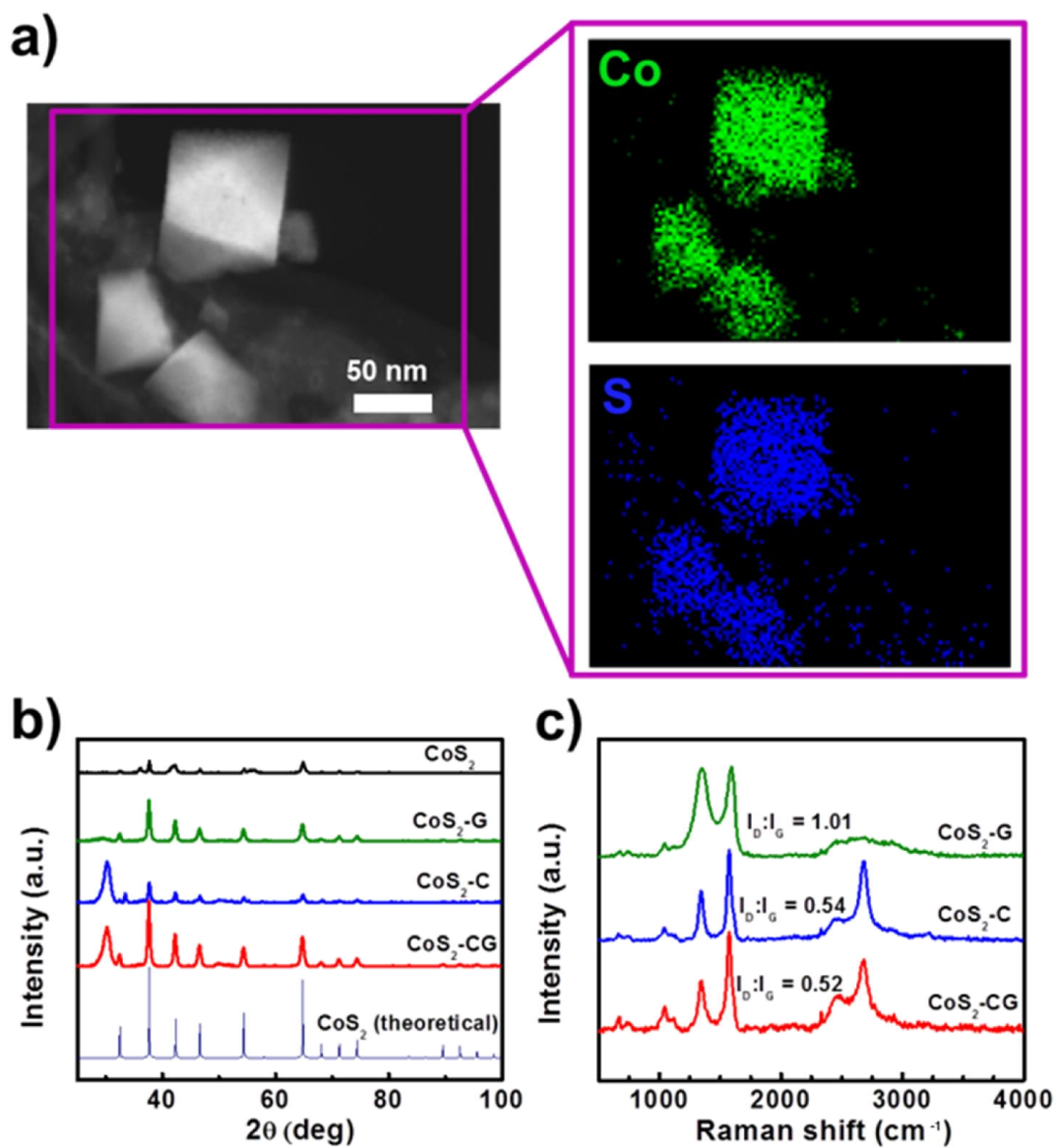
Figure 7-3: (a) EDX colour mapping of CoS₂-CG, (b) XRD patterns of prepared samples and theoretical CoS₂ pattern, and (c) Raman spectra for CoS₂-G, CoS₂-C and CoS₂-CG. Reproduced in adapted form from [253], with permission of the Royal Society of Chemistry.
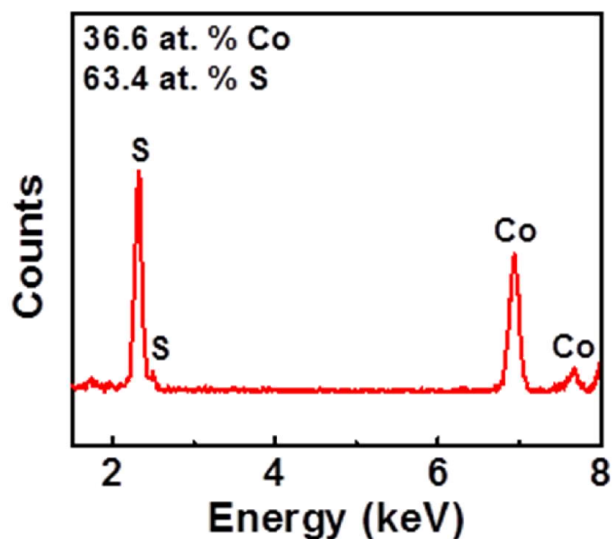
Figure 7-4: Energy dispersive x-ray spectrum of a single CoS$_2$ octahedral nanoparticle from the CoS$_2$-CG sample. Reproduced in adapted form from [253], with permission of the Royal Society of Chemistry.

XRD was used to confirm the phase structure of the prepared materials, with diffraction patterns of the prepared samples provided in **Figure 7-3b**. The diffraction peaks observed for CoS$_2$-G, CoS$_2$-C and CoS$_2$-CG were in direct agreement with the standard pattern of cubic CoS$_2$ with a lattice parameter of 0.554 nm (86351-ICSD). When prepared in the absence of any nanostructured carbon support, the diffraction pattern of the as-prepared CoS$_2$ materials demonstrated the CoS$_2$ phase, however minor CoS diffraction peaks were also observed. This reiterates the important role of the nanostructured carbon supports in preparing well-dispersed, homogeneous CoS$_2$ nanoparticles. The CoS phase could potentially be present as an intermediate species for CoS$_2$ formation that became entrapped within the large agglomerates during particle growth, or could arise due to the

effect (or lack thereof) that the nanostructured carbon species with electrostatically charged surface functional species has on the synthesis process.

Provided in **Figure 7-3c** are the Raman spectra for CoS_2-G, CoS_2-C and CoS_2-CG. Each sample clearly shows a "D-band" peak located at ca. 1339 cm^{-2}, attributed to defect induced structural vibrations and a "G-band" peak located at ca. 1580 cm^{-2} and attributed to the E_{2g} vibration spectra of sp^2 bonded carbon. These peaks, in addition to the 2D-band peak demonstrated at ca. 2683 cm^{-2} are characteristic of graphitic materials and arise from the nanostructured carbon materials used to support CoS_2 particles. Commonly the D-band to G-band peak ration ($I_D:I_G$) is used to gauge the degree of structural disorder present in CNT or graphene based materials.[214] CoS_2-G demonstrates an $I_D:I_G$ ratio of 1.01, which is in agreement with the values obtained previously for graphene-based materials[179, 301] and indicating that the solvothermal process was successful in reducing the surface oxygen species of GO. The $I_D:I_G$ ratios of CoS_2-C and CoS_2-CG were similar at 0.54 and 0.52, respectively. This value is consistent with results reported for CNT-based materials reported recently[301] and also provides indication that the CNT component of the composite supported CoS_2-CG contributes primarily to the observed Raman spectra, most likely due to the fact that CNTs are observed to be assembled on the surface of the graphene sheets.

Using CoS_2-CG as a representative sample, the Co2p and S2p spectra obtained by XPS are provided in **Figure 7-5a** and **b**, respectively. The Co2p spectra displays three spin-orbit couples, with the lower binding energy peaks displayed in the figure and located at ca. 778.9, 781.0 and 782.95 eV, respectively. The first peak comprises the majority of Co atoms scanned and can be attributed to the Co^{2+} species of CoS_2, an observation consistent

with results of previous spectroscopic investigations on cobalt sulfide materials.[262, 264, 300] The two minor peaks located at higher binding energies could be due to the presence of Co-NH bonds formed between residual ammonia species from the decomposition of thiourea[300] or satellite shake up peaks.[302] More rigorous investigations are required to elucidate the exact source of these observed peaks, although they comprise only a small amount of the surface cobalt ions scanned and therefore are not of significant concern. The S2p peak in **Figure 7-5b** demonstrates a main peak comprised or two $Sp_{1/2}$ and $Sp_{3/2}$ doublets. The first doublet, with peaks located at 162.4 and 163.6 eV are attributed to the CoS_2 phase.[264, 302] The second pair, with peaks located at 164.5 and 165.6 eV are attributed to thiophenic sulfur species incorporated into the CNT/graphene support matrix.[39, 303] While these results, in accordance with the previously discussed EDX colour mapping indicate successful doping of the nanostructured carbon supports through the solvothermal process, this phenomenon, including nitrogen doping, will be investigated and discussed in more detail later on. There is an additional pair of peaks in the S2p spectra observed at ca. 169.0 eV, which can be attributed to oxidized sulfur species, potentially sulfates,[304] that are present in small quantities on the surface of the developed materials.

111
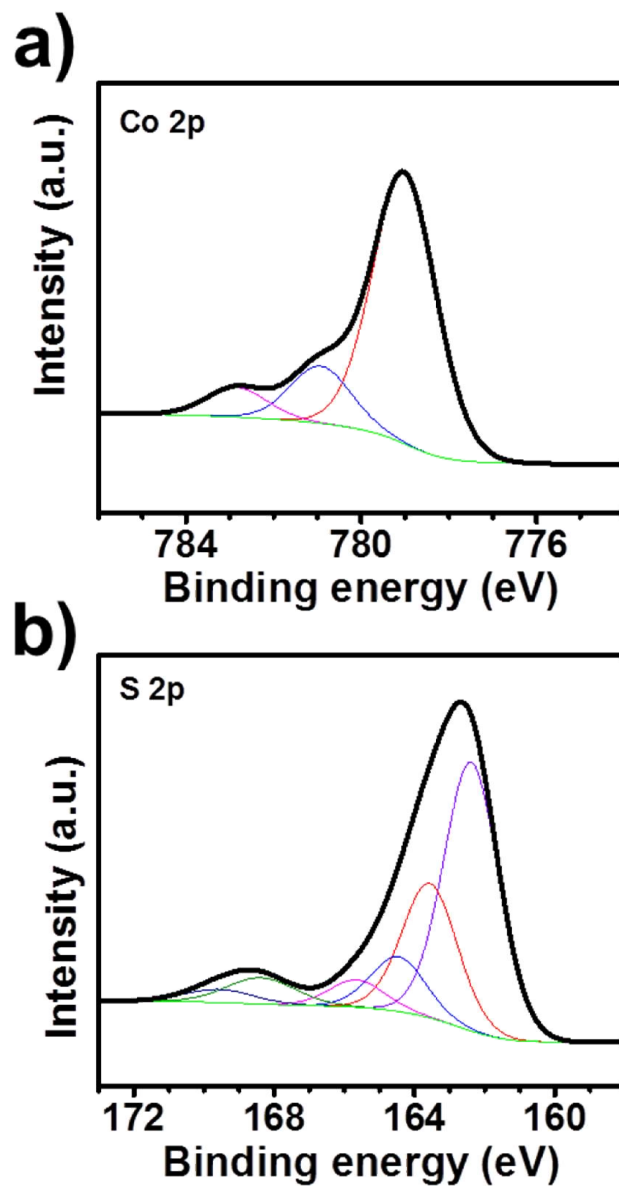
Figure 7-5: High resolution XPS (a) Co2p and (b) S2p spectra of CoS$_2$-CG. Reproduced in adapted form from [253], with permission of the Royal Society of Chemistry.

To understand the mechanistic process of CoS$_2$ octahedron particle formation and growth, a time dependent synthesis investigation was carried out using graphene as the representative support material. After initially heating the solvothermal reaction

temperature up to 120 $^{\circ}$C and maintaining it for 10 hours, the temperature was further increased to 220 $^{\circ}$C, after which the reaction was interrupted at various time intervals by removing the solvothermal reactor from the oven. After 0.5 h (**Figure 7-6a**, **Figure 7-7a**), only small, irregularly shaped nanoparticles were observed on the surface of the graphene sheets. This structure is consistent with the materials that resulted when a reaction temperature of only 120 $^{\circ}$C was used for the entire solvothermal reaction (CoSG-120), and the nanoparticles were determined to be amorphous based on XRD, high resolution TEM imaging and SAED patterns provided in **Figure 7-8**. As the reaction time at 220 $^{\circ}$C is lengthened to 2.5 h, the formation of larger, crystalline nanoparticles is observed (**Figure 7-6b**, **Figure 7-7b**). Further increasing the reaction time to 5 h, disappearance of the majority of amorphous nanoparticles occurs, and there is an abundance of larger particle structures starting to exhibit the single crystal octahedron morphology (**Figure 7-6c**, **Figure 7-7c**). Finally after a reaction time of 10 h, only octahedron nanoparticles, comprised of single crystals with varying sizes well-distributed across the surface of graphene remain (**Figure 7-6d**, **Figure 7-7d**), with minimal changes to morphology observed with a further increase in the reaction time to 20 h.
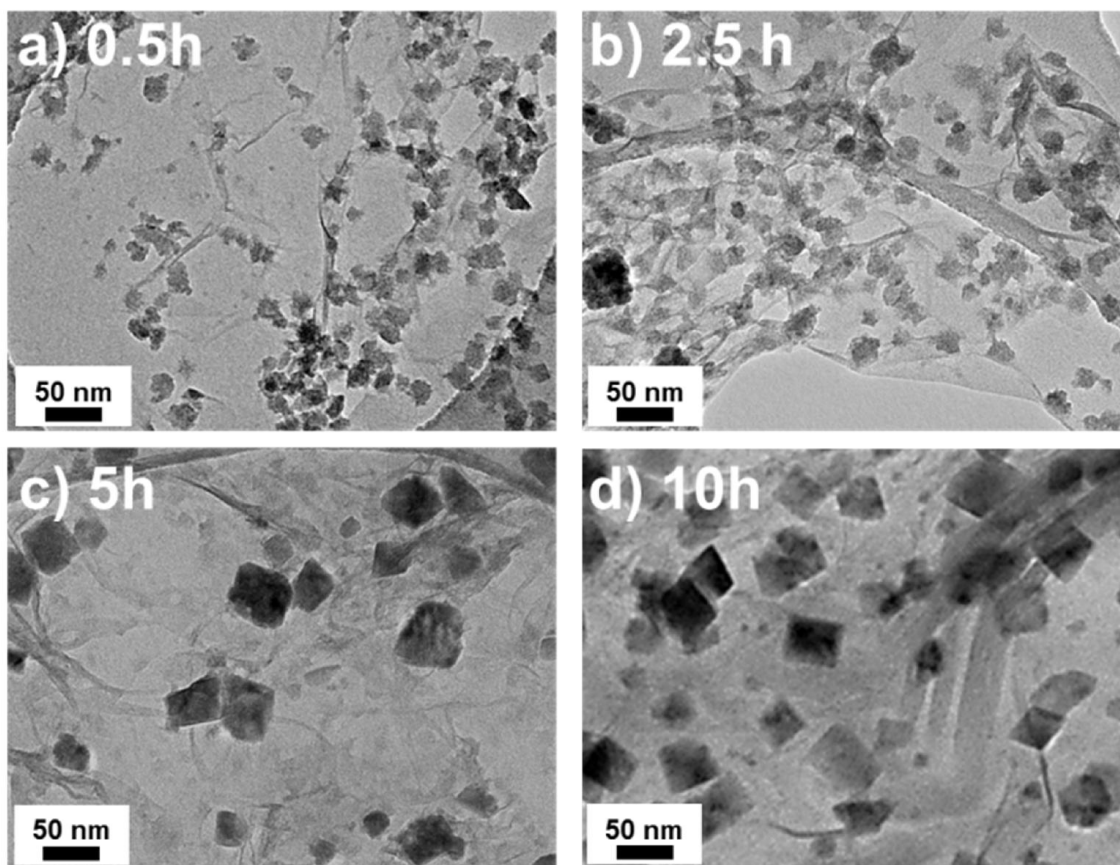
Figure 7-6: TEM images of the time dependent growth of CoS$_2$ supported on graphene held at 220 ^{o}C for (a) 0.5 h, (b) 2.5 h, (c) 5 h and (d) 10 h. Reproduced in adapted form from [253], with permission of the Royal Society of Chemistry.

Figure 7-7: SEM images of the time dependent growth of CoS$_2$ supported on graphene held at 220 °C for (a) 0.5 h, (b) 2.5 h, (c) 5 h and (d) 10 h. Reproduced in adapted form from [253]**, with permission of the Royal Society of Chemistry.**
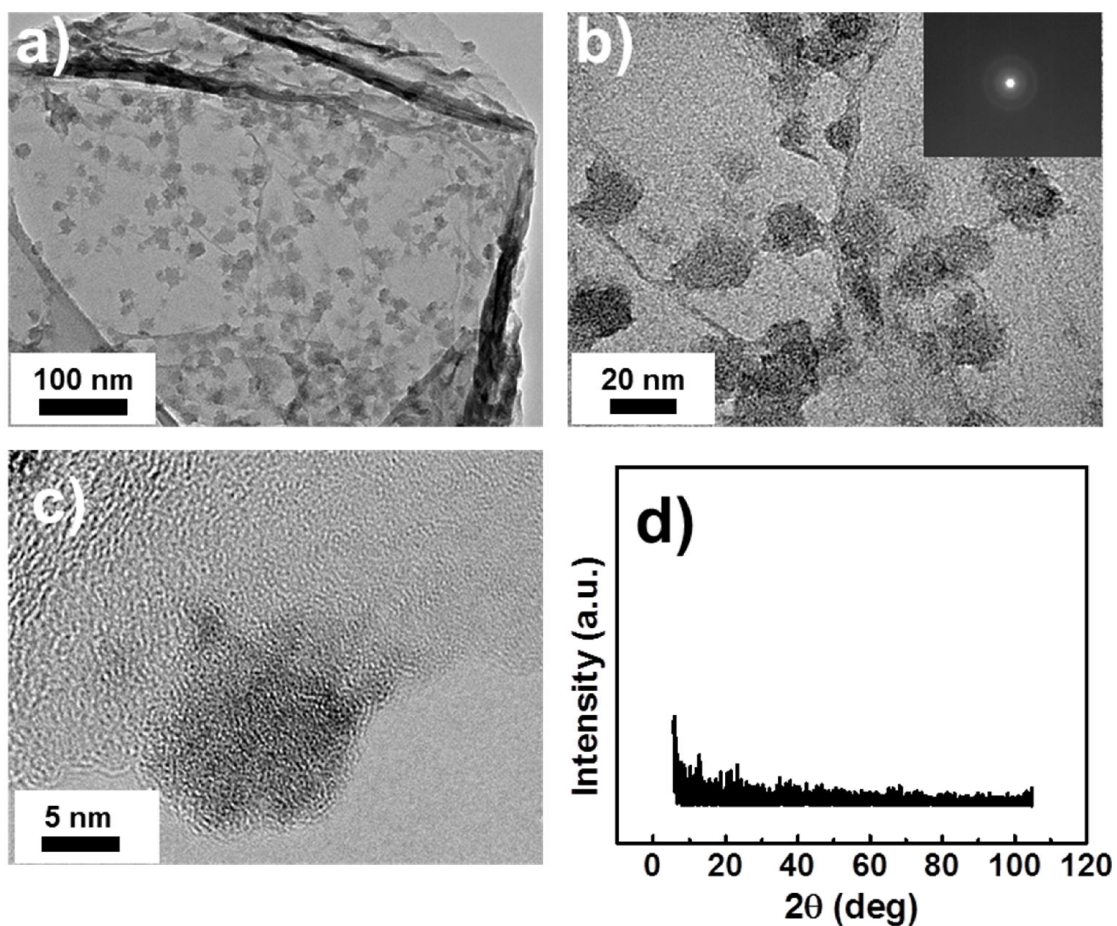
Figure 7-8: (a,b) TEM images, (c) high resolution TEM image, (d) XRD pattern and (b-inset) SAED pattern of CoSG-120. Reproduced in adapted form from [253], with permission of the Royal Society of Chemistry.

Drawing on these observations, a schematic outlining the crystal phase transformations and growth occurring on the surface of graphene during the solvothermal reaction is provided in **Figure 7-9**. It can also be seen that at increasing reaction times, the structure of the graphene substrates gradually evolve. Initially this material shows a relatively smooth, sheet-like structure (**Figure 7-6a, 7-7a**). Throughout the reaction process

and associated to the reduction of GO, the substrate takes on a wrinkled configuration with increasing amounts of edge plane exposure (**Figures 7-6b, c** and **d; 7-7b, c** and **d**).

Figure 7-9: Proposed growth schematic of CoS$_2$ octahedron nanoparticles supported on nitrogen and sulfur doped graphene. Reproduced in adapted form from [253], with permission of the Royal Society of Chemistry.

With the formation and growth process of octahedral CoS$_2$ nanoparticles elucidated, of particular importance in the present work is also the reduction and simultaneous doping (*i.e.,* nitrogen and sulfur) processes occurring in the nanostructured carbon supports. Because the presence of CoS$_2$ nanoparticles on the surface of the nanostructured carbon supports will confound the results of these spectroscopic investigations, graphene, CNT and CNT/graphene composite samples were prepared under the same reaction conditions, albeit in the absence of a cobalt precursor. These samples were found to be doped with both nitrogen and sulfur, and are therefore referred to as NS-G, NS-C and NS-CG, respectively.

The absence of cobalt precursor had a negligible impact on the microstructure of the obtained materials, with SEM images of NS-G, NS-C and NS-CG provided in **Figure 7-10a**, **b** and **c**, respectively. These materials demonstrated a very similar structure to those prepared with cobalt precursor, although as expected, without CoS_2 octahedron nanoparticles decorated on the surface. XPS was used to confirm the successful reduction of GO during the solvothermal process, with the oxygen surface content of NS-G quantified to be 7.21 at. %, significantly lower than the ca. 35 at. % commonly reported for GO[179].
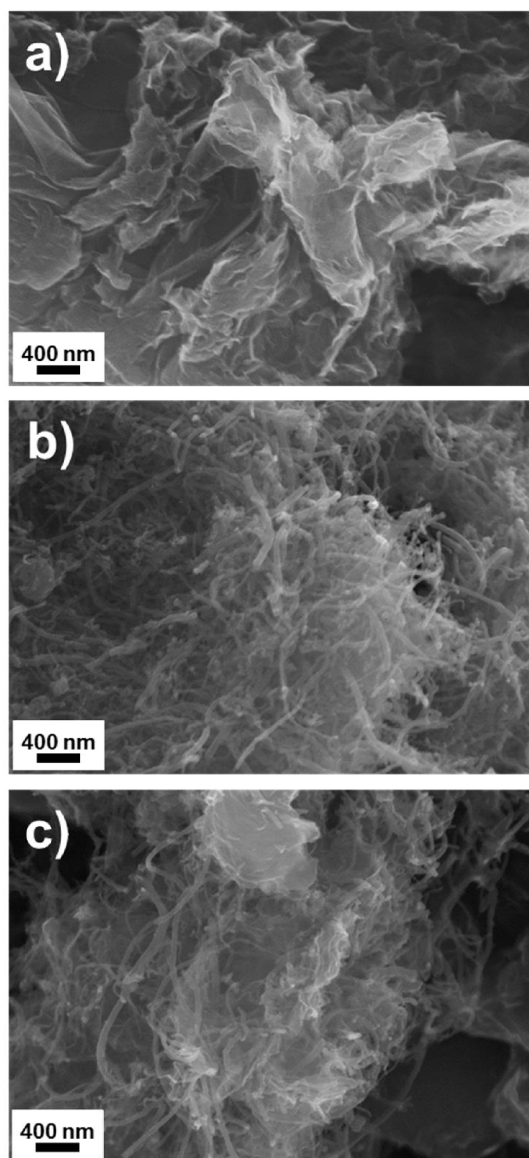
Figure 7-10: SEM images of (a) NS-G, (b) NS-C and (c) NS-CG. Reproduced in adapted form from [253], with permission of the Royal Society of Chemistry.

High resolution S2p and N1s spectra for the nitrogen/sulfur-doped nanostructured carbon supports are provided in **Figure 7-11**. The obtained signals indicate that the solvothermal procedure used in the present work were capable of incorporating both sulfur and nitrogen heteroatom dopants into the CNT/graphene materials. Double doping of

nanostructured carbons with more than one element has been reported before, commonly accomplished by high temperature heat treatment processes in the presence of heteroatom containing precursors.[301, 305] Reports on double doping by hydrothermal or solvothermal processes however are very rare,[306, 307] and to the best of our knowledge, only one report exists for the double doping of graphene or CNT structures with nitrogen and sulfur by hydro/solvothermal procedures.[308] NS-G was found to have the highest concentration of sulfur and nitrogen dopants within the structure, with a surface concentration of 2.98 and 2.75 at. %, respectively. This likely arises due to the highly tunable surface structures of GO, containing an abundance of oxygen-containing functional species that can serve as reactive sites for heteroatom incorporation[297]. For NS-C, the sulfur and nitrogen contents were lower at 0.71 and 0.95 at. %, respectively, indicating the incorporation of heteroatom species into functionalized CNTs by "post-treatment" methods is relatively more difficult, an observation consistent with previous investigations[301, 309]. The sulfur and nitrogen contents of NS-CG (0.68 and 1.09 at. %, respectively) were similar to that of NS-C, suggesting that the majority of XPS signal arises from the CNT constituent assembled on the surface of graphene sheets in the composite arrangement.
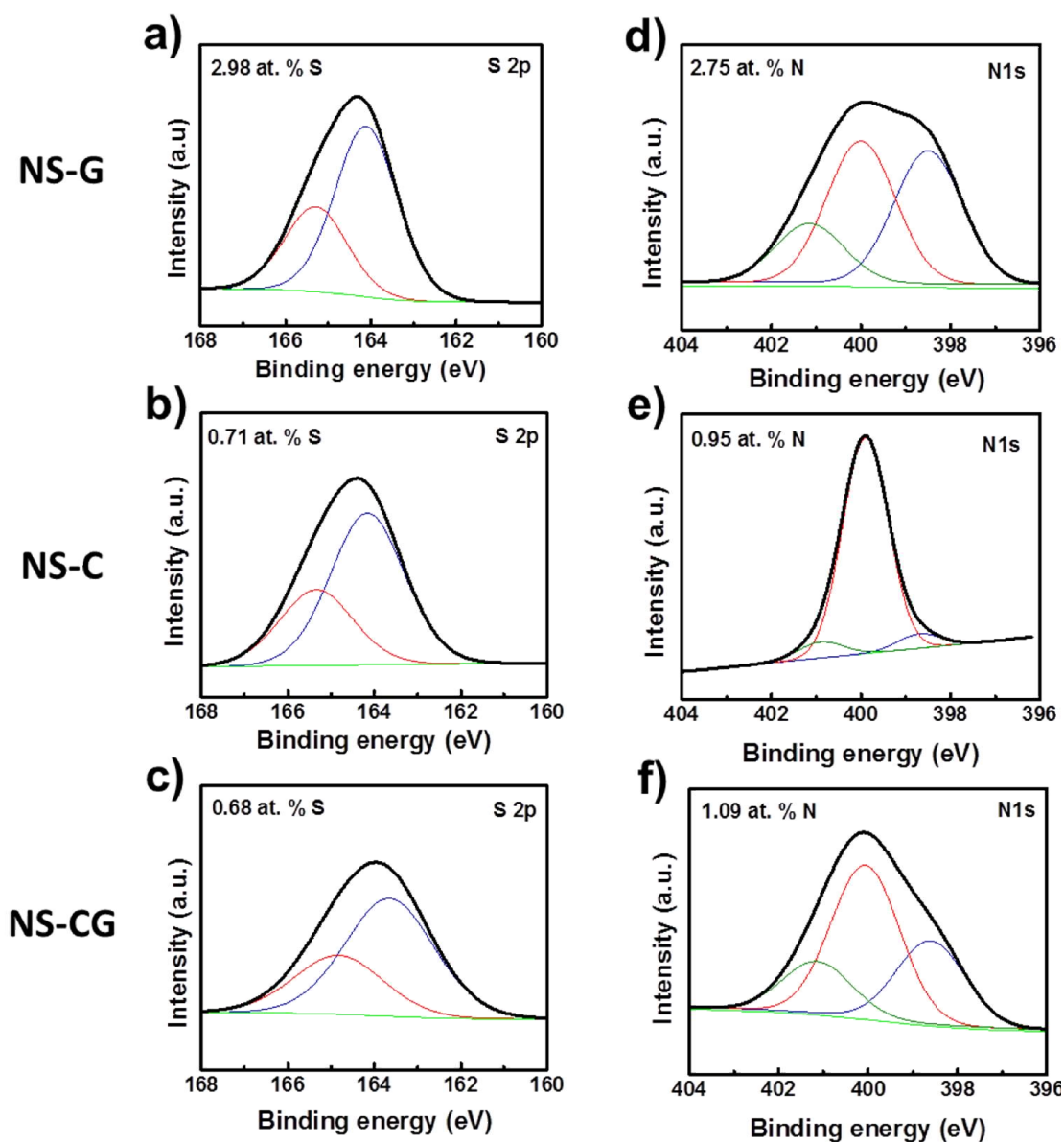
Figure 7-11: High resolution XPS (a-c) S2p and (d-f) N1s spectra for NS-G, NS-C and NS-CG. Reproduced in adapted form from [253], with permission of the Royal Society of Chemistry.

The S2p spectra of all three materials (**Figure 7-11a, b** and **c**) could be deconvoluted into the $S2p_{1/2}$ and $S2p_{3/2}$ doublet peaks of thiophenic sulfur, located at 164.1 and 165.3 eV, respectively.[39, 310] Thiophenic sulfur species reside on the edge plane of

graphene/CNT in a 5-membered heterocyclic ring arrangement. The N1s spectra of each sample was deconvoluted intro three individual contributions arising from pyridinic (ca. 398.6 eV), pyrrolic (400.1 eV) and graphitic (401.2 eV) nitrogen species [214, 311]. NS-G (**Figure 7-11d**) was comprised of mainly pyrrolic nitrogen species, however both pyridinic and graphitic nitrogen was observed in sufficient quantities. On the other hand, almost all of the nitrogen atoms scanned in NS-C (**Figure 7-11e**) were of pyrollic form, residing on edge plane of the CNTs and bonded to carbon in a 5-membered ring arrangement. It appears that the incorporation of pyridinic or graphitic nitrogen species into the 6-membered ring structures of CNTs is difficult at the relatively low (220 $^{\circ}$C) temperature used during the solvothermal synthesis. At higher temperatures (i.e. > 800 $^{\circ}$C) it has been well established that the pyridinic species are not as stable, at which conditions increased relative graphitic nitrogen contents are commonly observed.[180, 312] The N1s spectra of NS-CG (**Figure 7-11f**) indicates that pyrrolic nitrogen species are still dominant in the composite arrangement, although small peaks arising from graphitic and pyridinic nitrogen species are observed, most likely arising from the underlying doped graphene sheet structures.

The complex reaction mixture consisting of multiple organic and inorganic species, in combination with the "black box" nature of solvothermal syntheses renders *in situ* monitoring and speciation to elucidate the exact mechanistic process of material preparation very difficult. Notwithstanding these challenges, based on fundamental information available in the literature and results of our *ex situ* experimental results, we propose a mechanism for the fabrication of nitrogen and sulfur-doped graphene supported

CoS_2 octahedrons. After reacting solvothermally for 10h at 120 ^{o}C, amorphous particles were observed decorated on the surface of GO sheets (**Figure 7-8**). This most likely consists of Co-based intermediates (i.e. oxides, carbonates or hydroxides) formed through the decomposition of cobalt acetate,[313] and nucleated on the oxygen containing functional sites of GO owing to the favourable interactions of these species with inorganic nanoparticles.[283]

When the solvothermal reaction temperature is increased to 220 ^{o}C, this exceeds the decomposition temperature of thiourea (ca. 187 ^{o}C), a process that generates primarily ammonia, carbon disulfide and thiocyanic acid as the byproducts.[314] Owing to the isomeric complexity of thiourea with numerous potential decomposition intermediates and reaction pathways,[315] it is also likely that under the solvothermal reaction conditions the formation of other sulfur-containing species can occur. One such species is hydrogen sulfide, which has interestingly been attributed as a sulfur source for cobalt sulfide formation,[316] however is not a commonly observed species during the thermal decomposition of thiourea.[314, 317] Regardless, when the reaction temperature is increased to 220 ^{o}C, the decomposition of thiourea is evidenced by transformation of the solution colour to yellow, which becomes more pronounced at increasing reaction times (**Figure 7-12**). After 30 min at 220 ^{o}C, only slight discolouration of the solvothermal solution is observed (**Figure 7-12b**) and amorphous Co-based nanoparticles comprise the majority of species in existence on the surface of the graphene sheets (**Figure 7-6a**). This provides indication that the entire reaction mixture has not reached a uniform temperature of 220 ^{o}C, and/or the

decomposition of thiourea and the CoS_2 formation reactions did not have enough time to proceed.
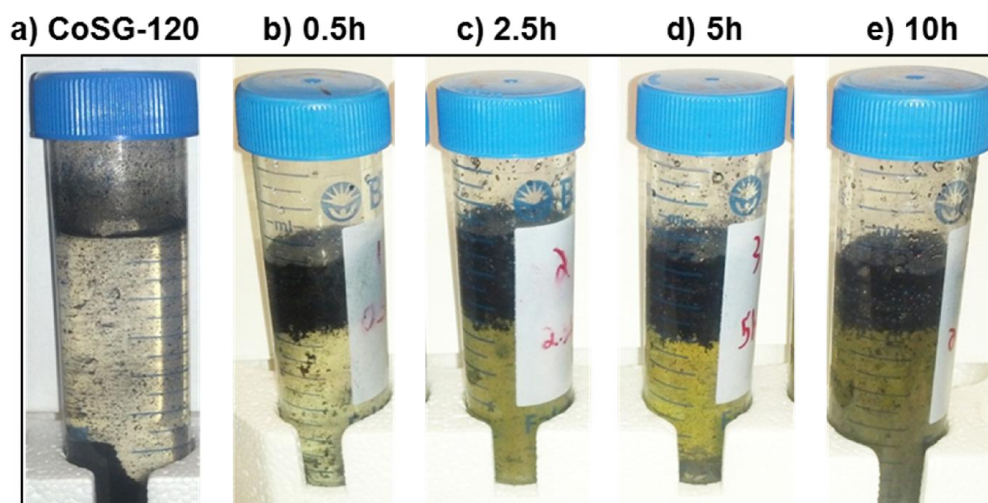
Figure 7-12: Solution obtained after solvothermal synthesis for (a) CoSG-120 and CoS₂ supported on graphene reaction mixture materials held at 220 °C for (b) 0.5 h, (c) 2.5 h, (d) 5 h and (e) 10 h. Reproduced in adapted form from [253], with permission of the Royal Society of Chemistry.

Once the thiourea species have a sufficient reaction temperature and time to decompose, the high concentration of available sulfur-containing intermediates will attach the amorphous nanoparticles decorating the graphene surface. This results in the formation or irregularly shaped CoS_2 particles that are observed after holding the reaction temperature at 220 ^{o}C for 2.5 h (**Figure 7-6b**). At increased reaction times, more CoS_2 species continue to form and Ostwald ripening processes comprise the subsequent structural transformations observed. During this time period, inhomogeneous CoS_2 species migrate and rearrange to form single crystal octahedral structures encased by the {111} crystal facets. This morphology likely forms as it the most thermodynamically stable structure due to the

relatively low surface energy of the (111) surface in comparison to other CoS_2 surface structures as predicted by theoretical simulations (*vide infra*).

In terms of the graphene based supports, it is not only expected that the covalently bonded oxygen functional species in GO play a crucial role in Co-based nanoparticle nucleation and growth,[283] but also serve as anchoring sites for the incorporation of heteroatom dopant species.[297] As a primary product of thiourea decomposition, ammonia (NH_3) species will be formed within the solvothermal reaction vessel. NH_3 is commonly used as a precursor for the simultaneous nitrogen doping and reduction of GO materials by annealing treatments,[179, 180, 301, 312] and more recently by hydro/solvothermal methods.[318, 319] Additionally, EG is a well-known reducing agent for GO during solvothermal synthesis,[320] and in tandem with NH_3 results in the effective reduction and nitrogen doping of the graphene supports. On the other hand, identification of the exact sulfur containing intermediate(s) formed during thiourea decomposition that are responsible for sulfur doping of graphene requires further, more stringent fundamental investigations.

ORR polarization plots for all of the prepared samples in 0.1 M $HClO_4$ and at an electrode rotation speed of 1600 rpm are provided in **Figure 7-13a**, with onset potential and half-wave potential ($E_{1/2}$) values summarized in **Table 7-1** versus the RHE. Linear potential sweeps at electrode rotation speeds varying from 100 to 2500 rpm are provided for CoS_2-CG in **Figure 7-13b**, and for CoS_2-G in **Figure 7-14a**, CoS_2-C in **Figure 7-14b** and as-prepared CoS_2 in **Figure 7-14c**. All of the nanostructured carbon supported CoS_2 octahedron catalysts displayed similar ORR onset potentials, suggesting that the active site structures present in these catalysts are the same. The unsupported, as-prepared CoS_2

materials demonstrated an on-set potential that was ca. 40-60 mV lower, along with reduced ORR current densities throughout almost the entire potential range investigated. The reduced performance of as-prepared CoS_2 can likely be linked to the large agglomerate structure of the catalyst, with ORR activity resembling that reported previously for a CoS_2 thin film structure.[264] The increased onset potential of the carbon supported CoS_2 octahedrons could also arise due to the more favourable adosprtion energy of oxygen on the (111) surface of CoS_2 in comparison to the (001) and (110) surfaces, as determined from our theoretical simulations *vide infra*. The supported octahedrons consist of only {111} surface facets, which could therefore be advantageous for ORR kinetics in comparison to the unsupported CoS_2 agglomerates consisting of a mix of various surface structures. Additionally, the minor presence of the CoS phase as illustrated by XRD within the unsupported CoS_2 could provide an impact on ORR performance, albeit to an unknown extent.
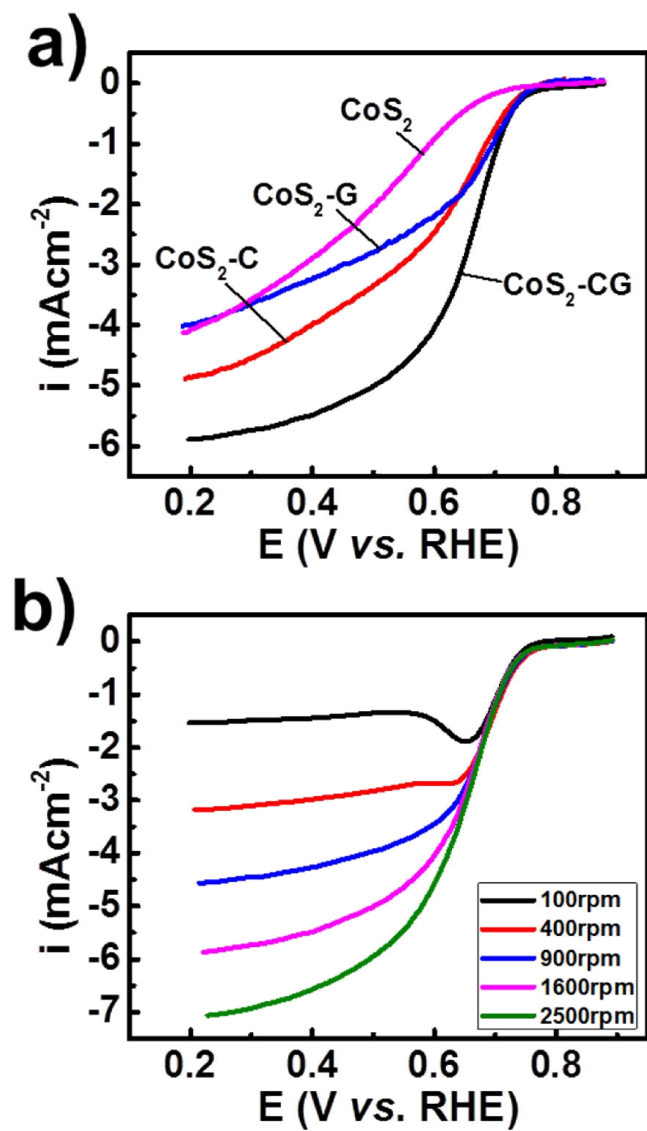
Figure 7-13: ORR polarization curves (a) at 1600 rpm for all samples, and (b) at various electrode rotation rates for CoS₂-CG. Reproduced in adapted form from [253], with permission of the Royal Society of Chemistry.

Table 7-1: Electrochemical performance evaluation results. Reproduced in adapted form from [253], with permission of the Royal Society of Chemistry.

Parameter (V *vs.* RHE)	CoS$_2$-CG	CoS$_2$-G	CoS$_2$-C	CoS$_2$
Onset potential[a]	0.78	0.76	0.76	0.72
E$_{1/2}$	0.66	0.64	0.61	0.51

[a]Taken as the potential that the current density reaches 0.1 mAcm^{-2}.
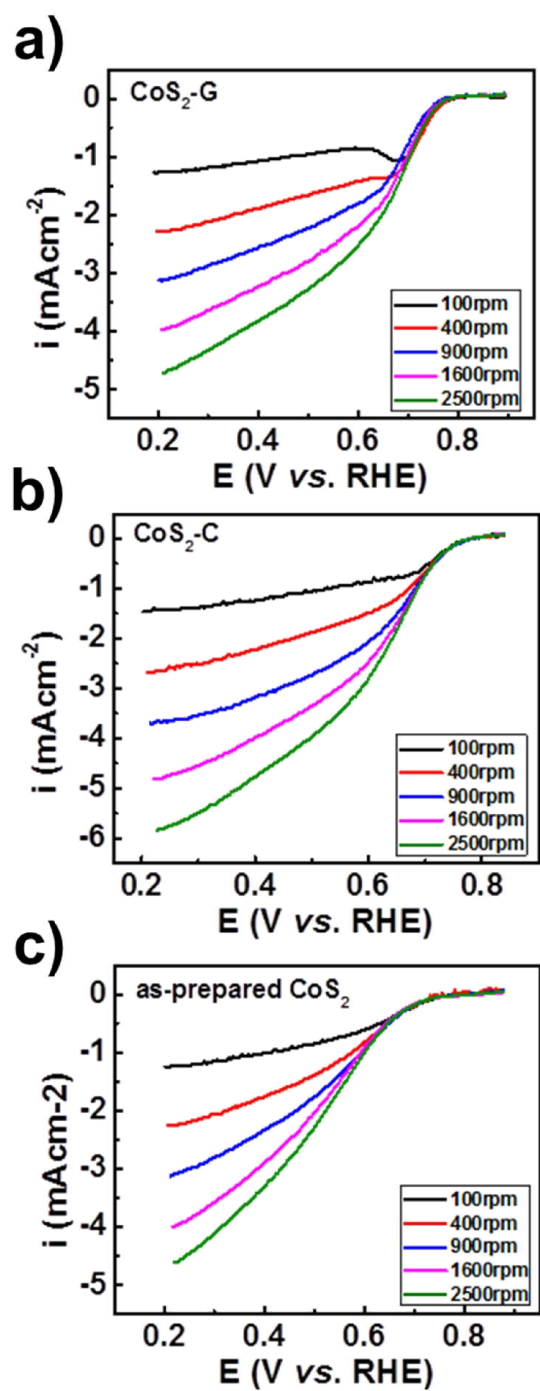
Figure 7-14: ORR polarization curve for (a) CoS₂-G, (b) CoS₂-C and (c) CoS₂ at various electrode rotation rates. Reproduced in adapted form from [253], with permission of the Royal Society of Chemistry.

It is clear that the incorporation of nanostructured carbon supports into the solvothermal reaction mixture can facilitate the formation of single crystal, shape controlled octahedral CoS_2 nanoparticles immobilized within a conductive network that can provide significant ORR performance enhancements. Of the three materials investigated, CoS_2-CG provides the best ORR performance, with a polarization curve resemblant of high ORR activity catalysts, demonstrating a current density that levels off at lower electrode potentials owing to the onset of mass transport limitations. Comparing the performance of CoS_2-G and CoS_2-C can provide some understanding regarding the impact of nanostructured carbon support type on ORR activity. Interestingly, CoS_2-G demonstrates slightly higher current densities at high electrode potentials (> 0.63 V *vs*. RHE). In this region, ORR kinetics play a dominant role in the observed catalyst performance, which can likely be attributed to the increased dispersion of well-defined CoS_2 octahedral crystals with smaller average sizes on CoS_2-G. This in turn provides a larger number of ORR active sites in order to facilitate the electrochemical reduction. Additionally, the increased nitrogen and sulfur dopant concentrations in the nanostructured carbon support for CoS_2-G could provide favourable catalyst-support interactions that beneficially influence ORR kinetics, similar to the effect commonly observed in Pt/doped-carbon catalyst systems.[17, 39, 279] At potentials below ca. 0.63 V *vs*. RHE, CoS_2-C provides relatively higher current densities that CoS_2-G. This can most likely be attributed to the highly porous, interconnected catalyst layer structures formed by one-dimensional CNTs. This provides ample pathways for electronic conductivity and access for O_2 reactant molecules, contributing to the increased current densities observed in the potential region that transport (electronic/reactant) properties play a dominant role.

The half-wave potential for CoS_2-CG is 0.66 V *vs*. RHE, a ca. 20 and 50 mV improvement over that of CoS_2-G and CoS_2-C, respectively. Additionally, Koutecky-Levich analysis[214, 255] indicated excellent selectivity towards the overall four electron ORR mechanism, with the number of electrons calculated to be greater than 3.7 over the entire range of potentials investigated. All of these results indicate that the microstructure of CoS_2-CG provides an ideal balance of inherent ORR active site structure density and turnover frequency, along with reactant access. This likely arises due to the complementary contributions of each component, whereby the graphene provides excellent octahedral nanoparticle dispersion owing to the high surface areas and ease of functionalization, and CNTs provide highly interconnected, conductive and porous morphologies that can facilitate the rapid access of electrons and oxygen throughout the entire catalyst layer. This notion is supported by the results of Brunauer–Emmett–Teller (BET) analysis, indicating a surface area of 123.9 m^2 g^{-1} for CoS_2-CG, which is higher than CoS_2-C (96.1 m^2 g^{-1}) yet lower than CoS_2-G (150.0 m^2 g^{-1}). The advantages of this synergistic arrangement have also been previously demonstrated for ORR activity in alkaline electroytes[318, 321, 322], solar cell,[323] lithium-ion battery[324] and supercapacitor[325-327] applications. Drawing on this, CoS_2-CG demonstrates a half-wave potential that is comparable to several precious metal (i.e. Ru) based chalcogenide materials reported previously.[328] Further comparison can be made to the most active non-precious metal chacogenide reported previously,[263] consisting of $Co_{1-x}S$ particles supported on reduced GO ($Co_{1-x}S$/RGO) and prepared by a two-step synthesis method employing a heat treatment process. CoS_2-CG demonstrates a comparable onset potential, although provides a current density of 1.3 $mAcm^{-2}$ at an electrode potential of 0.7 V vs. RHE, an over 15% improvement in comparison to $Co_{1-x}S$/RGO (1.1 $mAcm^{-2}$).

Combined with a simplistic preparation process, shape controlled CoS$_2$ octahedron nanoparticles supported on nitrogen and sulfur doped CNT/graphene composites comprises the best performance non-precious metal chalcogenide ORR catalyst reported to date.

Figure 7-15 shows the fully relaxed bulk CoS$_2$ structure. After stabilization, the lattice parameters of CoS$_2$ were evaluated to be 5.505, 5.505 and 5.505 Å, consistent with previous experimental work[329] and theoretical diffraction pattern data. From the bulk structure of CoS$_2$, slab models for the (111), (001) and (110) surfaces were designed as shown in Figure 7-16a, b and c, respectively. During model relaxation, we allowed the upper layers to relax, while maintaining the bottom five layers fixed in their bulk positions. The surface energy per unit area (σ) was calculated by Equation 7-1:

$$\sigma = \frac{1}{A}[E_{slab} - nE_{bulk}] \qquad (1)$$

Here, E$_{slab}$ is the total energy of a slab with CoS$_2$ layers and E$_{bulk}$ is the reference total energy per unit area of the bulk system. For the (111), (001) and (110) surfaces, the surface energies were evaluated to be 0.836, 1.497 and 1.328 J m^{-2}, respectively. It is clearly seen that the order of thermodynamic stability for the relaxed surfaces of CoS$_2$ are in the order of (111) > (110) > (001). Therefore, the CoS$_2$ octahedron morphology, encapsulated by (111) surfaces as confirmed by SAED and high resolution TEM imaging, is very likely a result of surface energy minimization occurring through the solvothermal synthesis.
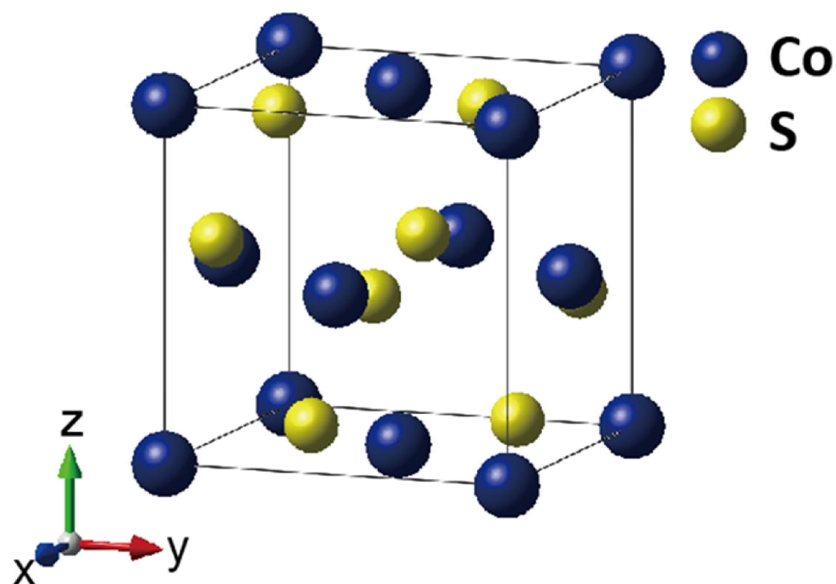
Figure 7-15: Fully relaxed bulk CoS$_2$ structure. Reproduced in adapted form from [253], with permission of the Royal Society of Chemistry.

We then wanted to investigate the chemical adsorption energies of atomic oxygen on the various CoS$_2$ surface structures. It is well known that the binding strength of adsorbates play an important role governing ORR activity. This is due to the Sabatier principle that states that catalytic reaction rates are favourable when there exists an appropriately moderate interaction between the adsorbate species and the catalytically active surface.[330-332] **Figures 7-16d**, **e** and **f** illustrate the oxygen adsorption sites on the (111), (001) and (110) surface structures of CoS$_2$, respectively. The adsorption energy (E$_{ads,O}$) was then calculated according to Equation 7-2:

$$\Delta E_{ads,O} = E_{O-CoS_2} - E_O - E_{CoS_2} \qquad (7\text{-}2)$$

Here, E_{O-CoS2}, E_O and E_{CoS2} are energies of the CoS_2 surface with adsorbed oxygen, the isolated oxygen atom and a clean CoS_2 surface, respectively. The adsorption energies of oxygen (ΔE_{ads}) were evaluated to be -3.940, -3.928 and -5.297 eV for the (111), (001) and (110) surfaces of CoS_2, respectively. Taking into account the E_{ads} value of -4.36 eV for oxygen on a bulk Pt(111) surface (calculated for a 1/4 monolayer of oxygen on a (2 × 2) unit cell, and consistent with values previously reported in the literature[20, 333]), significantly weaker oxygen adsorption in observed on the (111) and (001) surfaces of CoS_2, whereas significantly stronger oxygen adsorption is observed on the (110) surface. Regardless, the (111) surface of CoS_2 has an oxygen adsorption energy that is closest to the optimal value of ca. -4.08 eV, that can be achieved on Pt_3Ni surfaces.[20] This highlights that the (111) surface of CoS_2 can provide the highest activity towards the ORR among others investigated, and can serve to explain the relatively excellent performance of the {111} facet encased octahedrons observed through RDE evaluation.
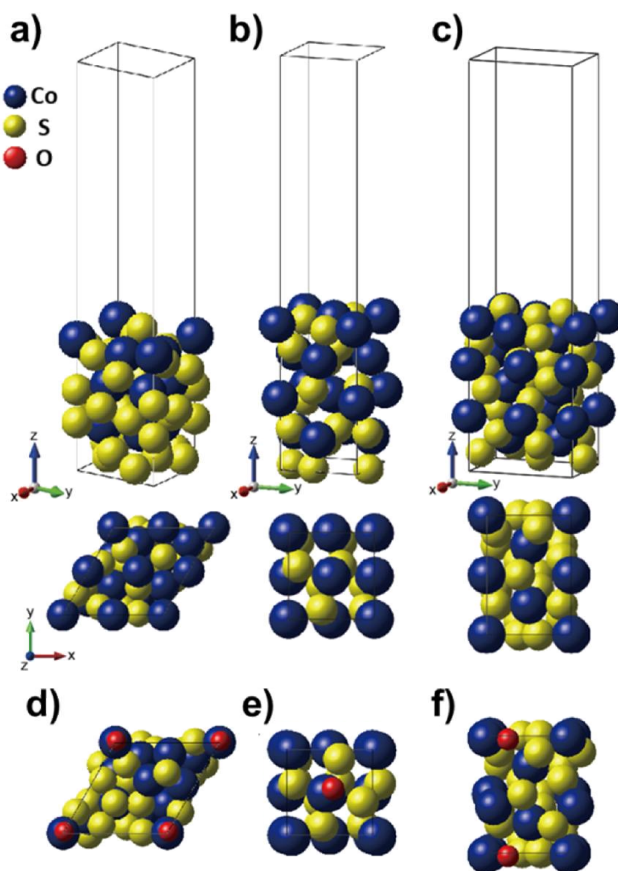
Figure 7-16: Slab models of CoS$_2$ with the (a) (111), (b) (001) and (c) (110) surfaces. Oxygen adsorbed on the (d) (111), (e) (001) and (f) (110) surfaces. Reproduced in adapted form from [253], with permission of the Royal Society of Chemistry.

7.4 Conclusions

Using a one-pot solvothermal technique, CoS$_2$ octahedra nanoparticles supported on nitrogen and sulfur doped graphene, CNTs or a graphene/CNT composite were prepared. The incorporation of these nanostructured carbon supports into the reaction mixture was essential for achieving excellent CoS$_2$ phase purity and well-defined octahedra nanoparticles encased by the {111} facets. The growth of the CoS$_2$ nanoparticles was investigated by a time-dependent study, and was found to occur first by amorphous

nanoparticle formation, followed by the continuous evolution into single crystal octahedral achieved after 10 hours of reaction time at 220 $^{\circ}$C. This evolution is very likely thermodynamically driven, owing to computational simulations revealing that the (111) surface of CoS_2 possesses a significantly lower surface energy than (001) and (110). The simultaneous reduction and doping of the GO and HNO_3-CNT precursors was probed by conducting control experiments in the absence of the cobalt precursors. After the solvothermal reaction, the nanostructured carbon supports were doped with nitrogen and sulfur hetero-atoms, primarily in the pyrollic and thiophenic forms, respectively. Electrochemical half-cell testing in 0.1 M $HClO_4$ revealed that CoS_2-CG provided an ORR on-set and half-wave potential of 0.78 and 0.66 V *vs*. RHE, respectively. The performance was higher than that of CoS_2-C and CoS_2-G, highlighting the synergistic benefits of using the graphene/CNT composite arrangements as a support material. Significantly improved ORR activity of CoS_2-CG was also observed in comparison to the CoS_2 nanoparticle agglomerate structured formed when no nanostructured carbon supports were included in the reaction mixture. These performance likely arise due to the theoretical calculations that indicate a more favourable adsorption energy of oxygen on the (111) surface of CoS_2 that the octahedral are composed of. By coupling the synergistic effects of the graphene/CNT composite support with the well-dispersed {111} facet terminated single crystal octahedral nanoparticles, CoS_2-CG is presented as the most active transition metal-chalcogenide towards the ORR reported to date.

8. Conclusions and future work

8.1 Summary and conclusions

The objectives of the present thesis are to independently deliver both platinum catalysts and non-PGM catalysts with high ORR that can be coupled together into reduced platinum electrode configurations for PEFC cathodes. This approach is being taken in an attempt to reduce the overall platinum requirement of PEFC systems and lower system costs to levels that are economical for transportation applications. The hypothesis is that combining high activity platinum (or platinum alloy) catalysts can reduce activation losses, while the non-PGM catalyst can be used both as a scaffold to support the platinum, and to provide high current and power densities in the intermediate voltage range.

In Chapter 4, platinum nanoparticles supported on newly developed core-shell TiN-CNT composites were prepared. The materials were rigorously characterized both physicochemically and electrochemically to determine their activity towards the ORR. Improved performance in comparison to commercial Pt/C catalyst was observed, attributed to the one-dimensional structure of the composites, and also speculated to arise due to catalyst-support interactions between the titanium nitride and platinum nanoparticles. While titanium nitride is commonly considered a very stable material, under electrochemical conditions it has recently come to light that a thin, passivating layer of titanium oxide will be formed on the surface. Therefore while the activity of these materials was good, detrimental performance loss will occur under PEFC operative conditions.

To overcome this issue of catalyst support corrosion, unsupported platinum cobalt alloy nanowires were prepared by a microwave assisted solvothermal procedure as described in Chapter 5. Cobalt was chosen as an alloying element owing to its ability to fine tune the adsorptive properties of platinum and induce dramatic ORR activity enhancements. The prepared Pt-Co-NWs demonstrated excellent activity towards ORR through half-cell testing. Most notably, excellent electrochemical stability was found for these materials by employing a half-cell electrochemical ADT experiments. A negligible loss in ORR activity occurred after 1000 CV cycles from 0 to 1.5 V vs. RHE at 50 °C, conditions that are very harsh. This activity retention was superior to that of commercial Pt/C and Pt-B. The main challenge remaining with these materials was that the solvothermal synthesis procedure offered very little flexibility in terms of nanowire composition and size. The Pt-Co-NWs were relatively thick (40-70 nm) resulting in inaccessible platinum atoms within the bulk that would effectively reduce ORR activity on a precious metal basis.

Chapter 6 adopted the electrospinning technique to prepare PtCoNWs. An optimal synthesis "recipe" was developed, with the ability to fine tune the nanowire diameters and compositions achieved by varying the fabrication parameters. The developed PtCoNWs were found to provide excellent activity and stability towards the ORR in acidic electrolytes. The beneficial impact of alloying with cobalt was exclusively demonstrated by comparing the activity of PtCoNWs with PtNWs. More than four-times higher Pt mass-based activities at 0.9 V vs. RHE was achieved with the incorporation of Co. A dramatic ~7-fold improvement in specific activity (based on ECSA) over commercial Pt/C was

achieved for PtCoNWs. Improved ECSA retention through ADT potential cycling was also observed. While it is likely that further mass activity improvements can be achieved, these PtCoNWs can be reliably and inexpensively prepared for MEA integration with non-PGM catalysts.

The development of non-PGM catalysts is described in Chapter 7. Shape controlled CoS_2 octahedra nanoparticles supported on nitrogen and sulfur doped carbon supports were prepared by a one-pot solvothermal technique. The carbon supports investigated were graphene, CNTs or a graphene/CNT composite. A time dependent study was employed to investigated the growth process of the CoS_2 into octahedral nanoparticles with preferential (111) surface exposure. Electrochemical half-cell testing showed that CoS_2-CG could achieve an ORR on-set and half-wave potential of 0.78 and 0.66 V *vs.* RHE, respectively. The synergistic benefits of using the graphene/CNT composite arrangements as a support material was clear, with inferior performance observed for CoS_2-C and CoS_2-G. These materials, prepared using a very straightforward process are the most ORR active transition metal-chalcogenides reported to date and can be composited with PtCoNWs for MEA integration investigations.

8.2 Proposed future work

It is recommended that future projects are rationally designed to leverage the progress and catalyst technologies realized throughout the present thesis. These projects should focus on: (i) rigorously investigating and understanding the operational durability of the PtCoNWs and CoS_2-CG catalysts under PEFC conditions and elucidate mechanistic pathway(s) of performance loss; (ii) further optimization of developed catalyst properties to

improve activity and mitigate the occurrence of the aforementioned degradation mechanisms; and most importantly (iii) integration of PtCoNWs and CoS_2-CG catalysts into hybrid electrode configurations for practical PEFC demonstration.

(i) Rigorous durability investigations

With the preparation process and physicochemical properties of the developed catalyst technologies well established, it is highly desirable to rigorously evaluate the durability capabilities. Initial studies should include half-cell ADT procedures (such as those employed throughout this thesis), with the testing conditions systematically varied to investigate their effect on the catalytic activity and structures. For example, CoS_2-CG should be subjected to ADT at varying conditions, such as from 0.2 to 1.0 V vs. RHE under oxygen saturated electrolyte to investigate the dissolution of the CoS_2 octahedra nanoparticles, and at potential values higher than 1.0 V vs. RHE to elucidate corrosion of the graphene/CNT composite support materials.

The different ADT protocols should be coupled with post testing characterization of the catalyst materials. Catalyst samples can be collected from the working electrodes and analyzed using the array of physicochemical characterization techniques used throughout this thesis, in addition to any further techniques deemed appropriate for elucidating physical and chemical changes to the catalysts. For example, PtCoNWs subjected to different ADT protocols designed to induce different degradation pathways can be investigated by TEM to understand structural changes to the nanowires (*i.e.,* diameter reduction) and EDX colour mapping to elucidate dissolution of the cobalt and changes to

the atomic distribution of the nanowires (*i.e.,* formation of a platinum shell). By rigorously investigating catalyst stability and the mechanisms of performance loss, new strategies can be designed to mitigate these occurrences and increase electrochemical stability.

(ii) Further electrocatalyst optimization

While the studies presented throughout this thesis were systematic in nature, there is still opportunity for the different catalyst technologies developed to achieve further activity and stability improvements. Looking at PtCoNWs, the electrospinning procedure is ideal because it allows for deliberate tuning of nanowire properties. This paves the way for very fundamental investigations directed at understanding the impact of diameter, composition and atomic distribution on both electrochemical activity and stability. Particularly, it is highly expected that further mass activity improvements can be achieved by careful control of the morphology (*i.e.,* diameter) and atomic compositions of the PtCoNWs. An appropriate design of experiment can further our understanding of the preparation parameters and allow for development of well controlled PtCoNWs that can be investigated for activity and durability. The fundamental insight generated throughout these studies can be used in tandem with insight obtained from the previously mentioned durability investigations to apply rational design strategies to optimize the catalysts. For the CoS_2-CG catalysts, methods to improve activity and stability can include the development of techniques to reduce the size of the CoS_2 octahedra, and by optimization of the graphene to CNT ratios in the catalyst support composites.

(iii) Hybrid electrode and membrane electrode assembly integration

From a practical standpoint, integration of the PtCoNWs and CoS_2-CG catalysts into operational hybrid electrode structures is the ultimate objective. This will allow researchers to translate the success in this project towards real world applications, in particular PEFCs for automotive applications. It is suggested that hybrid electrode integration studies first involve optimization of the catalyst layer preparation by systematically investigating the impact of catalyst ink solvent, concentrations and deposition method (*i.e.*, painting, spraying, decal) on MEA performance. Once established, the foundation is set for an engineering approach to the design of hybrid electrodes. The electrode thickness, catalyst loading and PtCoNW to non-PGM catalyst ratios can be varied to determine the impact on resulting PEFC performance. An interesting strategy that may be beneficial is to have a platinum loading in the catalyst layer that varies with electrode thickness (**Figure 8-1**). With a gradient distribution of platinum, improved performance may be realized by achieving almost complete platinum utilization. Understanding and controlling the electrode structure and properties will also allow for performance improvements. By correlating structural characterizations of the hybrid electrodes to MEA performance data, the impact of porosity, ionomer distribution and electrode interconnectivity can be elucidated. This knowledge will be the first of its type for platinum/non-PGM hybrid electrodes, with the potential to change conventional approaches for MEA fabrication.
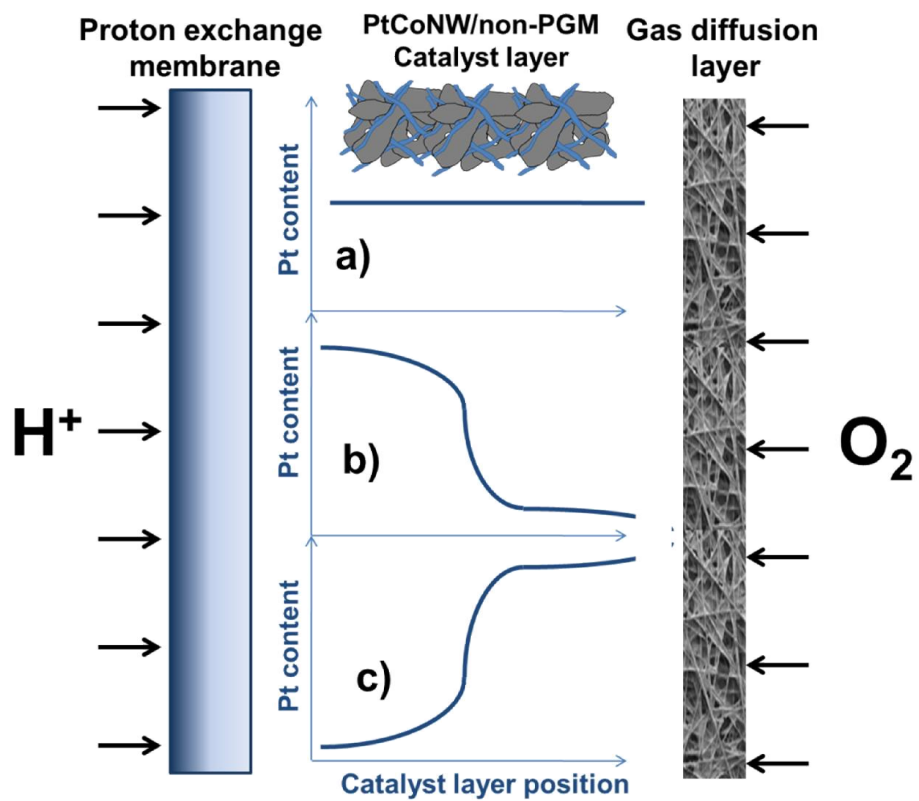
Figure 8-1: Method of integrating PtCoNWs and non-PGM catalysts into hybrid electrode structures for MEA evaluation.

References

1. B. G. Pollet, I. Staffell, J. L. Shang (2012) "Current status of hybrid, battery and fuel cell electric vehicles: From electrochemistry to market prospects", *Electrochimica Acta*, **84**, 235-249.

2. B. C. H. Steele, A. Heinzel (2001) "Materials for fuel-cell technologies", *Nature*, **414**, 345-352.

3. Kitco (2015) "Multi Year Platinum Pricing". Available online at: http://www.kitco.com/scripts/hist_charts/yearly_graphs.plx.

4. J. Moton B. James, W. Colella (2014) "U.S. Department of Energy's 2014 Annual Merit Review and Peer Evaluation Meeting Presentation. Fuel cell transportation cost analysis". Available online at: http://www.hydrogen.energy.gov/pdfs/review14/fc018_james_2014_o.pdf.

5. M. K. Debe (2012) "Electrocatalyst approaches and challenges for automotive fuel cells", *Nature*, **486**, 43-51.

6. R. Borup, J. Meyers, B. Pivovar, Y. Kim, R. Mukundan, N. Garland, D. Myers, M. Wilson, F. Garzon, D. Wood (2007) "Scientific aspects of polymer electrolyte fuel cell durability and degradation", *Chemical reviews*, **107**, 3904-3951.

7. J. Larminie, A. Dicks, Knovel (2003) "Fuel cell systems explained, Second Edition", John Wiley & Sons Ltd, West Sussex, England.

8. US. Department of Energy - Energy Efficiency & Renewable Energy (2014) "2013 Fuel Cell Technologies Market Report". Available online at: http://energy.gov/sites/prod/files/2014/11/f19/fcto_2013_market_report.pdf.

9. U.S. Drive (2013) "Fuel Cell Technical Team Roadmap". Available online at: http://energy.gov/sites/prod/files/2014/02/f8/fctt_roadmap_june2013.pdf.

10. D. Banham, S. Ye, K. Pei, J.-i. Ozaki, T. Kishimoto, Y. Imashiro (2015) "A review of the stability and durability of non-precious metal catalysts for the oxygen reduction reaction in proton exchange membrane fuel cells", *Journal of Power Sources*, **285**, 334-348.

11. T. J. Peckham, S. Holdcroft (2010) "Structure-Morphology-Property Relationships of Non-Perfluorinated Proton-Conducting Membranes", *Advanced Materials*, **22**, 4667-4690.

12. S. Subianto, M. Pica, M. Casciola, P. Cojocaru, L. Merlo, G. Hards, D. J. Jones (2013) "Physical and chemical modification routes leading to improved mechanical properties of perfluorosulfonic acid membranes for PEM fuel cells", *Journal of Power Sources*, **233**, 216-230.

13. R. Taherian (2014) "A review of composite and metallic bipolar plates in proton exchange membrane fuel cell: Materials, fabrication, and material selection", *Journal of Power Sources*, **265**, 370-390.

14. A. Chandan, M. Hattenberger, A. El-kharouf, S. Du, A. Dhir, V. Self, B. G. Pollet, A. Ingram, W. Bujalski (2013) "High temperature (HT) polymer electrolyte membrane fuel cells (PEMFC) – A review", *Journal of Power Sources*, **231**, 264-278.

15. M. Uchida, Y.-C. Park, K. Kakinuma, H. Yano, D. A. Tryk, T. Kamino, H. Uchida, M. Watanabe (2013) "Effect of the state of distribution of supported Pt nanoparticles on effective Pt utilization in polymer electrolyte fuel cells", *Physical Chemistry Chemical Physics*, **15**, 11236-11247.

16. D. C. Higgins, J.-Y. Choi, J. Wu, A. Lopez, Z. Chen (2012) "Titanium nitride-carbon nanotube core-shell composites as effective electrocatalyst supports for low temperature fuel cells", *Journal of Materials Chemistry*, **22**, 3727-3732.

17. D. C. Higgins, D. Meza, Z. Chen (2010) "Nitrogen-Doped Carbon Nanotubes as Platinum Catalyst Supports for Oxygen Reduction Reaction in Proton Exchange Membrane Fuel Cells", *The Journal of Physical Chemistry C*, **114**, 21982-21988.

18. W. Li, C. Liang, J. Qiu, W. Zhou, H. Han, Z. Wei, G. Sun, Q. Xin (2002) "Carbon nanotubes as support for cathode catalyst of a direct methanol fuel cell", *Carbon*, **40**, 787-790.

19. B. Seger, P. V. Kamat (2009) "Electrocatalytically active graphene-platinum nanocomposites. Role of 2-D carbon support in PEM fuel cells", *The Journal of Physical Chemistry C*, **113**, 7990-7995.

20. J. Greeley, I. Stephens, A. Bondarenko, T. P. Johansson, H. A. Hansen, T. Jaramillo, J. Rossmeisl, I. Chorkendorff, J. K. Nørskov (2009) "Alloys of platinum and early transition metals as oxygen reduction electrocatalysts", *Nature Chemistry*, **1**, 552-556.

21. F. Maillard, L. Dubau, J. Durst, M. Chatenet, J. André, E. Rossinot (2010) "Durability of Pt3Co/C nanoparticles in a proton-exchange membrane fuel cell: direct evidence of bulk Co segregation to the surface", *Electrochemistry Communications*, **12**, 1161-1164.

22. U. Paulus, A. Wokaun, G. Scherer, T. Schmidt, V. Stamenkovic, V. Radmilovic, N. Markovic, P. Ross (2002) "Oxygen Reduction on Carbon-Supported Pt- Ni and Pt- Co Alloy Catalysts", *The Journal of Physical Chemistry B*, **106**, 4181-4191.

23. M. Saha, Y. Chen, R. Li, X. Sun (2009) "Enhancement of PEMFC performance by using carbon nanotubes supported Pt Co alloy catalysts", *Asia Pacific Journal of Chemical Engineering*, **4**, 12-16.

24. J. Salgado, E. Antolini, E. Gonzalez (2004) "Structure and Activity of Carbon-Supported Pt- Co Electrocatalysts for Oxygen Reduction", *The Journal of Physical Chemistry B*, **108**, 17767-17774.

25. J. L. Shui, J. W. Zhang, J. C. M. Li (2011) "Making Pt-shell Pt30Ni70 nanowires by mild dealloying and heat treatments with little Ni loss", *Journal of Materials Chemistry*, **21**, 6225-6229.

26. S. Sun, G. Zhang, D. Geng, Y. Chen, R. Li, M. Cai, X. Sun (2011) "A Highly Durable Platinum Nanocatalyst for Proton Exchange Membrane Fuel Cells: Multiarmed Starlike Nanowire Single Crystal", *Angewandte Chemie*, **50**, 422-426.

27. Z. Chen, M. Waje, W. Li, Y. Yan (2007) "Supportless Pt and PtPd Nanotubes as Electrocatalysts for Oxygen Reduction Reactions", *Angewandte Chemie*, **119**, 4138-4141.

28. Y. Yu, H. Li, H. Wang, X.-Z. Yuan, G. Wang, M. Pan (2012) "A review on performance degradation of proton exchange membrane fuel cells during startup and shutdown processes: Causes, consequences, and mitigation strategies", *Journal of Power Sources*, **205**, 10-23.

29. J. C. Meier, C. Galeano, I. Katsounaros, J. Witte, H. J. Bongard, A. A. Topalov, C. Baldizzone, S. Mezzavilla, F. Schüth, K. J. J. Mayrhofer (2014) "Design criteria for stable Pt/C fuel cell catalysts", *Beilstein Journal of Nanotechnology*, **5**, 44-67.

30. H. Li, C. Song, J. Zhang, J. Zhang, Catalyst Contamination in PEM Fuel Cells, in: Jiujun Zhang (Ed.) PEM Fuel Cell Electrocatalysts and Catalyst Layers, Springer London2008, pp. 331-354.

31. X. Cheng, Z. Shi, N. Glass, L. Zhang, J. Zhang, D. Song, Z.-S. Liu, H. Wang, J. Shen (2007) "A review of PEM hydrogen fuel cell contamination: Impacts, mechanisms, and mitigation", *Journal of Power Sources*, **165**, 739-756.

32. Y. Shao, G. Yin, Y. Gao (2007) "Understanding and approaches for the durability issues of Pt-based catalysts for PEM fuel cell", *Journal of Power Sources*, **171**, 558-566.

33. F. Jaouen, J.-P. Dodelet (2007) "Non-Noble Electrocatalysts for O2 Reduction: How Does Heat Treatment Affect Their Activity and Structure? Part I. Model for Carbon Black Gasification by NH3: Parametric Calibration and Electrochemical Validation", *The Journal of Physical Chemistry C*, **111**, 5963-5970.

34. S. Y. Huang, P. Ganesan, B. N. Popov (2011) "Titania supported platinum catalyst with high electrocatalytic activity and stability for polymer electrolyte membrane fuel cell", *Applied Catalysis B: Environmental*, **102**, 71-77.

35. S.-Y. Huang, P. Ganesan, S. Park, B. N. Popov (2009) "Development of a Titanium Dioxide-Supported Platinum Catalyst with Ultrahigh Stability for Polymer Electrolyte Membrane Fuel Cell Applications", *Journal of the American Chemical Society*, **131**, 13898-13899.

36. M. S. Wilson, F. H. Garzon, K. E. Sickafus, S. Gottesfeld (1993) "Surface Area Loss of Supported Platinum in Polymer Electrolyte Fuel Cells", *Journal of The Electrochemical Society*, **140**, 2872-2877.

37. Y. Shao-Horn, W. C. Sheng, S. Chen, P. J. Ferreira, E. F. Holby, D. Morgan (2007) "Instability of Supported Platinum Nanoparticles in Low-Temperature Fuel Cells", *Topics in Catalysis*, **46**, 285-305.

38. Y. Chen, J. Wang, H. Liu, R. Li, X. Sun, S. Ye, S. Knights (2009) "Enhanced stability of Pt electrocatalysts by nitrogen doping in CNTs for PEM fuel cells", *Electrochemistry Communications*, **11**, 2071-2076.

39. D. Higgins, M. A. Hoque, M. H. Seo, R. Wang, F. Hassan, J.-Y. Choi, M. Pritzker, A. Yu, J. Zhang, Z. Chen (2014) "Development and Simulation of Sulfur-doped Graphene Supported Platinum with Exemplary Stability and Activity Towards Oxygen Reduction", *Advanced Functional Materials*, **24**, 4325-4336.

40. S.-H. Liu, M.-T. Wu, Y.-H. Lai, C.-C. Chiang, N. Yu, S.-B. Liu (2011) "Fabrication and electrocatalytic performance of highly stable and active platinum nanoparticles supported on nitrogen-doped ordered mesoporous carbons for oxygen reduction reaction", *Journal of Materials Chemistry*, **21**, 12489-12496.

41. D. C. Higgins, S. Ye, S. Knights, Z. Chen (2012) "Highly Durable Platinum-Cobalt Nanowires by Microwave Irradiation as Oxygen Reduction Catalyst for PEM Fuel Cell", *Electrochemical and Solid-State Letters*, **15**, B83-B85.

42. S. Sun, G. Zhang, D. Geng, Y. Chen, M. N. Banis, R. Li, M. Cai, X. Sun (2010) "Direct Growth of Single‐Crystal Pt Nanowires on Sn@ CNT Nanocable: 3D Electrodes for Highly Active Electrocatalysts", *Chemistry-a European Journal*, **16**, 829-835.

43. S. Sun, G. Zhang, Y. Zhong, H. Liu, R. Li, X. Zhou, X. Sun (2009) "Ultrathin single crystal Pt nanowires grown on N-doped carbon nanotubes", *Chemical Communications (Cambridge, United Kingdom)*, 7048-7050.

44. R. Wang, D. Higgins, S. Prabhudev, D. U. Lee, J.-Y. Choi, M. A. Hoque, G. Botton, Z. Chen (2015) "Synthesis and structural evolution of Pt nanotubular skeletons: revealing the source of instability for nanostructured electrocatalysts", *Journal of Materials Chemistry A*,

45. Y. Shao, J. Liu, Y. Wang, Y. Lin (2009) "Novel catalyst support materials for PEM fuel cells: current status and future prospects", *Journal of Materials Chemistry*, **19**, 46-59.

46. K.-Y. Chan, J. Ding, J. Ren, S. Cheng, K. Y. Tsang (2004) "Supported mixed metal nanoparticles as electrocatalysts in low temperature fuel cells", *Journal of Materials Chemistry*, **14**, 505-516.

47. Y. J. Wang, D. P. Wilkinson, J. Zhang (2011) "Noncarbon support materials for polymer electrolyte membrane fuel cell electrocatalysts", *Chemical reviews*, **111**, 7625-7651.

48. D. H. Lim, W. J. Lee, J. Wheldon, N. L. Macy, W. H. Smyrl (2010) "Electrochemical Characterization and Durability of Sputtered Pt Catalysts on TiO2 Nanotube Arrays as a Cathode Material for PEFCs", *Journal of The Electrochemical Society*, **157**, B862-B867.

49. J.-Y. Choi, D. Higgins, Z. Chen (2011) "Highly Durable Graphene Nanosheet Supported Iron Catalyst for Oxygen Reduction Reaction in PEM Fuel Cells", *Journal of The Electrochemical Society*, **159**, B86-B89.

50. M. A. Hoque, F. M. Hassan, D. Higgins, J.-Y. Choi, M. Pritzker, S. Knights, S. Ye, Z. Chen (2015) "Multigrain Platinum Nanowires Consisting of Oriented Nanoparticles Anchored on Sulfur-Doped Graphene as a Highly Active and Durable Oxygen Reduction Electrocatalyst", *Advanced Materials*, **27**, 1229-1234.

51. T. Ioroi, H. Senoh, S. Yamazaki, Z. Siroma, N. Fujiwara, K. Yasuda (2008) "Stability of corrosion-resistant Magnéli-phase Ti4O7-supported PEMFC catalysts at high potentials", *Journal of The Electrochemical Society*, **155**, B321-B326.

52. T. Ioroi, Z. Siroma, N. Fujiwara, S. Yamazaki, K. Yasuda (2005) "Sub-stoichiometric titanium oxide-supported platinum electrocatalyst for polymer electrolyte fuel cells", *Electrochemistry Communications*, **7**, 183-188.

53. S. Zhang, H. Zhu, H. Yu, J. Hou, B. Yi, P. Ming (2007) "The oxidation resistance of tungsten carbide as catalyst support for proton exchange membrane fuel cells", *Chinese Journal of Catalysis*, **28**, 109-111.

54. M. A. Hoque, D. C. Higgins, F. M. Hassan, J.-Y. Choi, M. D. Pritzker, Z. Chen (2014) "Tin oxide - mesoporous carbon composites as platinum catalyst supports for ethanol oxidation and oxygen reduction", *Electrochimica Acta*, **121**, 421-427.

55. D. Meza, D. C. Higgins, J. Wu, Z. Chen (2011) "One-Step Synthesized Tungsten Oxide/Carbon Nanotube Composites as Pt Catalyst Supports for Oxygen Reduction Reaction in Proton Exchange Membrane Fuel Cells", *Journal of Nanoengineering and Nanomanufacturing*, **1**, 280-286.

56. Y. H. Li, T. H. Hung, C. W. Chen (2009) "A first-principles study of nitrogen-and boron-assisted platinum adsorption on carbon nanotubes", *Carbon*, **47**, 850-855.

57. Y. Zhou, K. Neyerlin, T. S. Olson, S. Pylypenko, J. Bult, H. N. Dinh, T. Gennett, Z. Shao, R. O'Hayre (2010) "Enhancement of Pt and Pt-alloy fuel cell catalyst activity and durability via nitrogen-modified carbon supports", *Energy & Environmental Science*, **3**, 1437-1446.

58. R. Wang, D. C. Higgins, M. A. Hoque, D. Lee, F. Hassan, Z. Chen (2013) "Controlled Growth of Platinum Nanowire Arrays on Sulfur Doped Graphene as High Performance Electrocatalyst", *Scientific Reports*, **3**,

59. N. Rajalakshmi, N. Lakshmi, K. Dhathathreyan (2008) "Nano titanium oxide catalyst support for proton exchange membrane fuel cells", *International journal of hydrogen energy*, **33**, 7521-7526.

60. F. Walsh, R. Wills (2010) "The continuing development of Magnéli phase titanium sub-oxides and Ebonex< sup>®</sup> electrodes", *Electrochimica Acta*, **55**, 6342-6351.

61. J. E. Graves, D. Pletcher, R. L. Clarke, F. C. Walsh (1991) "The electrochemistry of Magnéli phase titanium oxide ceramic electrodes Part I. The deposition and properties of metal coatings", *Journal of Applied Electrochemistry*, **21**, 848-857.

62. P. Krishnan, S. G. Advani, A. K. Prasad (2012) "Magneli phase Ti n O 2n− 1 as corrosion-resistant PEM fuel cell catalyst support", *Journal of Solid State Electrochemistry*, 1-7.

63. C. Yao, F. Li, X. Li, D. Xia (2012) "Fiber-like nanostructured Ti4O7 used as durable fuel cell catalyst support in oxygen reduction catalysis", *Journal of Materials Chemistry*, **22**, 16560-16565.

64. H. A. Gasteiger, S. S. Kocha, B. Sompalli, F. T. Wagner (2005) "Activity benchmarks and requirements for Pt, Pt-alloy, and non-Pt oxygen reduction catalysts for PEMFCs", *Applied Catalysis B: Environmental*, **56**, 9-35.

65. V. Stamenkovic, B. S. Mun, K. J. J. Mayrhofer, P. N. Ross, N. M. Markovic, J. Rossmeisl, J. Greeley, J. K. Nørskov (2006) "Changing the activity of electrocatalysts for oxygen reduction by tuning the surface electronic structure", *Angewandte Chemie*, **118**, 2963-2967.

66. J. K. Nørskov, J. Rossmeisl, A. Logadottir, L. Lindqvist, J. R. Kitchin, T. Bligaard, H. Jónsson (2004) "Origin of the Overpotential for Oxygen Reduction at a Fuel-Cell Cathode", *The Journal of Physical Chemistry B*, **108**, 17886-17892.

67. P. Strasser, S. Koh, T. Anniyev, J. Greeley, K. More, C. Yu, Z. Liu, S. Kaya, D. Nordlund, H. Ogasawara (2010) "Lattice-strain control of the activity in dealloyed core–shell fuel cell catalysts", *Nature chemistry*, **2**, 454-460.

68. V. R. Stamenkovic, B. Fowler, B. S. Mun, G. Wang, P. N. Ross, C. A. Lucas, N. M. Marković (2007) "Improved Oxygen Reduction Activity on Pt3Ni(111) via Increased Surface Site Availability", *Science*, **315**, 493-497.

69. P. Mani, R. Srivastava, P. Strasser (2008) "Dealloyed Pt-Cu core-shell nanoparticle electrocatalysts for use in PEM fuel cell cathodes", *The Journal of Physical Chemistry C*, **112**, 2770-2778.

70. J. Shui, C. Chen, J. Li (2011) "Evolution of Nanoporous Pt–Fe Alloy Nanowires by Dealloying and their Catalytic Property for Oxygen Reduction Reaction", *Advanced Functional Materials*, **21**, 3357-3362.

71. C. W. B. Bezerra, L. Zhang, H. Liu, K. Lee, A. L. B. Marques, E. P. Marques, H. Wang, J. Zhang (2007) "A review of heat-treatment effects on activity and stability of PEM fuel cell catalysts for oxygen reduction reaction", *Journal of Power Sources*, **173**, 891-908.

72. E. Antolini, J. R. C. Salgado, E. R. Gonzalez (2006) "The stability of Pt–M (M= first row transition metal) alloy catalysts and its effect on the activity in low temperature fuel cells: a literature review and tests on a Pt–Co catalyst", *Journal of Power Sources*, **160**, 957-968.

73. B. N. Wanjala, J. Luo, R. Loukrakpam, B. Fang, D. Mott, P. N. Njoki, M. Engelhard, H. R. Naslund, J. K. Wu, L. Wang, O. Malis, C.-J. Zhong (2010) "Nanoscale Alloying, Phase-Segregation, and Core−Shell Evolution of Gold−Platinum Nanoparticles and Their Electrocatalytic Effect on Oxygen Reduction Reaction", *Chemistry of Materials*, **22**, 4282-4294.

74. C. Chen, Y. Kang, Z. Huo, Z. Zhu, W. Huang, H. L. Xin, J. D. Snyder, D. Li, J. A. Herron, M. Mavrikakis, M. Chi, K. L. More, Y. Li, N. M. Markovic, G. A. Somorjai, P. Yang, V. R. Stamenkovic (2014) "Highly Crystalline Multimetallic Nanoframes with Three-Dimensional Electrocatalytic Surfaces", *Science*, **343**, 1339-1343.

75. B. Y. Xia, H. B. Wu, Y. Yan, X. W. Lou, X. Wang (2013) "Ultrathin and Ultralong Single-Crystal Platinum Nanowire Assemblies with Highly Stable Electrocatalytic Activity", *Journal of the American Chemical Society*, **135**, 9480-9485.

76. B. Y. Xia, H. B. Wu, X. Wang, X. W. Lou (2013) "Highly Concave Platinum Nanoframes with High-Index Facets and Enhanced Electrocatalytic Properties", *Angewandte Chemie International Edition*, **52**, 12337-12340.

77. C. Koenigsmann, W.-p. Zhou, R. R. Adzic, E. Sutter, S. S. Wong (2010) "Size-Dependent Enhancement of Electrocatalytic Performance in Relatively Defect-Free, Processed Ultrathin Platinum Nanowires", *Nano Letters*, **10**, 2806-2811.

78. Q. Li, P. Xu, B. Zhang, G. Wu, H. Zhao, E. Fu, H.-L. Wang (2013) "Self-supported Pt nanoclusters via galvanic replacement from Cu2O nanocubes as efficient electrocatalysts", *Nanoscale*, **5**, 7397-7402.

79. G. Zhang, S. Sun, M. Cai, Y. Zhang, R. Li, X. Sun (2013) "Porous Dendritic Platinum Nanotubes with Extremely High Activity and Stability for Oxygen Reduction Reaction", *Scientific Reports*, **3**,

80. S. Sun, G. Zhang, D. Geng, Y. Chen, M. Banis, R. Li, M. Cai, X. Sun (2010) "Direct Growth of Single Crystal Pt Nanowires on Sn@ CNT Nanocable: 3D Electrodes for Highly Active Electrocatalysts", *Chemistry – A European Journal*, **16**, 829-835.

81. S. Sun, G. Zhang, D. Geng, Y. Chen, R. Li, M. Cai, X. Sun (2011) "A Highly Durable Platinum Nanocatalyst for Proton Exchange Membrane Fuel Cells: Multiarmed Starlike Nanowire Single Crystal", *Angew. Chem. Int. Edit.*, **50**, 422-426.

82. H. Zhou, W. Zhou, R. Adzic, S. Wong (2009) "Enhanced Electrocatalytic Performance of One-Dimensional Metal Nanowires and Arrays Generated via an Ambient, Surfactantless Synthesis", *Journal of Physical Chemistry C*, **113**, 5460-5466.

83. D. C. Higgins, R. Wang, M. A. Hoque, P. Zamani, S. Abureden, Z. Chen (2014) "Morphology and composition controlled platinum–cobalt alloy nanowires prepared by electrospinning as oxygen reduction catalyst", *Nano Energy*, **10**, 135-143.

84. S. M. Alia, S. Pylypenko, K. C. Neyerlin, D. A. Cullen, S. S. Kocha, B. S. Pivovar (2014) "Platinum-Coated Cobalt Nanowires as Oxygen Reduction Reaction Electrocatalysts", *ACS Catalysis*, **4**, 2680-2686.

85. B. Li, Z. Yan, D. C. Higgins, D. Yang, Z. Chen, J. Ma (2014) "Carbon-supported Pt nanowire as novel cathode catalysts for proton exchange membrane fuel cells", *Journal of Power Sources*, **262**, 488-493.

86. K. Lee, J. Zhang, H. Wang, D. Wilkinson (2006) "Progress in the synthesis of carbon nanotube-and nanofiber-supported Pt electrocatalysts for PEM fuel cell catalysis", *Journal of Applied Electrochemistry*, **36**, 507-522.

87. E. Lee, Z. Peng, W. Chen, S. Chen, H. Yang, Y. Xia (2008) "Electrocatalytic Properties of Pt Nanowires Supported on Pt and W Gauzes", *ACS nano*, **2**, 2167-2173.

88. S. Choi, J. Kim, J. Jung, E. Yoon, W. Kim (2008) "Pt nanowires prepared via a polymer template method: Its promise toward high Pt-loaded electrocatalysts for methanol oxidation", *Electrochimica Acta*, **53**, 5804-5811.

89. Z. Zhang, M. Li, Z. Wu, W. Li (2011) "Ultra-thin PtFe-nanowires as durable electrocatalysts for fuel cells", *Nanotechnology*, **22**, 015602.

90. H. Chen, C. Hsin, P. Chen, R. Liu, S. Hu, C. Huang, J. Lee, L. Jang (2009) "Ferromagnetic CoPt3 Nanowires: Structural Evolution from fcc to Ordered L12", *Journal of the American Chemical Society*, **131**, 15794-15801.

91. L. Liu, E. Pippel, R. Scholz, U. Go sele (2009) "Nanoporous Pt- Co Alloy Nanowires: Fabrication, Characterization, and Electrocatalytic Properties", *Nano Letters*, **9**, 4352-4358.

92. L. Liu, W. Zhou, S. Xie, O. Albrecht, K. Nielsch (2008) "Microstructure and temperature-dependent magnetic properties of Co/Pt multilayered nanowires", *Chemical Physics Letters*, **466**, 165-169.

93. J. H. Song, Y. Wu, B. Messer, H. Kind, P. Yang (2001) "Metal Nanowire Formation Using Mo3Se3- as Reducing and Sacrificing Templates", *Journal of the American Chemical Society*, **123**, 10397-10398.

94. J. Fu, S. Cherevko, C. H. Chung (2008) "Electroplating of metal nanotubes and nanowires in a high aspect-ratio nanotemplate", *Electrochemistry Communications*, **10**, 514-518.

95. D. C. Higgins, Z. Chen (2013) "Recent progress in non-precious metal catalysts for PEM fuel cell applications", *The Canadian Journal of Chemical Engineering*, **91**, 1881-1895.

96. Z. Chen, D. Higgins, A. Yu, L. Zhang, J. Zhang (2011) "A review on non-precious metal electrocatalysts for PEM fuel cells", *Energy & Environmental Science*, **4**, 3167-3192.

97. Y. Liu, A. Ishihara, S. Mitsushima, N. Kamiya, K. Ota (2007) "Transition metal oxides as DMFC cathodes without platinum", *Journal of The Electrochemical Society*, **154**, B664-B669.

98. J. Kim, T. Oh, Y. Shin, J. Bonnett, K. Weil (2011) "A novel non-platinum group electrocatalyst for PEM fuel cell application", *International journal of hydrogen energy*, **36**, 4557-4564.

99. J. H. Kim, A. Ishihara, S. Mitsushima, N. Kamiya, K. I. Ota (2007) "Catalytic activity of titanium oxide for oxygen reduction reaction as a non-platinum catalyst for PEFC", *Electrochimica Acta*, **52**, 2492-2497.

100. K. C. Lee, A. Ishihara, S. Mitsushima, N. Kamiya, K. I. Ota (2004) "Stability and electrocatalytic activity for oxygen reduction in WC plus Ta catalyst", *Electrochimica Acta*, **49**, 3479-3485.

101. H. X. Zhong, H. M. Zhang, G. Liu, Y. M. Liang, J. W. Hu, B. L. Yi (2006) "A novel non-noble electrocatalyst for PEM fuel cell based on molybdenum nitride", *Electrochemistry Communications*, **8**, 707-712.

102. H. Behret, H. Binder, G. Sandstede (1975) "Electrocatalytic Oxygen Reduction with Thiospinels and Other Sulfides of Transition-Metals", *Electrochimica Acta*, **20**, 111-117.

103. D. Susac, L. Zhu, M. Teo, A. Sode, K. C. Wong, P. C. Wong, R. R. Parsons, D. Bizzotto, K. A. R. Mitchell, S. A. Campbell (2007) "Characterization of FeS2-based thin films as model catalysts for the oxygen reduction reaction", *Journal of Physical Chemistry C*, **111**, 18715-18723.

104. E. Vayner, R. A. Sidik, A. B. Anderson, B. N. Popov (2007) "Experimental and theoretical study of cobalt selenide as a catalyst for O-2 electroreduction", *Journal of Physical Chemistry C*, **111**, 10508-10513.

105. Y. J. Feng, T. He, N. Alonso-Vante (2008) "In situ free-surfactant synthesis and ORR-Electrochemistry of carbon-supported Co3S4 and CoSe2 nanoparticles", *Chemistry of Materials*, **20**, 26-28.

106. K. Lee, L. Zhang, J. J. Zhang (2007) "Ternary non-noble metal chalcogenide (W-Co-Se) as electrocatalyst for oxygen reduction reaction", *Electrochemistry Communications*, **9**, 1704-1708.

107. R. Bashyam, P. Zelenay (2006) "A class of non-precious metal composite catalysts for fuel cells", *Nature*, **443**, 63-66.

108. W. M. Millan, M. A. Smit (2009) "Study of Electrocatalysts for Oxygen Reduction Based on Electroconducting Polymer and Nickel", *Journal of Applied Polymer Science*, **112**, 2959-2967.

109. W. M. Millan, T. T. Thompson, L. G. Arriaga, M. A. Smit (2009) "Characterization of composite materials of electroconductive polymer and cobalt as electrocatalysts for the oxygen reduction reaction", *International journal of hydrogen energy*, **34**, 694-702.

110. R. Sulub, W. Martinez-Millan, M. A. Smit (2009) "Study of the Catalytic Activity for Oxygen Reduction of Polythiophene Modified with Cobalt or Nickel", *International Journal of Electrochemical Science*, **4**, 1015-1027.

111. F. Jaouen, E. Proietti, M. Lefevre, R. Chenitz, J.-P. Dodelet, G. Wu, H. T. Chung, C. M. Johnston, P. Zelenay (2011) "Recent advances in non-precious metal catalysis for oxygen-reduction reaction in polymer electrolyte fuel cells", *Energy & Environmental Science*, **4**, 114-130.

112. W. Li, J. Wu, D. C. Higgins, J.-Y. Choi, Z. Chen (2012) "Determination of Iron Active Sites in Pyrolyzed Iron-Based Catalysts for the Oxygen Reduction Reaction", *ACS Catalysis*, **2**, 2761-2768.

113. G. Wu, K. L. More, C. M. Johnston, P. Zelenay (2011) "High-Performance Electrocatalysts for Oxygen Reduction Derived from Polyaniline, Iron, and Cobalt", *Science*, **332**, 443-447.

114. J. Wu, W. Li, D. Higgins, Z. Chen (2011) "Heat-Treated Nonprecious Catalyst Using Fe and Nitrogen-Rich 2,3,7,8-Tetra(pyridin-2-yl)pyrazino[2,3-g]quinoxaline Coordinated Complex for Oxygen Reduction Reaction in PEM Fuel Cells", *The Journal of Physical Chemistry C*, **115**, 18856-18862.

115. G. Wu, P. Zelenay (2013) "Nanostructured Nonprecious Metal Catalysts for Oxygen Reduction Reaction", *Accounts of Chemical Research*, **46**, 1878-1889.

116. G. Wu, C. M. Johnston, N. H. Mack, K. Artyushkova, M. Ferrandon, M. Nelson, J. S. Lezama-Pacheco, S. D. Conradson, K. L. More, D. J. Myers, P. Zelenay (2011) "Synthesis-structure-performance correlation for polyaniline-Me-C non-precious metal cathode catalysts for oxygen reduction in fuel cells", *Journal of Materials Chemistry*, **21**, 11392-11405.

117. A. Serov, K. Artyushkova, P. Atanassov (2014) "Fe-N-C Oxygen Reduction Fuel Cell Catalyst Derived from Carbendazim: Synthesis, Structure, and Reactivity", *Advanced Energy Materials*, **4**, n/a-n/a.

118. A. Serov, U. Tylus, K. Artyushkova, S. Mukerjee, P. Atanassov (2014) "Mechanistic studies of oxygen reduction on Fe-PEI derived non-PGM electrocatalysts", *Applied Catalysis B: Environmental*, **150–151**, 179-186.

119. A. Serov, M. H. Robson, M. Smolnik, P. Atanassov (2013) "Tri-metallic transition metal–nitrogen–carbon catalysts derived by sacrificial support method synthesis", *Electrochimica Acta*, **109**, 433-439.

120. United States Department of Energy (2011) "Technical Plan - Fuel Cells". Available online at: http://www1.eere.energy.gov/hydrogenandfuelcells/mypp/pdfs/fuel_cells.pdf.

121. D. Higgins, G. Wu, H. T. Chung, U. Martinez, S. Ma, Z. Chen, P. Zelenay (2014) "Manganese-Based Non-Precious Metal Catalyst for Oxygen Reduction in Acidic Media", *ECS Transactions*, **61**, 35-42.

122. D. Higgins, Z. Chen, Recent development of non-precious metal catalysts, in: Minhua Shao (Ed.) Electrocatalysis in Fuel Cells A non- and low- platinum approach, Springer-Verlag, London, UK, 2013, pp. 247-269.

123. R. Jasinski (1964) "New Fuel Cell Cathode Catalyst", *Nature*, **201**, 1212-1213.

124. H. Alt, H. Binder, Sandsted.G (1973) "Mechanism of Electrocatalytic Reduction of Oxygen on Metal-Chelates", *Journal of Catalysis*, **28**, 8-19.

125. N. Cheng, C. Kemna, S. Goubert-Renaudin, A. Wieckowski (2012) "Reduction Reaction by Porphyrin-Based Catalysts for Fuel Cells", *Electrocatalysis*, **3**, 238-251.

126. R. Franke, D. Ohms, K. Wiesener (1989) "Investigation of the Influence of Thermal-Treatment on the Properties of Carbon Materials Modified by N-4-Chelates for the Reduction of Oxygen in Acidic Media", *Journal of Electroanalytical Chemistry*, **260**, 63-73.

127. D. Scherson, A. A. Tanaka, S. L. Gupta, D. Tryk, C. Fierro, R. Holze, E. B. Yeager, R. P. Lattimer (1986) "Transition-Metal Macrocycles Supported on High Area Carbon - Pyrolysis Mass-Spectrometry Studies", *Electrochimica Acta*, **31**, 1247-1258.

128. J. A. R. van Veen, H. A. Colijn, J. F. van Baar (1988) "On the Effect of a Heat-Treatment on the Structure of Carbon-Supported Metalloporphyrins and Phthalocyanines", *Electrochimica Acta*, **33**, 801-804.

129. S. Gupta, D. Tryk, I. Bae, W. Aldred, E. Yeager (1989) "Heat-Treated Polyacrylonitrile-Based Catalysts for Oxygen Electroreduction", *Journal of Applied Electrochemistry*, **19**, 19-27.

130. M. Ferrandon, A. J. Kropf, D. J. Myers, K. Artyushkova, U. Kramm, P. Bogdanoff, G. Wu, C. M. Johnston, P. Zelenay (2012) "Multitechnique Characterization of a Polyaniline–Iron–Carbon Oxygen Reduction Catalyst", *The Journal of Physical Chemistry C*, **116**, 16001-16013.

131. A. L. Bouwkamp-Wijnoltz, W. Visscher, J. A. R. van Veen, E. Boellaard, A. M. van der Kraan, S. C. Tang (2002) "On active-site heterogeneity in pyrolyzed carbon-supported iron porphyrin catalysts for the electrochemical reduction of oxygen: An in situ Mossbauer study", *Journal of Physical Chemistry B*, **106**, 12993-13001.

132. L. Birry, J. Zagal, J. Dodelet (2010) "Does CO poison Fe-based catalysts for ORR?", *Electrochemistry Communications*, **12**, 628-631.

133. S. L. Gojkovic, S. Gupta, R. F. Savinell (1998) "Heat-treated iron(III) tetramethoxyphenyl porphyrin supported on high-area carbon as an electrocatalyst for oxygen reduction - I. Characterization of the electrocatalyst", *Journal of The Electrochemical Society*, **145**, 3493-3499.

134. S. L. Gojkovic, S. Gupta, R. F. Savinell (1999) "Heat-treated iron(III) tetramethoxyphenyl porphyrin chloride supported on high-area carbon as an electrocatalyst for oxygen reduction: Part III. Detection of hydrogen-peroxide during oxygen reduction", *Electrochimica Acta*, **45**, 889-897.

135. J. Herranz, M. Lefevre, J. P. Dodelet (2009) "Metal-Precursor Adsorption Effects on Fe-Based Catalysts for Oxygen Reduction in PEM Fuel Cells", *Journal of The Electrochemical Society*, **156**, B593-B601.

136. R. Kothandaraman, V. Nallathambi, K. Artyushkova, S. C. Barton (2009) "Non-precious oxygen reduction catalysts prepared by high-pressure pyrolysis for low-temperature fuel cells", *Applied Catalysis B-Environmental*, **92**, 209-216.

137. X. G. Li, C. P. Liu, W. Xing, T. H. Lu (2009) "Development of durable carbon black/titanium dioxide supported macrocycle catalysts for oxygen reduction reaction", *Journal of Power Sources*, **193**, 470-476.

138. H. Meng, N. Larouche, M. Lefèvre, F. Jaouen, B. Stansfield, J. Dodelet (2010) "Iron porphyrin-based cathode catalysts for polymer electrolyte membrane fuel cells: Effect of NH3 and Ar mixtures as pyrolysis gases on catalytic activity and stability", *Electrochimica Acta*, **55**, 6450-6461.

139. E. Proietti, S. Ruggeri, J. P. Dodelet (2008) "Fe-based electrocatalysts for oxygen reduction in PEMFCs using ballmilled graphite powder as a carbon support", *Journal of The Electrochemical Society*, **155**, B340-B348.

140. F. Charreteur, F. Jaouen, J. P. Dodelet (2009) "Iron porphyrin-based cathode catalysts for PEM fuel cells: Influence of pyrolysis gas on activity and stability", *Electrochimica Acta*, **54**, 6622-6630.

141. F. Charreteur, F. Jaouen, S. Ruggeri, J. P. Dodelet (2008) "Fe/N/C non-precious catalysts for PEM fuel cells: Influence of the structural parameters of pristine commercial carbon blacks on their activity for oxygen reduction", *Electrochimica Acta*, **53**, 2925-2938.

142. M. Lefevre, J. P. Dodelet (2003) "Fe-based catalysts for the reduction of oxygen in polymer electrolyte membrane fuel cell conditions: determination of the amount of peroxide released during electroreduction and its influence on the stability of the catalysts", *Electrochimica Acta*, **48**, 2749-2760.

143. M. Lefevre, J. P. Dodelet, P. Bertrand (2005) "Molecular oxygen reduction in PEM fuel cell conditions: ToF-SIMS analysis of Co-based electrocatalysts", *Journal of Physical Chemistry B*, **109**, 16718-16724.

144. M. Lefevre, E. Proietti, F. Jaouen, J. P. Dodelet (2009) "Iron-Based Catalysts with Improved Oxygen Reduction Activity in Polymer Electrolyte Fuel Cells", *Science*, **324**, 71-74.

145. E. J. Biddinger, U. S. Ozkan (2007) "Methanol Tolerance of CN x Oxygen Reduction Catalysts", *Topics in Catalysis*, **46**, 339-348.

146. E. J. Biddinger, D. von Deak, U. S. Ozkan (2009) "Nitrogen-Containing Carbon Nanostructures as Oxygen-Reduction Catalysts", *Topics in Catalysis*, **52**, 1566-1574.

147. X. G. Li, G. Liu, B. N. Popov (2010) "Activity and stability of non-precious metal catalysts for oxygen reduction in acid and alkaline electrolytes", *Journal of Power Sources*, **195**, 6373-6378.

148. G. Liu, X. G. Li, P. Ganesan, B. N. Popov (2009) "Development of non-precious metal oxygen-reduction catalysts for PEM fuel cells based on N-doped ordered porous carbon", *Applied Catalysis B-Environmental*, **93**, 156-165.

149. G. Liu, X. G. Li, P. Ganesan, B. N. Popov (2010) "Studies of oxygen reduction reaction active sites and stability of nitrogen-modified carbon composite catalysts for PEM fuel cells", *Electrochimica Acta*, **55**, 2853-2858.

150. S. Maldonado, K. J. Stevenson (2004) "Direct preparation of carbon nanofiber electrodes via pyrolysis of iron(II) phthalocyanine: Electrocatalytic aspects for oxygen reduction", *Journal of Physical Chemistry B*, **108**, 11375-11383.

151. P. H. Matter, U. S. Ozkan (2006) "Non-metal catalysts for dioxygen reduction in an acidic electrolyte", *Catalysis Letters*, **109**, 115-123.

152. P. H. Matter, E. Wang, M. Arias, E. J. Biddinger, U. S. Ozkan (2006) "Oxygen reduction reaction catalysts prepared from acetonitrile pyrolysis over alumina-supported metal particles", *Journal of Physical Chemistry B*, **110**, 18374-18384.

153. P. H. Matter, E. Wang, J. M. M. Millet, U. S. Ozkan (2007) "Characterization of the iron phase in CNx-based oxygen reduction reaction catalysts", *Journal of Physical Chemistry C*, **111**, 1444-1450.

154. P. H. Matter, L. Zhang, U. S. Ozkan (2006) "The role of nanostructure in nitrogen-containing carbon catalysts for the oxygen reduction reaction", *Journal of Catalysis*, **239**, 83-96.

155. V. Nallathambi, J. W. Lee, S. P. Kumaraguru, G. Wu, B. N. Popov (2008) "Development of high performance carbon composite catalyst for oxygen reduction reaction in PEM Proton Exchange Membrane fuel cells", *Journal of Power Sources*, **183**, 34-42.

156. J. Ozaki, S. Tanifuji, A. Furuichi, K. Yabutsuka (2010) "Enhancement of oxygen reduction activity of nanoshell carbons by introducing nitrogen atoms from metal phthalocyanines", *Electrochimica Acta*, **55**, 1864-1871.

157. B. N. Popov, X. Li, G. Liu, J. Lee (2010) "Power source research at USC: Development of advanced electrocatalysts for polymer electrolyte membrane fuel cells", *International journal of hydrogen energy*, **36**, 1794-1802.

158. X. Q. Wang, J. S. Lee, Q. Zhu, J. Liu, Y. Wang, S. Dai (2010) "Ammonia-Treated Ordered Mesoporous Carbons as Catalytic Materials for Oxygen Reduction Reaction", *Chemistry of Materials*, **22**, 2178-2180.

159. N. Alonso-Vante, H. Tributsch, O. Solorza-Feria (1995) "Kinetics Studies of Oxygen Reduction in Acid-Medium on Novel Semiconducting Transition-Metal Chalcogenides", *Electrochimica Acta*, **40**, 567-576.

160. D. X. Cao, A. Wieckowski, J. Inukai, N. Alonso-Vante (2006) "Oxygen reduction reaction on ruthenium and rhodium nanoparticles modified with selenium and sulfur", *Journal of The Electrochemical Society*, **153**, A869-A874.

161. C. Delacote, A. Bonakdarpour, C. M. Johnston, P. Zelenay, A. Wieckowski (2008) "Aqueous-based synthesis of ruthenium-selenium catalyst for oxygen reduction reaction", *Faraday Discussions*, **140**, 269-281.

162. C. Fischer, N. Alonsovante, S. Fiechter, H. Tributsch (1995) "Electrocatalytic Properties of Mixed Transition-Metal Tellurides (Chevrel-Phases) for Oxygen Reduction", *Journal of Applied Electrochemistry*, **25**, 1004-1008.

163. K. Lee, L. Zhang, J. J. Zhang (2007) "A novel methanol-tolerant Ir-Se chalcogenide electrocatalyst for oyxgen reduction", *Journal of Power Sources*, **165**, 108-113.

164. A. Lewera, J. Inukai, W. P. Zhou, D. Cao, H. T. Duong, N. Alonso-Vante, A. Wieckowski (2007) "Chalcogenide oxygen reduction reaction catalysis: X-ray photoelectron spectroscopy with Ru, Ru/Se and Ru/S samples emersed from aqueous media", *Electrochimica Acta*, **52**, 5759-5765.

165. N. Alonso-Vante, W. Jaegermann, H. Tributsch, W. Honle, K. Yvon (1987) "Electrocatalysis of Oxygen Reduction by Chalcogenides Containing Mixed Transition-Metal Clusters", *Journal of the American Chemical Society*, **109**, 3251-3257.

166. N. Alonso-Vante, H. Tributsch (1986) "Energy-Conversion Catalysis Using Semiconducting Transition-Metal Cluster Compounds", *Nature*, **323**, 431-432.

167. R. A. Sidik, A. B. Anderson (2006) "Co9S8 as a catalyst for electroreduction of O-2: Quantum chemistry predictions", *Journal of Physical Chemistry B*, **110**, 936-941.

168. D. Susac, A. Sode, L. Zhu, P. C. Wong, M. Teo, D. Bizzotto, K. A. R. Mitchell, R. R. Parsons, S. A. Campbell (2006) "A methodology for investigating new nonprecious metal catalysts for PEM fuel cells", *Journal of Physical Chemistry B*, **110**, 10762-10770.

169. E. Ahlberg, A. E. Broo (1996) "Oxygen reduction at sulphide minerals .1. A rotating ring disc electrode (RRDE) study at galena and pyrite", *International Journal of Mineral Processing*, **46**, 73-89.

170. Y. Feng, T. He, N. Alonso-Vante (2008) "Novel Non-Precious Metal Electrocatalysts for Oxygen Reduction Based on Nanostructured Cobalt Chalcogenide", *ECS Transactions*, **11**, 67-73.

171. Y. J. Feng, N. Alonso-Vante (2008) "Nonprecious metal catalysts for the molecular oxygen-reduction reaction", *Physica Status Solidi B-Basic Solid State Physics*, **245**, 1792-1806.

172. Y. J. Feng, T. He, N. Alonso-Vante (2009) "Oxygen reduction reaction on carbon-supported CoSe2 nanoparticles in an acidic medium", *Electrochimica Acta*, **54**, 5252-5256.

173. J. Goldstein, D. E. Newbury, D. C. Joy, P. Echlin, C. E. Lyman, E. Lifshin (2003) "Scanning electron microscopy and X-ray microanalysis", Springer, USA.

174. J. F. Shackelford (2005) "Introduction to materials science for engineers: Sixth Edition", Pearson Prentice Hall, New Jersey, USA.

175. Z. Chen, D. Higgins, Z. Chen (2010) "Nitrogen doped carbon nanotubes and their impact on the oxygen reduction reaction in fuel cells", *Carbon*, **48**, 3057-3065.

176. Z. Chen, D. Higgins, Z. Chen (2010) "Electrocatalytic activity of nitrogen doped carbon nanotubes with different morphologies for oxygen reduction reaction", *Electrochimica Acta*, **55**, 4799-4804.

177. Z. Chen, D. Higgins, H. Tao, R. S. Hsu, Z. Chen (2009) "Highly Active Nitrogen-Doped Carbon Nanotubes for Oxygen Reduction Reaction in Fuel Cell Applications", *The Journal of Physical Chemistry C*, **113**, 21008-21013.

178. Z. Chen, A. Yu, D. Higgins, H. Li, H. Wang, Z. Chen (2012) "Highly Active and Durable Core–Corona Structured Bifunctional Catalyst for Rechargeable Metal–Air Battery Application", *Nano Letters*, **12**, 1946-1952.

179. D. Higgins, Z. Chen, D. U. Lee, Z. Chen (2013) "Activated and nitrogen-doped exfoliated graphene as air electrodes for metal-air battery applications", *Journal of Materials Chemistry A*, **1**, 2639-2645.

180. D. U. Lee, H. W. Park, D. Higgins, L. Nazar, Z. Chen (2013) "Highly Active Graphene Nanosheets Prepared via Extremely Rapid Heating as Efficient Zinc-Air Battery Electrode Material", *Journal of The Electrochemical Society*, **160**, F910-F915.

181. Y. Garsany, O. A. Baturina, K. E. Swider-Lyons, S. S. Kocha (2010) "Experimental Methods for Quantifying the Activity of Platinum Electrocatalysts for the Oxygen Reduction Reaction", *Analytical Chemistry*, **82**, 6321-6328.

182. W. T. Hong, M. Risch, K. A. Stoerzinger, A. Grimaud, J. Suntivich, Y. Shao-Horn (2015) "Toward the rational design of non-precious transition metal oxides for oxygen electrocatalysis", *Energy & Environmental Science*,

183. Z. Chen, L. Xu, W. Li, M. Waje, Y. Yan (2006) "Polyaniline nanofibre supported platinum nanoelectrocatalysts for direct methanol fuel cells", *Nanotechnology*, **17**, 5254-5257.

184. A. Pozio, M. De Francesco, A. Cemmi, F. Cardellini, L. Giorgi (2002) "Comparison of high surface Pt/C catalysts by cyclic voltammetry", *Journal of Power Sources*, **105**, 13-19.

185. Y. Garsany S. Kocha, D. Myers (2013) "Testing Oxygen Reduction Reaction Activity with the Rotating Disc Electrode Technique". Available online at: http://energy.gov/sites/prod/files/2014/03/f12/webinarslides_rde_technique_031213.pdf.

186. Q. Li, H. Pan, D. Higgins, R. Cao, G. Zhang, H. Lv, K. Wu, J. Cho, G. Wu (2015) "Metal–Organic Framework-Derived Bamboo-like Nitrogen-Doped Graphene Tubes as an Active Matrix for Hybrid Oxygen-Reduction Electrocatalysts", *Small*, **11**, 1443-1452.

187. Y. Chen, J. Wang, H. Liu, R. Li, X. Sun, S. Ye, S. Knights (2009) "Enhanced stability of Pt electrocatalysts by nitrogen doping in CNTs for PEM fuel cells", *Electrochem. Comm.*, **11**, 2071-2076.

188. D. C. Higgins, D. Meza, Z. Chen (2010) "Nitrogen-Doped Carbon Nanotubes as Platinum Catalyst Supports for Oxygen Reduction Reaction in Proton Exchange Membrane Fuel Cells", *J. Phys. Chem. C*, **114**, 21982-21988.

189. M. S. Saha, R. Li, X. Sun, S. Ye (2009) "3-D composite electrodes for high performance PEM fuel cells composed of Pt supported on nitrogen-doped carbon nanotubes grown on carbon paper", *Electrochemistry Communications*, **11**, 438-441.

190. L. Dong, R. R. S. Gari, Z. Li, M. M. Craig, S. Hou (2010) "Graphene-supported platinum and platinum-ruthenium nanoparticles with high electrocatalytic activity for methanol and ethanol oxidation", *Carbon*, **48**, 781-787.

191. B. Seger, P. V. Kamat (2009) "Electrocatalytically active graphene-platinum nanocomposites. Role of 2-D carbon support in PEM fuel cells", *J. Phys. Chem. C*, **113**, 7990-7995.

192. R. S. Hsu, D. Higgins, Z. Chen (2010) "Tin-oxide-coated single-walled carbon nanotube bundles supporting platinum electrocatalysts for direct ethanol fuel cells", *Nanotechnology*, **21**, 165705-165810.

193. T. Ioroi, Z. Siroma, N. Fujiwara, S. Yamazaki, K. Yasuda (2005) "Sub-stoichiometric titanium oxide-supported platinum electrocatalyst for polymer electrolyte fuel cells", *Electrochem. Comm.*, **7**, 183-188.

194. B. Avasarala, T. Murray, W. Li, P. Haldar (2009) "Titanium nitride nanoparticles based electrocatalysts for proton exchange membrane fuel cells", *Journal of Materials Chemistry*, **19**, 1803-1805.

195. J. M. Lee, S. B. Han, Y. J. Song, J. Y. Kim, B. Roh, I. Hwang, W. Choi, K. W. Park (2010) "Methanol electrooxidation of Pt catalyst on titanium nitride nanostructured support", *Applied Catalysis A*, **375**, 149-155.

196. O. T. M. Musthafa, S. Sampath (2008) "High performance platinized titanium nitride catalyst for methanol oxidation", *Chemical Communications*, 67-69.

197. M. M. O. Thotiyl, T. Ravikumar, S. Sampath (2010) "Platinum particles supported on titanium nitride: an efficient electrode material for the oxidation of methanol in alkaline media", *Journal of Materials Chemistry*, **20**, 10643–10651.

198. E. Hosono, Y. Wang, N. Kida, M. Enomoto, N. Kojima, M. Okubo, H. Matsuda, Y. Saito, T. Kudo, I. Honma (2009) "Synthesis of Triaxial LiFePO4 Nanowire with a VGCF Core Column and a Carbon Shell through the Electrospinning Method", *ACS Applied Materials & Interfaces*, **2**, 212-218.

199. H. Y. Du, C. H. Wang, H. C. Hsu, S. T. Chang, S. C. Yen, L. C. Chen, B. Viswanathan, K. H. Chen (2011) "High performance of catalysts supported by directly grown PTFE-free micro-porous CNT layer in a proton exchange membrane fuel cell", *Journal of Materials Chemistry*, **21**, 2512-2516.

200. M. Rauber, I. Alber, S. Mu ller, R. Neumann, O. Picht, C. Roth, A. Scho kel, M. E. Toimil-Molares, W. Ensinger (2011) "Highly-Ordered Supportless Three-Dimensional Nanowire Networks with Tunable Complexity and Interwire Connectivity for Device Integration", *Nano Letters*, **6**, 2304–2310.

201. D. C. Higgins, Z. Chen (2010) "Nitrogen Doped Carbon Nanotube Thin Films as Efficient Oxygen Reduction Catalyst for Alkaline Anion Exchange Membrane Fuel Cell", *ECS Transactions*, **28**, 63-68.

202. W. Li, X. Wang, Z. Chen, M. Waje, Y. Yan (2005) "Carbon nanotube film by filtration as cathode catalyst support for proton-exchange membrane fuel cell", *Langmuir*, **21**, 9386-9389.

203. L. Jiang, L. Gao (2005) "Carbon nanotubes-metal nitride composites: a new class of nanocomposites with enhanced electrical properties", *Journal of Materials Chemistry*, **15**, 260-266.

204. L. Jiang, L. Gao (2006) "Fabrication and Characterization of Carbon Nanotube–Titanium Nitride Composites with Enhanced Electrical and Electrochemical Properties", *Journal of the American Chemical Society*, **89**, 156-161.

205. F. F. Cao, Y. G. Guo, S. F. Zheng, X. L. Wu, L. Y. Jiang, R. R. Bi, L. J. Wan, J. Maier (2010) "Symbiotic coaxial nanocables: Facile synthesis and an efficient and elegant morphological solution to the lithium storage problem", *Chemistry of Materials*, **22**, 1908-1914.

206. O. Schulz, N. Eisenreich, H. Fietzek, M. M. Juez Lorenzo, E. Kondratenko (2010) "Oxidation of Nanometer Sized Titanium Nitride and Micrometer Sized Titanium Particles

with Titanium Nitride Traces up to 1473 K in Air", *Particle & Particle Systems Characterizations*, **27**, 58-68.

207. F. Jaouen, F. Charreteur, J. Dodelet (2006) "Fe-based catalysts for oxygen reduction in PEMFCs", *Journal of The Electrochemical Society*, **153**, A689-A698.

208. H. Y. Du, C. H. Wang, H. C. Hsu, S. T. Chang, U. S. Chen, S. Yen, L. Chen, H. C. Shih, K. Chen (2008) "Controlled platinum nanoparticles uniformly dispersed on nitrogen-doped carbon nanotubes for methanol oxidation", *Diamond and Related Materials*, **17**, 535-541.

209. W. Li, C. Liang, W. Zhou, J. Qiu, Z. Zhou, G. Sun, Q. Xin (2003) "Preparation and characterization of multiwalled carbon nanotube-supported platinum for cathode catalysts of direct methanol fuel cells", *Journal of Physical Chemistry B*, **107**, 6292-6299.

210. D. Banham, F. Feng, T. Fürstenhaupt, K. Pei, S. Ye, V. Birss (2011) "Effect of Pt-loaded carbon support nanostructure on oxygen reduction catalysis", *Journal of Power Sources*, **196**, 5438–5445.

211. N. M. Markovic, H. A. Gasteiger, P. N. Ross Jr (1995) "Oxygen reduction on platinum low-index single-crystal surfaces in sulfuric acid solution: rotating ring-Pt (hkl) disk studies", *Journal of Physical Chemistry*, **99**, 3411-3415.

212. D. Meza, U. Morales, P. Roquero, L. Salgado (2010) "Oxygen reduction on carbon supported Pt-W electrocatalysts", *International journal of hydrogen energy*, **35**, 12111-12114.

213. Y. H. Shih, G. V. Sagar, S. D. Lin (2008) "Effect of Electrode Pt Loading on the Oxygen Reduction Reaction Evaluated by Rotating Disk Electrode and Its Implication on the Reaction Kinetics", *Journal of Physical Chemistry C*, **112**, 123-130.

214. D. Higgins, Z. Chen, Z. Chen (2011) "Nitrogen doped carbon nanotubes synthesized from aliphatic diamines for oxygen reduction reaction", *Electrochimica Acta*, **56**, 1570-1575.

215. B. Avasarala, P. Haldar (2010) "Electrochemical Oxidation Behavior of Titanium Nitride based Catalyst Supports under PEM Fuel Cell Conditions", *Electrochim. Acta*, **55**, 9024-9034.

216. Y. Bing, H. Liu, L. Zhang, D. Ghosh, J. Zhang (2010) "Nanostructured Pt-alloy electrocatalysts for PEM fuel cell oxygen reduction reaction", *Chemical Society Reviews*, **39**, 2184-2202.

217. S. Sun, G. Zhang, D. Geng, Y. Chen, R. Li, M. Cai, X. Sun (2011) "A Highly Durable Platinum Nanocatalyst for Proton Exchange Membrane Fuel Cells: Multiarmed Starlike Nanowire Single Crystal", *Angewandte Chemie International Edition*, **123**, 442-446.

218. B. Y. Xia, W. T. Ng, H. B. Wu, X. Wang, X. W. Lou (2012) "Self-Supported Interconnected Pt Nanoassemblies as Highly Stable Electrocatalysts for Low-Temperature Fuel Cells", *Angewandte Chemie International Edition*, **124**, 7325-7328.

219. V. T. T. Ho, N. G. Nguyen, C.-J. Pan, J.-H. Cheng, J. Rick, W.-N. Su, J.-F. Lee, H.-S. Sheu, B.-J. Hwang (2012) "Advanced nanoelectrocatalyst for methanol oxidation and oxygen reduction reaction, fabricated as one-dimensional pt nanowires on nanostructured robust Ti0.7Ru0.3O2 support", *Nano Energy*, **1**, 687-695.

220. A. L. Tiano, C. Koenigsmann, A. C. Santulli, S. S. Wong (2010) "Solution-based synthetic strategies for one-dimensional metal-containing nanostructures", *Chemical Communications*, **46**, 8093-8130.

221. S. Sun, F. Jaouen, J.-P. Dodelet (2008) "Controlled Growth of Pt Nanowires on Carbon Nanospheres and Their Enhanced Performance as Electrocatalysts in PEM Fuel Cells", *Advanced Materials*, **20**, 3900-3904.

222. R. Wang, C. Xu, X. Bi, Y. Ding (2012) "Nanoporous surface alloys as highly active and durable oxygen reduction reaction electrocatalysts", *Energy & Environmental Science*, **5**, 5281-5286.

223. N. V. Long, Y. Yang, C. Minh Thi, N. V. Minh, Y. Cao, M. Nogami (2013) "The development of mixture, alloy, and core-shell nanocatalysts with nanomaterial supports for energy conversion in low-temperature fuel cells", *Nano Energy*, **2**, 636-676.

224. V. Stamenkovic, B. Mun, K. Mayrhofer, P. Ross, N. Markovic (2006) "Effect of surface composition on electronic structure, stability, and electrocatalytic properties of Pt-transition metal alloys: Pt-skin versus Pt-skeleton surfaces", *Journal of the American Chemical Society*, **128**, 8813-8819.

225. Y. Wang, J. Yang, J. Zhang, H. Liu, Z. Zhang (2005) "Microwave-assisted preparation of titanate nanotubes", *Chemistry Letters*, **34**, 1168-1169.

226. Z. Zhang, D. Blom, Z. Gai, J. Thompson, J. Shen, S. Dai (2003) "High-yield solvothermal formation of magnetic CoPt alloy nanowires", *Journal of the American Chemical Society*, **125**, 7528-7529.

227. S. Koh, J. Leisch, M. Toney, P. Strasser (2007) "Structure-Activity-Stability Relationships of Pt- Co Alloy Electrocatalysts in Gas-Diffusion Electrode Layers", *Journal of Physical Chemistry C*, **111**, 3744-3752.

228. T. Moffat, J. Mallett, S. Hwang (2009) "Oxygen Reduction Kinetics on Electrodeposited Pt, PtNi, and PtCo", *Journal of The Electrochemical Society*, **156**, B238.

229. S. Mukerjee, S. Srinivasan (1993) "Enhanced electrocatalysis of oxygen reduction on platinum alloys in proton exchange membrane fuel cells", *Journal of Electroanalytical Chemistry*, **357**, 201-224.

230. U. Paulus, A. Wokaun, G. Scherer, T. Schmidt, V. Stamenkovic, V. Radmilovic, N. Markovic, P. Ross (2002) "Oxygen Reduction on Carbon-Supported Pt- Ni and Pt- Co Alloy Catalysts", *J. Phys. Chem. B*, **106**, 4181-4191.

231. M. Saha, Y. Chen, R. Li, X. Sun (2009) "Enhancement of PEMFC performance by using carbon nanotubes supported Pt Co alloy catalysts", *Asia Pac. J. Chem. Eng.*, **4**, 12-16.

232. X. Liao, J. Zhu, J. Xu, H. Chen, J. Zhu (2001) "Preparation of monodispersed nanocrystalline CeO 2 powders by microwave irradiation", *Chem. Comm.*, **2001**, 937-938.

233. F. Liu, Y. Chang, P. Huang, F. Ko, T. Chu (2004) "Preparation of silver nanorods by rapid microwave heating", *Chemistry Letters*, **33**, 1050-1051.

234. E. Hong, K. Lee, S. Oh, C. Park (2003) "Synthesis of carbon nanotubes using microwave radiation", *Advanced Functional Materials*, **13**, 961-966.

235. A. Panda, G. Glaspell, M. El-Shall (2006) "Microwave synthesis of highly aligned ultra narrow semiconductor rods and wires", *Journal of the American Chemical Society*, **128**, 2790-2791.

236. Z. Chen, L. Xu, W. Li, M. Waje, Y. Yan (2006) "Polyaniline nanofibre supported platinum nanoelectrocatalysts for direct methanol fuel cells", *Nanotechnology*, **17**, 5254.

237. J. Salgado, E. Antolini, E. Gonzalez (2004) "Structure and Activity of Carbon-Supported Pt- Co Electrocatalysts for Oxygen Reduction", *J. Phys. Chem. B*, **108**, 17767-17774.

238. F. Maillard, L. Dubau, J. Durst, M. Chatenet, J. André, E. Rossinot (2010) "Durability of Pt3Co/C nanoparticles in a proton-exchange membrane fuel cell: direct evidence of bulk Co segregation to the surface", *Electrochem. Comm.*, **12**, 1161-1164.

239. S. Axnanda, K. Cummins, T. He, D. Goodman, M. Soriaga (2010) "Structural, Compositional and Electrochemical Characterization of Pt–Co Oxygen Reduction Catalysts", *ChemPhysChem*, **11**, 1468-1475.

240. M. Inaba, H. Yamada, J. Tokunaga, A. Tasaka (2004) "Effect of agglomeration of Pt/C catalyst on hydrogen peroxide formation", *Electrochemical and Solid-State Letters*, **7**, A474.

241. C. Koenigsmann, M. E. Scofield, H. Liu, S. S. Wong (2012) "Designing Enhanced One-Dimensional Electrocatalysts for the Oxygen Reduction Reaction: Probing Size- and Composition-Dependent Electrocatalytic Behavior in Noble Metal Nanowires", *The Journal of Physical Chemistry Letters*, **3**, 3385-3398.

242. D. Li, Y. Wang, Y. Xia (2003) "Electrospinning of Polymeric and Ceramic Nanofibers as Uniaxially Aligned Arrays", *Nano Letters*, **3**, 1167-1171.

243. H. J. Kim, Y. S. Kim, M. H. Seo, S. M. Choi, W. B. Kim (2009) "Pt and PtRh nanowire electrocatalysts for cyclohexane-fueled polymer electrolyte membrane fuel cell", *Electrochemistry Communications*, **11**, 446-449.

244. J. Wu, H. W. Park, A. Yu, D. Higgins, Z. Chen (2012) "Facile Synthesis and Evaluation of Nanofibrous Iron–Carbon Based Non-Precious Oxygen Reduction Reaction Catalysts for Li–O2 Battery Applications", *The Journal of Physical Chemistry C*, **116**, 9427-9432.

245. V. R. Stamenkovic, B. S. Mun, M. Arenz, K. J. J. Mayrhofer, C. A. Lucas, G. Wang, P. N. Ross, N. M. Markovic (2007) "Trends in electrocatalysis on extended and nanoscale Pt-bimetallic alloy surfaces", *Nature Materials*, **6**, 241-247.

246. D. van der Vliet, D. S. Strmcnik, C. Wang, V. R. Stamenkovic, N. M. Markovic, M. T. M. Koper (2010) "On the importance of correcting for the uncompensated Ohmic resistance

in model experiments of the Oxygen Reduction Reaction", *Journal of Electroanalytical Chemistry*, **647**, 29-34.

247. D. Wang, H. L. Xin, R. Hovden, H. Wang, Y. Yu, D. A. Muller, F. J. DiSalvo, H. D. Abruña (2013) "Structurally ordered intermetallic platinum–cobalt core–shell nanoparticles with enhanced activity and stability as oxygen reduction electrocatalysts", *Nature Materials*, **12**, 81-87.

248. B. P. Vinayan, R. Nagar, N. Rajalakshmi, S. Ramaprabhu (2012) "Novel Platinum–Cobalt Alloy Nanoparticles Dispersed on Nitrogen-Doped Graphene as a Cathode Electrocatalyst for PEMFC Applications", *Advanced Functional Materials*, **22**, 3519-3526.

249. K. C. Neyerlin, B. A. Larsen, S. Pylypenko, S. S. Kocha, B. S. Pivovar (2013) "Activity of Pt Extended Network Electrocatalyst Structures Made from Spontaneous Galvanic Displacement", *ECS Transactions*, **50**, 1405-1413.

250. I. E. L. Stephens, A. S. Bondarenko, U. Gronbjerg, J. Rossmeisl, I. Chorkendorff (2012) "Understanding the electrocatalysis of oxygen reduction on platinum and its alloys", *Energy & Environmental Science*, **5**, 6744-6762.

251. H. A. Gasteiger, S. S. Kocha, B. Sompalli, F. T. Wagner (2005) "Activity benchmarks and requirements for Pt, Pt-alloy, and non-Pt oxygen reduction catalysts for PEMFCs", *Appl. Catal. B*, **56**, 9-35.

252. K. J. J. Mayrhofer, D. Strmcnik, B. B. Blizanac, V. Stamenkovic, M. Arenz, N. M. Markovic (2008) "Measurement of oxygen reduction activities via the rotating disc electrode method: From Pt model surfaces to carbon-supported high surface area catalysts", *Electrochimica Acta*, **53**, 3181-3188.

253. D. C. Higgins, F. M. Hassan, M. H. Seo, J. Y. Choi, M. A. Hoque, D. U. Lee, Z. Chen (2015) "Shape-controlled octahedral cobalt disulfide nanoparticles supported on nitrogen and sulfur-doped graphene/carbon nanotube composites for oxygen reduction in acidic electrolyte", *Journal of Materials Chemistry A*, **3**, 6340-6350.

254. J.-Y. Choi, D. Higgins, G. Jiang, R. Hsu, J. Qiao, Z. Chen (2015) "Iron-tetracyanobenzene complex derived non-precious catalyst for oxygen reduction reaction", *Electrochimica Acta*, **162**, 224-229.

255. P. Zamani, D. Higgins, F. Hassan, G. Jiang, J. Wu, S. Abureden, Z. Chen (2014) "Electrospun Iron–Polyaniline–Polyacrylonitrile Derived Nanofibers as Non–Precious Oxygen Reduction Reaction Catalysts for PEM Fuel Cells", *Electrochimica Acta*, **139**, 111-116.

256. H. T. Chung, C. M. Johnston, K. Artyushkova, M. Ferrandon, D. J. Myers, P. Zelenay (2010) "Cyanamide-derived non-precious metal catalyst for oxygen reduction", *Electrochemistry Communications*, **12**, 1792-1795.

257. E. Proietti, F. Jaouen, M. Lefèvre, N. Larouche, J. Tian, J. Herranz, J.-P. Dodelet (2011) "Iron-based cathode catalyst with enhanced power density in polymer electrolyte membrane fuel cells", *Nature Communications*, **2**, 416.

258. W. Li, A. Yu, D. C. Higgins, B. G. Llanos, Z. Chen (2010) "Biologically Inspired Highly Durable Iron Phthalocyanine Catalysts for Oxygen Reduction Reaction in Polymer Electrolyte Membrane Fuel Cells", *Journal of the American Chemical Society*, **132**, 17056-17058.

259. M. H. Seo, D. Higgins, G. Jiang, S. M. Choi, B. Han, Z. Chen (2014) "Theoretical insight into highly durable iron phthalocyanine derived non-precious catalysts for oxygen reduction reactions", *Journal of Materials Chemistry A*, **2**, 19707-19716.

260. M. R. Gao, Y. F. Xu, J. Jiang, S. H. Yu (2013) "Nanostructured metal chalcogenides: synthesis, modification, and applications in energy conversion and storage devices", *Chemical Society Reviews*, **42**, 2986-3017.

261. N. Kumar, N. Raman, A. Sundaresan (2014) "Synthesis and Properties of Cobalt Sulfide Phases: CoS2 and Co9S8", *Zeitschrift für anorganische und allgemeine Chemie*, **640**, 1069-1074.

262. Q. Liu, J. Zhang (2013) "A general and controllable synthesis of ComSn (Co9S8, Co3S4, and Co1-xS) hierarchical microspheres with homogeneous phases", *CrystEngComm*, **15**, 5087-5092.

263. H. Wang, Y. Liang, Y. Li, H. Dai (2011) "Co1−xS–Graphene Hybrid: A High-Performance Metal Chalcogenide Electrocatalyst for Oxygen Reduction", *Angewandte Chemie International Edition*, **50**, 10969-10972.

264. L. Zhu, D. Susac, M. Teo, K. C. Wong, P. C. Wong, R. R. Parsons, D. Bizzotto, K. A. R. Mitchell, S. A. Campbell (2008) "Investigation of CoS2-based thin films as model catalysts for the oxygen reduction reaction", *Journal of Catalysis*, **258**, 235-242.

265. Y. X. Zhou, H. B. Yao, Y. Wang, H. L. Liu, M. R. Gao, P. K. Shen, S. H. Yu (2010) "Hierarchical Hollow Co9S8 Microspheres: Solvothermal Synthesis, Magnetic, Electrochemical, and Electrocatalytic Properties", *Chemistry – A European Journal*, **16**, 12000-12007.

266. J. S. Jirkovský, A. Björling, E. Ahlberg (2012) "Reduction of Oxygen on Dispersed Nanocrystalline CoS2", *The Journal of Physical Chemistry C*, **116**, 24436-24444.

267. G. Wu, N. H. Mack, W. Gao, S. Ma, R. Zhong, J. Han, J. K. Baldwin, P. Zelenay (2012) "Nitrogen-Doped Graphene-Rich Catalysts Derived from Heteroatom Polymers for Oxygen Reduction in Nonaqueous Lithium–O2 Battery Cathodes", *ACS nano*, **6**, 9764-9776.

268. C. Zhao, D. Li, Y. Feng (2013) "Size-controlled hydrothermal synthesis and high electrocatalytic performance of CoS2 nanocatalysts as non-precious metal cathode materials for fuel cells", *Journal of Materials Chemistry A*, **1**, 5741-5746.

269. Q. Wang, L. Jiao, H. Du, Y. Si, Y. Wang, H. Yuan (2012) "Co3S4 hollow nanospheres grown on graphene as advanced electrode materials for supercapacitors", *Journal of Materials Chemistry*, **22**, 21387-21391.

270. J. Xiao, L. Wan, S. Yang, F. Xiao, S. Wang (2014) "Design Hierarchical Electrodes with Highly Conductive NiCo2S4 Nanotube Arrays Grown on Carbon Fiber Paper for High-Performance Pseudocapacitors", *Nano Letters*, **14**, 831-838.

271. A. N. Grace, R. Ramachandran, M. Vinoba, S. Y. Choi, D. H. Chu, Y. Yoon, S. C. Nam, S. K. Jeong (2014) "Facile Synthesis and Electrochemical Properties of Co3S4-Nitrogen-Doped Graphene Nanocomposites for Supercapacitor Applications", *Electroanalysis*, **26**, 199-208.

272. J. Wang, S. H. Ng, G. X. Wang, J. Chen, L. Zhao, Y. Chen, H. K. Liu (2006) "Synthesis and characterization of nanosize cobalt sulfide for rechargeable lithium batteries", *Journal of Power Sources*, **159**, 287-290.

273. Q. Wang, L. Jiao, Y. Han, H. Du, W. Peng, Q. Huan, D. Song, Y. Si, Y. Wang, H. Yuan (2011) "CoS2 Hollow Spheres: Fabrication and Their Application in Lithium-Ion Batteries", *The Journal of Physical Chemistry C*, **115**, 8300-8304.

274. Y. Gu, Y. Xu, Y. Wang (2013) "Graphene-Wrapped CoS Nanoparticles for High-Capacity Lithium-Ion Storage", *ACS Applied Materials & Interfaces*, **5**, 801-806.

275. J. Y. Lin, J. H. Liao, S. W. Chou (2011) "Cathodic electrodeposition of highly porous cobalt sulfide counter electrodes for dye-sensitized solar cells", *Electrochimica Acta*, **56**, 8818-8826.

276. C. W. Kung, H. W. Chen, C. Y. Lin, K. C. Huang, R. Vittal, K. C. Ho (2012) "CoS Acicular Nanorod Arrays for the Counter Electrode of an Efficient Dye-Sensitized Solar Cell", *ACS nano*, **6**, 7016-7025.

277. E. Bi, H. Chen, X. Yang, W. Peng, M. Gratzel, L. Han (2014) "A quasi core-shell nitrogen-doped graphene/cobalt sulfide conductive catalyst for highly efficient dye-sensitized solar cells", *Energy & Environmental Science*, **7**, 2637-2641.

278. D. Geng, Y. Chen, Y. Chen, Y. Li, R. Li, X. Sun, S. Ye, S. Knights (2011) "High oxygen-reduction activity and durability of nitrogen-doped graphene", *Energy & Environmental Science*, **4**, 760-764.

279. Y. Chen, J. Wang, H. Liu, M. N. Banis, R. Li, X. Sun, T.-K. Sham, S. Ye, S. Knights (2011) "Nitrogen Doping Effects on Carbon Nanotubes and the Origin of the Enhanced Electrocatalytic Activity of Supported Pt for Proton-Exchange Membrane Fuel Cells", *The Journal of Physical Chemistry C*, **115**, 3769-3776.

280. J. P. Paraknowitsch, A. Thomas (2013) "Doping carbons beyond nitrogen: an overview of advanced heteroatom doped carbons with boron, sulphur and phosphorus for energy applications", *Energy & Environmental Science*, **6**, 2839-2855.

281. H. Wang, T. Maiyalagan, X. Wang (2012) "Review on Recent Progress in Nitrogen-Doped Graphene: Synthesis, Characterization, and Its Potential Applications", *ACS Catalysis*, **2**, 781-794.

282. H. Wang, M. Xie, L. Thia, A. Fisher, X. Wang (2013) "Strategies on the Design of Nitrogen-Doped Graphene", *The Journal of Physical Chemistry Letters*, **5**, 119-125.

283. Y. Liang, Y. Li, H. Wang, H. Dai (2013) "Strongly Coupled Inorganic/Nanocarbon Hybrid Materials for Advanced Electrocatalysis", *Journal of the American Chemical Society*, **135**, 2013-2036.

284. B. Xia, Y. Yan, X. Wang, X. W. Lou (2014) "Recent progress on graphene-based hybrid electrocatalysts", *Materials Horizons*, **1**, 379-399.

285. M. N. Banis, S. Sun, X. Meng, Y. Zhang, Z. Wang, R. Li, M. Cai, T.-K. Sham, X. Sun (2013) "TiSi2Ox Coated N-Doped Carbon Nanotubes as Pt Catalyst Support for the Oxygen Reduction Reaction in PEMFCs", *The Journal of Physical Chemistry C*, **117**, 15457-15467.

286. J. Xu, G. Dong, C. Jin, M. Huang, L. Guan (2013) "Sulfur and Nitrogen Co-Doped, Few-Layered Graphene Oxide as a Highly Efficient Electrocatalyst for the Oxygen-Reduction Reaction", *ChemSusChem*, **6**, 493-499.

287. B. J. Kim, D. U. Lee, J. Wu, D. Higgins, A. Yu, Z. Chen (2013) "Iron- and Nitrogen-Functionalized Graphene Nanosheet and Nanoshell Composites as a Highly Active Electrocatalyst for Oxygen Reduction Reaction", *The Journal of Physical Chemistry C*, **117**, 26501-26508.

288. G. Kresse, J. Furthmüller (1996) "Efficient iterative schemes for ab initio total-energy calculations using a plane-wave basis set", *Physical Review B*, **54**, 11169-11186.

289. P. Hohenberg, W. Kohn (1964) "Inhomogeneous Electron Gas", *Physical Review*, **136**, B864–B871.

290. W. Kohn, L. J. Sham (1965) "Self-Consistent Equations Including Exchange and Correlation Effects", *Physical Review A*, **140**, 1133–A1138.

291. J. P. Perdew, K. Burke, M. Ernzerhof (1996) "Generalized Gradient Approximation Made Simple", *Physical Review Letters*, **77**, 3865-3868.

292. G. Kresse, J. Furthmuller (1996) "Efficiency of ab-initio total energy calculations for metals and semiconductors using a plane-wave basis set", *Computational Materials Science*, **6**, 15-50.

293. J. P. Perdew, K. Burke, Y. Wang (1996) "Generalized gradient approximation for the exchange-correlation hole of a many-electron system", *Physical Review B*, **54**, 16533-16539.

294. G. Kresse, D. Joubert (1999) "From ultrasoft pseudopotentials to the projector augmented-wave method", *Physical Review B*, **59**, 1758 -1775.

295. P. E. Blöchl (1994) "Projector augmented-wave method", *Physical Review B*, **50**, 17953-17979.

296. M. Methfessel, A. T. Paxton (1989) "High-Precision Sampling for Brillouin-Zone Integration in Metals", *Physical Review B*, **40**, 3616-3621.

297. V. Chabot, D. Higgins, A. Yu, X. Xiao, Z. Chen, J. Zhang (2014) "A review of graphene and graphene oxide sponge: material synthesis and applications to energy and the environment", *Energy & Environmental Science*, **7**, 1564-1596.

298. C. Zhang, L. Ren, X. Wang, T. Liu (2010) "Graphene Oxide-Assisted Dispersion of Pristine Multiwalled Carbon Nanotubes in Aqueous Media", *The Journal of Physical Chemistry C*, **114**, 11435-11440.

299. L. Qiu, X. Yang, X. Gou, W. Yang, Z.-F. Ma, G. G. Wallace, D. Li (2010) "Dispersing Carbon Nanotubes with Graphene Oxide in Water and Synergistic Effects between Graphene Derivatives", *Chemistry – A European Journal*, **16**, 10653-10658.

300. S. J. Bao, Y. Li, C. M. Li, Q. Bao, Q. Lu, J. Guo (2008) "Shape Evolution and Magnetic Properties of Cobalt Sulfide", *Crystal Growth & Design*, **8**, 3745-3749.

301. D. C. Higgins, M. A. Hoque, F. Hassan, J.-Y. Choi, B. Kim, Z. Chen (2014) "Oxygen Reduction on Graphene–Carbon Nanotube Composites Doped Sequentially with Nitrogen and Sulfur", *ACS Catalysis*, **4**, 2734-2740.

302. H. van der Heide, R. Hemmel, C. F. van Bruggen, C. Haas (1980) "X-ray photoelectron spectra of 3d transition metal pyrites", *Journal of Solid State Chemistry*, **33**, 17-25.

303. Z. Yang, Z. Yao, G. Li, G. Fang, H. Nie, Z. Liu, X. Zhou, X. a. Chen, S. Huang (2011) "Sulfur-Doped Graphene as an Efficient Metal-free Cathode Catalyst for Oxygen Reduction", *ACS nano*, **6**, 205-211.

304. Z. P. Xu, R. Xu, H. C. Zeng (2001) "Sulfate-Functionalized Carbon/Metal-Oxide Nanocomposites from Hydrotalcite-like Compounds", *Nano Letters*, **1**, 703-706.

305. J. Liang, Y. Jiao, M. Jaroniec, S. Z. Qiao (2012) "Sulfur and Nitrogen Dual-Doped Mesoporous Graphene Electrocatalyst for Oxygen Reduction with Synergistically Enhanced Performance", *Angewandte Chemie International Edition*, **51**, 11496-11500.

306. S. M. Jung, E. K. Lee, M. Choi, D. Shin, I. Y. Jeon, J. M. Seo, H. Y. Jeong, N. Park, J. H. Oh, J. B. Baek (2014) "Direct Solvothermal Synthesis of B/N-Doped Graphene", *Angewandte Chemie International Edition*, **53**, 2398-2401.

307. S. A. Wohlgemuth, R. J. White, M. G. Willinger, M. M. Titirici, M. Antonietti (2012) "A one-pot hydrothermal synthesis of sulfur and nitrogen doped carbon aerogels with enhanced electrocatalytic activity in the oxygen reduction reaction", *Green Chemistry*, **14**, 1515-1523.

308. Y. Su, Y. Zhang, X. Zhuang, S. Li, D. Wu, F. Zhang, X. Feng (2013) "Low-temperature synthesis of nitrogen/sulfur co-doped three-dimensional graphene frameworks as efficient metal-free electrocatalyst for oxygen reduction reaction", *Carbon*, **62**, 296-301.

309. Q. Shi, F. Peng, S. Liao, H. Wang, H. Yu, Z. Liu, B. Zhang, D. Su (2013) "Sulfur and nitrogen co-doped carbon nanotubes for enhancing electrochemical oxygen reduction activity in acidic and alkaline media", *Journal of Materials Chemistry A*, **1**, 14853-14857.

310. Y. Chang, F. Hong, C. He, Q. Zhang, J. Liu (2013) "Nitrogen and Sulfur Dual-Doped Non-Noble Catalyst Using Fluidic Acrylonitrile Telomer as Precursor for Efficient Oxygen Reduction", *Advanced Materials*, **25**, 4794-4799.

311. D. C. Higgins, J. Wu, W. Li, Z. Chen (2012) "Cyanamide derived thin film on carbon nanotubes as metal free oxygen reduction reaction electrocatalyst", *Electrochimica Acta*, **59**, 8-13.

312. X. Li, H. Wang, J. T. Robinson, H. Sanchez, G. Diankov, H. Dai (2009) "Simultaneous Nitrogen Doping and Reduction of Graphene Oxide", *Journal of the American Chemical Society*, **131**, 15939-15944.

313. T. Wanjun, C. Donghua (2007) "Mechanism of thermal decomposition of cobalt acetate tetrahydrate", *Chemical Papers*, **61**, 329-332.

314. S. Wang, Q. Gao, J. Wang (2005) "Thermodynamic Analysis of Decomposition of Thiourea and Thiourea Oxides", *The Journal of Physical Chemistry B*, **109**, 17281-17289.

315. Z. D. Wang, M. Yoshida, B. George (2013) "Theoretical study on the thermal decomposition of thiourea", *Computational and Theoretical Chemistry*, **1017**, 91-98.

316. W. Dong, X. Wang, B. Li, L. Wang, B. Chen, C. Li, X. Li, T. Zhang, Z. Shi (2011) "Hydrothermal synthesis and structure evolution of hierarchical cobalt sulfide nanostructures", *Dalton Transactions*, **40**, 243-248.

317. J. Madarász, G. Pokol (2007) "Comparative evolved gas analyses on thermal degradation of thiourea by coupled TG-FTIR and TG/DTA-MS instruments", *Journal of Thermal Analysis and Calorimetry*, **88**, 329-336.

318. P. Chen, T. Y. Xiao, Y. H. Qian, S. S. Li, S. H. Yu (2013) "A Nitrogen-Doped Graphene/Carbon Nanotube Nanocomposite with Synergistically Enhanced Electrochemical Activity", *Advanced Materials*, **25**, 3192-3196.

319. P. Chen, J. J. Yang, S. S. Li, Z. Wang, T. Y. Xiao, Y. H. Qian, S. H. Yu (2013) "Hydrothermal synthesis of macroscopic nitrogen-doped graphene hydrogels for ultrafast supercapacitor", *Nano Energy*, **2**, 249-256.

320. C. Nethravathi, M. Rajamathi (2008) "Chemically modified graphene sheets produced by the solvothermal reduction of colloidal dispersions of graphite oxide", *Carbon*, **46**, 1994-1998.

321. S. Ratso, I. Kruusenberg, M. Vikkisk, U. Joost, E. Shulga, I. Kink, T. Kallio, K. Tammeveski (2014) "Highly active nitrogen-doped few-layer graphene/carbon nanotube composite electrocatalyst for oxygen reduction reaction in alkaline media", *Carbon*, **73**, 361-370.

322. H. W. Park, D. U. Lee, Y. Liu, J. Wu, L. F. Nazar, Z. Chen (2013) "Bi-Functional N-Doped CNT/Graphene Composite as Highly Active and Durable Electrocatalyst for Metal Air Battery Applications", *Journal of The Electrochemical Society*, **160**, A2244-A2250.

323. V. C. Tung, L. M. Chen, M. J. Allen, J. K. Wassei, K. Nelson, R. B. Kaner, Y. Yang (2009) "Low-Temperature Solution Processing of Graphene−Carbon Nanotube Hybrid Materials for High-Performance Transparent Conductors", *Nano Letters*, **9**, 1949-1955.

324. Y. Hu, X. Li, J. Wang, R. Li, X. Sun (2013) "Free-standing graphene–carbon nanotube hybrid papers used as current collector and binder free anodes for lithium ion batteries", *Journal of Power Sources*, **237**, 41-46.

325. D. Yu, L. Dai (2009) "Self-Assembled Graphene/Carbon Nanotube Hybrid Films for Supercapacitors", *The Journal of Physical Chemistry Letters*, **1**, 467-470.

326. Q. Cheng, J. Tang, J. Ma, H. Zhang, N. Shinya, L. C. Qin (2011) "Graphene and carbon nanotube composite electrodes for supercapacitors with ultra-high energy density", *Physical Chemistry Chemical Physics*, **13**, 17615-17624.

327. H. Sun, X. You, J. Deng, X. Chen, Z. Yang, J. Ren, H. Peng (2014) "Novel Graphene/Carbon Nanotube Composite Fibers for Efficient Wire-Shaped Miniature Energy Devices", *Advanced Materials*, **26**, 2868-2873.

328. Y. Feng, A. Gago, L. Timperman, N. Alonso-Vante (2011) "Chalcogenide metal centers for oxygen reduction reaction: Activity and tolerance", *Electrochimica Acta*, **56**, 1009-1022.

329. P. J. Brown, K. U. Neumann, A. Simon, F. Ueno, K. R. A. Ziebeck (2005) "Magnetization distribution in COS2; is it a half metallic ferromagnet?", *Journal of Physics-Condensed Matter*, **17**, 1583-1592.

330. M. H. Shao, T. Huang, P. Liu, J. Zhang, K. Sasaki, M. B. Vukmirovic, R. R. Adzic (2006) "Palladium monolayer and Palladium alloy electrocatalysts for oxygen reduction", *Langmuir*, **22**, 10409–10415.

331. G. A. Tritsaris, J. Rossmeisl (2012) "Methanol Oxidation on Model Elemental and Bimetallic Transition Metal Surfaces", *The Journal of Physical Chemistry C*, **116**, 11980−11986.

332. I. Chorkendorff, J. W. Niemantsverdriet (2007) "Concepts of Modern Catalysis and Kinetics", Wiley-VCH Verlag GmbH & Co KGaA, Weinheim, Germany.

333. M. H. Seo, S. M. Choi, E. J. Lim, I. H. Kwon, J. K. Seo, S. H. Noh, W. B. Kim, B. Han (2014) "Toward New Fuel Cell Support Materials: A Theoretical and Experimental Study of Nitrogen-Doped Graphene", *ChemSusChem*, **7**, 2609-2620.